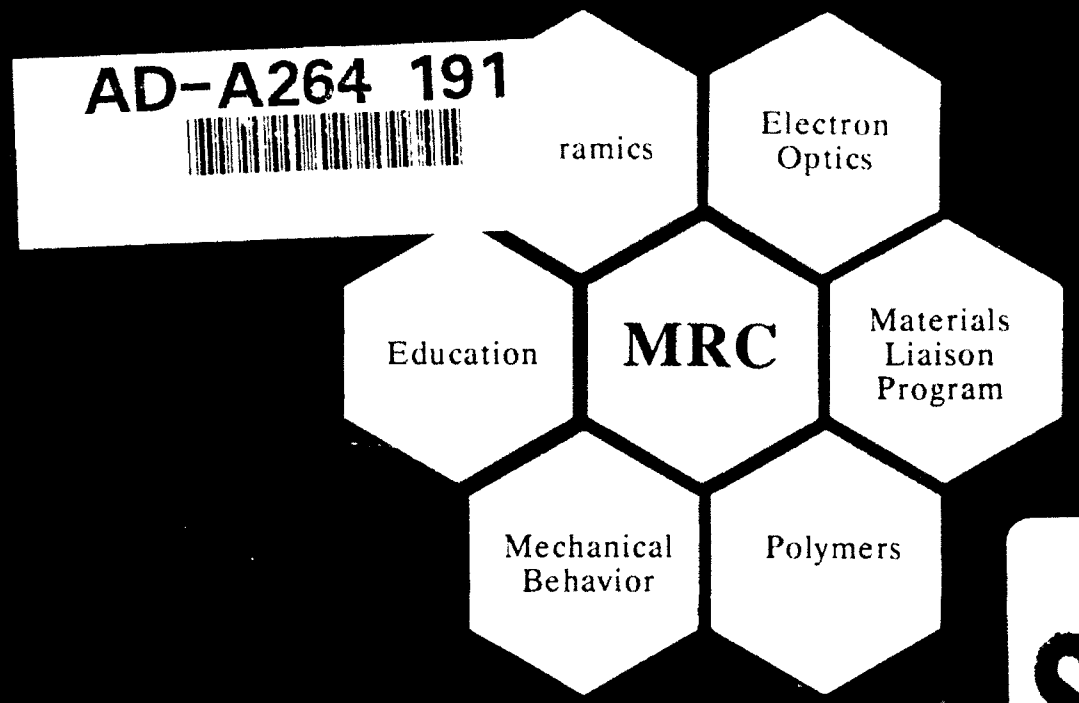

First Annual Report

PROCESSING OF NOVEL NANOPARTICLE DISPERSION STRENGTHENED CERAMICS FOR IMPROVED MECHANICAL PERFORMANCE

Professors H. M. Chan (P.I.), M. P. Harmer (Co-P.I.), and Research Assistants/Associates M. Thompson, J. Zhao, J. Fang, I. Chou

Sponsored by

U.S. Office of Naval Research and The Electric Power Research Institute

ONR Grant No.: N00014-92-J-1635

EPRI Contract: RP2426-54

Report Period: 15 December 1991 - 14 December 1992

Materials Research Center, MRC
Lehigh Univers

ABSTRACT

"Nanocomposites" have continued to show promise both as structural ceramic materials and as ideal systems in which to design multiphase microstructures. This report focuses on successful techniques for fabricating Al_2O_3/SiC "nanocomposites", the strengthening obtained by the addition of sub-micron SiC particles to Al_2O_3, and the technological advantages of the nanocomposite Some of the most significant conclusions of this work are:

(1) A technique has been developed to reproducibly fabricate fine-grained nanocomposites of Al_2O_3 containing 0.15 μm SiC particles.

(2) It has been confirmed that "nanocomposites" of Al_2O_3 containing 5 vol% 0.15 μm SiC have exceptionally high unindented strengths. A subsequent annealing step improves these unindented strengths to greater than 1 GPa.

(3) The strengthening effect appears to be grain size independent: the strengthening does not diminish even after the matrix grain size is coarsened to the level of 60 μm. This is in marked contrast to undoped Al_2O_3 in which the unindented strengths decrease significantly as the grain size coarsens.

(3) The strengthening mechanism in the "nanocomposite" is believed to arise from machining-induced residual surface stresses. The function of the annealing step is to relax these stresses slightly (as indicated in preliminary x-ray stress measurements) while significantly decreasing the size of the machining flaws.

(4) The flaw healing behavior of the Al_2O_3 "nanocomposite" and the undoped Al_2O_3 has been characterized in an indentation-annealing study. The two materials show remarkably different responses to the annealing step used to strengthen the nanocomposite. In the nanocomposite, the indentation cracks close and diffusionally bond, whereas in Al_2O_3 the cracks grow. These observations are explained by considering the toughening mechanism and fracture mode in each material.

(5) Microstructural investigation of the as-ground and polished surfaces of Al_2O_3 and Al_2O_3/SiC "nanocomposite" has revealed possibly one of the greatest technological advantages of the nanocomposite system. The nanocomposite can be easily ground flat, without the grain pullout and chipping that usually accompanies the machining of Al_2O_3. This material property is believed to arise from the mechanical keying of the Al_2O_3 matrix grains by the SiC particles.

St-A per telecon, Dr. Fishman, ONR/
Code 1131S. Arl., VA 22217
5-13-93 JK

TABLE OF CONTENTS

Section 1.1

UNIQUE OPPORTUNITIES FOR MICROSTRUCTURAL ENGINEERING WITH DUPLEX AND LAMINAR CERAMIC COMPOSITES

by

Martin P. Harmer, Helen M. Chan, and Gary A. Miller

Featured article in Journal of the American Ceramic Society, Volume 75, page 1715.

journal

J. Am. Ceram. Soc., 75 [7] 1715–28 (1992)

Unique Opportunities for Microstructural Engineering with Duplex and Laminar Ceramic Composites

Martin P. Harmer,* Helen M. Chan,* and Gary A. Miller

Department of Materials Science and Engineering, and Materials Research Center, Lehigh University, Bethlehem, Pennsylvania 18015

Duplex (two-phase) microstructures and laminar composites offer some unique opportunities for improving the room-temperature mechanical reliability (e.g., flaw tolerance) and the high-temperature microstructural stability (e.g., resistance to grain growth and creep damage) of structural ceramic materials. Examples illustrating the approach to designing novel multiphase microstructures and laminar composites with enhanced structural reliability are given. These are based on current work on various alumina-based ceramics as well as zirconia-, silicon nitride-, and silicon carbide-containing ceramics. Critical issues and areas for future work are discussed. [Key words: ceramics, composites, multiphase, laminates, microstructure.]

I. Introduction

MUCH of the past emphasis in ceramic powder-processing science has been placed on achieving the highest degree of homogeneity in monophase ceramics.[1,2] This strategy has been successful in producing both powders that are highly sinterable and fired ceramics that have fewer flaws and, consequently, higher mechanical strength. Extensive work on alumina gives an indication of the progress that has been made to date.[3,4] Recently, three new strategies have emerged for achieving greater mechanical reliability that are fundamentally different from the conventional "flaw elimination" approach. These strategies are "flaw tolerance," "nanoparticle dispersion strengthening," and "laminates."

In the flaw tolerance approach to nontransforming ceramics, the microstructure is designed to promote grain-localized bridging behind the crack tip, which leads, in the ideal case, to the strength being independent of flaw size.[5,6] From the processing standpoint, the advantage is that the strength is then less sensitive to processing defects and accidents. Improvements in flaw tolerance depend upon having a multiphase ceramic with a controlled, heterogeneous microstructure. This requires a processing strategy for flaw tolerance that is in contrast to that for flaw elimination.

In the nanoparticle-dispersion-strengthening approach, it has been reported that the incorporation of a dispersion of ultrafine (100 to 300 nm) second-phase particles into a matrix of higher expansion coefficient gives rise to significant strengthening.[7]

Laminar composites also provide a unique opportunity for tailoring the microstructure and mechanical properties of structural ceramics.

The first part of this paper reviews some of the new approaches for room-temperature mechanical stability, and the

S. M. Wiederhorn—contributing editor

Manuscript No. 196300. Received October 3, 1991; approved March 16, 1992.

Supported by U.S. Air Force Office of Scientific Research, Ceramics Program, monitored by L. Schioler and L. W. Burggraf, under Contract No. AFOSR-87-0396.

*Member, American Ceramic Society.

feature

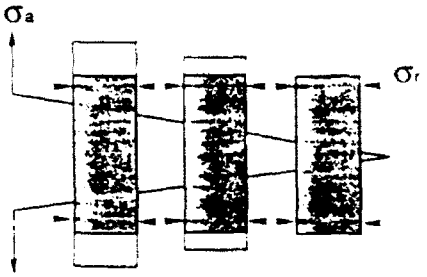

Fig. 1. Schematic diagram of grain-localized bridging in crack wake leading to *R*-curve behavior. Bridging grains are clamped in place by residual stress σ_r.

balance deals with specific examples of elevated-temperature microstructural stability. The examples include grain-growth resistance and tolerance to creep damage, which are inherent to some interpenetrating duplex (two-phase) ceramic microstructures.

II. Mechanical Reliability at Low Temperatures

(1) Flaw Tolerance

One of the major toughening mechanisms believed to be responsible for flaw tolerance in nontransforming ceramics is grain-localized bridging[9-11] (see Fig. 1). The concept (which is an extension of the earlier works of Lange,[14] Becher,[15] Lewis,[16] and others on fibrous and whisker-reinforced ceramics) is that bridging grains are wedged in the microstructure by internal compressive stresses, which lead to an increase in fracture toughness as the crack grows (*R*-curve behavior). For noncubic materials, these wedging stresses are augmented by thermal expansion mismatch between adjacent grains. The extent of toughening, i.e., the form of the *R*-curve, is postulated to depend upon such factors as the size and shape of the bridging grains, the spacing between the bridges, and the residual stress field surrounding the bridging sites.[17]

In single-phase ceramics, such as alumina, it has been demonstrated that one way to enhance the microstructural bridging is to increase the grain size.[18] Although this is effective in increasing the grain pullout distance and, hence, promoting flaw tolerance, it does so at the expense of strength at small flaw sizes. This is because scaling up the microstructure also increases the bridge spacing (i.e., it increases the distance the crack must propagate before it encounters a bridge). A more effective approach is to introduce a high number density of isolated elongated grains (effective bridge sites) into the microstructure *in situ*. The classic example is Lange's[14] early work on silicon nitride. In that study, he showed that the elongated grain microstructure had 4 times the fracture toughness and 2 times the strength of the equiaxed microstructure. More recently the approach has been successfully applied to the development of a new generation of silicon nitride ceramics with strong *R*-curve behavior, high peak fracture toughness (8 to 12 MPa·m$^{1/2}$) and high strength (~800 MPa) (see Fig. 2).[19] However, the technique for the in situ formation of such duplex microstructures is based largely on empiricism. As yet there is no easy method to predict from first principles how to form controlled, elongated-grain duplex structures in other systems, even those as well studied as alumina. At the core of the problem is a basic lack of understanding of the effect of sintering additives and chemical composition on grain shape anisotropy and abnormal grain growth nucleation. This is a critical area for future research in powder-processing science. It is ironic that, after many years of effort, learning how to eliminate elongated-grain growth in *materials such as alumina, now that* we want it, albeit in a controlled fashion, we are not able to predict how to achieve it!

This brings us to the new approach, which is to augment the "clamping" stresses on the bridging grains by increasing the magnitude of the grain-boundary residual stresses. As mentioned earlier, such internal residual stresses often result from thermal expansion anisotropy. In single-phase materials, the magnitude of the stresses generated is limited by the degree of anisotropy, since this determines the maximum possible mismatch in thermal expansion coefficient between neighboring grains. In two-phase materials, however, we can achieve much greater flexibility. Thus, the residual stresses may be enhanced by the addition of a second phase whose thermal expansion coefficient shows the desired degree of mismatch with that of the matrix. The mechanical behavior of such two-phase composites have been studied by several workers.[20-23]

In particular, the effectiveness of this approach in producing increased *R*-curve behavior (and, hence, flaw tolerance) has been successfully demonstrated in several studies. Padture *et al.*[24] showed that the addition of aluminum titanate to alumina results in improved flaw tolerance compared to single-phase alumina. Similar results were obtained in the alumina–mullite system by Stuart *et al.*;[25] i.e., both the addition of mullite

Fig. 2. SEM micrograph of cracks interacting with elongated grains in a high-toughness silicon nitride. Fracture toughness of this material is ~9 MPa·m$^{1/2}$ at a crack size of ~800 μm. (Courtesy C. W. Li.)

to single-phase alumina and of alumina to single-phase mullite gave improved flaw tolerance with respect to the single-phase matrix materials. In particular, the importance of the role of residual stresses in determining *R*-curve behavior was clearly demonstrated in the alumina–anorthite system.[26] In this study, two alumina–anorthite composites were prepared; their microstructures were identical in every respect, except that in one case the intergranular anorthite was crystalline (A-AN(C)), and in the other it was glassy (A-AN(G)). Comparison of the mechanical behavior showed that A-AN(C) exhibited significantly enhanced *R*-curve behavior compared to A-AN(G) (see Fig. 3). This result can be readily explained with respect to the bridging model, because, in the case of A-AN(G), viscous flow of the glassy second phase would be expected to allow the relaxation of the residual stresses. This in turn would reduce the effectiveness of grain bridging.

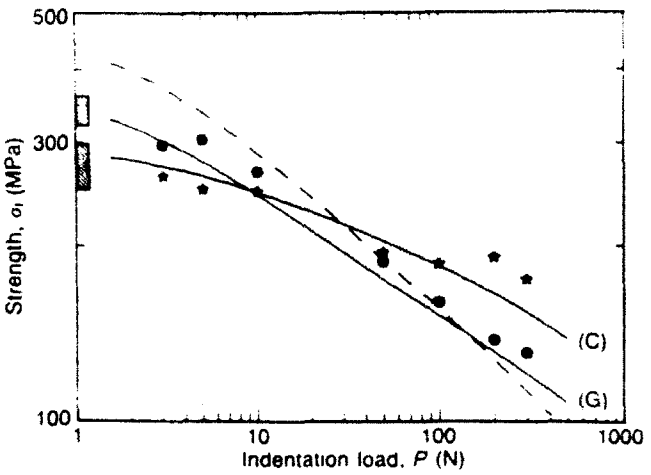

Fig. 3. Strength versus indentation load for alumina containing crystalline (C) and glassy (G) anorthite second phase. Dashed line represents behavior of undoped alumina of equivalent grain size. (Courtesy N. Padture.)

Several groups have shown that, in addition to increasing the level of residual stresses (by the addition of second phases), further enhancement in *R*-curve behavior can be achieved by the deliberate introduction of microstructural inhomogeneities. A processing route developed at Lehigh University that seems to show great promise is the production of a bimodal structure by the addition of spray-dried agglomerates. Another excellent example of the controlled heterogeneity approach is the work by Claussen and co-workers.[27-30] Specifically, Lutz *et al.*[28-30] showed that the incorporation of microstruc-

Panel A. Flaw Tolerance and *R*-Curve Behavior

Comparison of strength–crack size and toughness–crack size relationships for materials exhibiting non-*R*-curve and *R*-curve behavior.

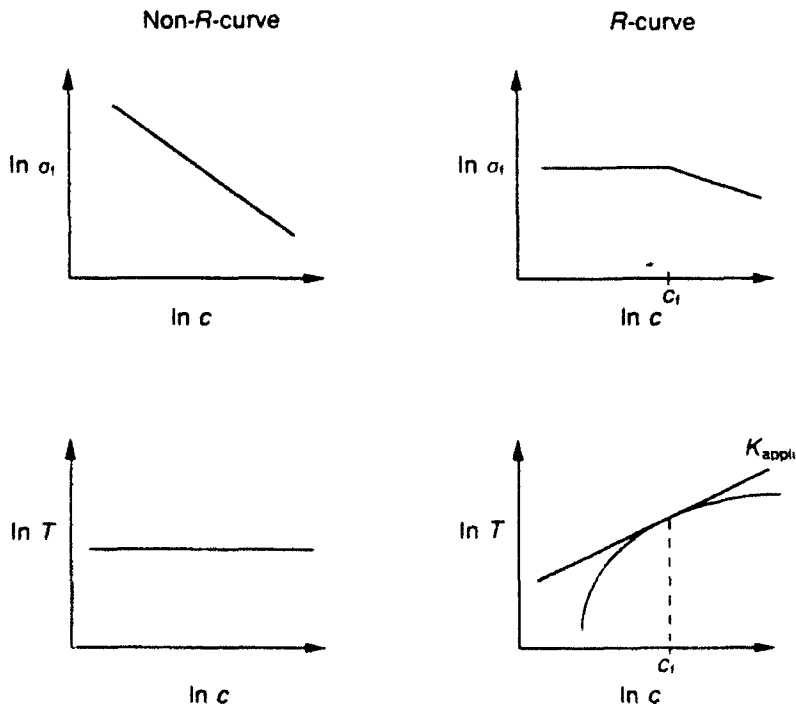

For non-*R*-curve materials, strength decreases with increasing flaw size. *R*-curve materials, however, exhibit a range of crack size over which strength is invariant; i.e., they are "flaw tolerant".

For non-*R*-curve materials, the toughness (T) is a constant, independent of crack size. For *R*-curve materials, the toughness increases with crack size. C_i denotes the crack size below which the fracture stress is constant.

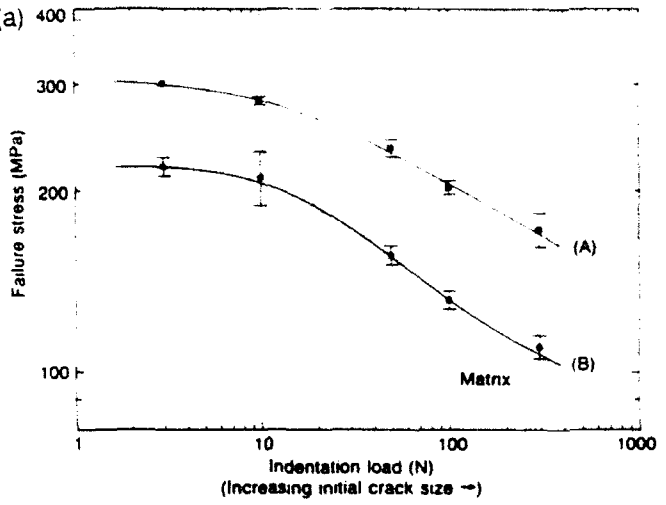

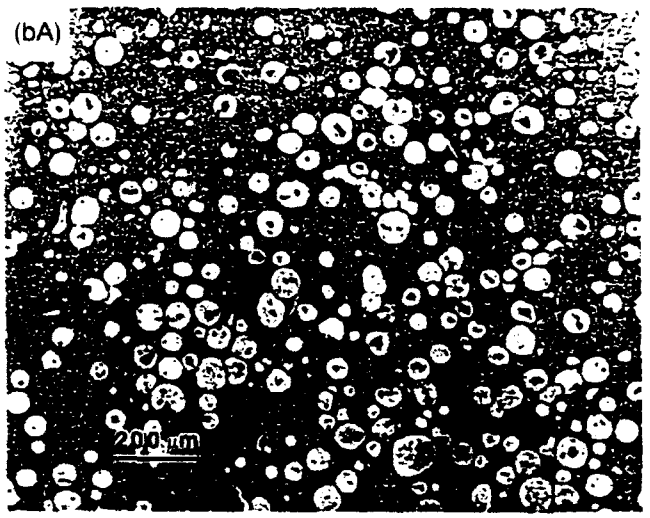

Fig. 4. (a) Strength versus indentation load for (matrix) alumina–56% mullite (AM56); (A) alumina–56 vol% mullite plus 30 vol% alumina agglomerates (AM56 + 30A) and (B) alumina–56 vol% mullite plus 30% mullite agglomerates (AM56 + 30M) (Courtesy M. Stuart.) (b) Optical micrographs of polished and etched (A) AM56 + 30A and (B) AM56 + 30M. Lighter phase is alumina and the darker phase is mullite. (Courtesy M. Stuart.)

tural "pressure" zones (consisting of alumina and monoclinic zirconia) led to increased crack-resistance curves which were markedly improved over that of the matrix alone. These workers studied a wide range of duplex compositions and, using in situ observation techniques, obtained evidence for toughening by microcracking, crack deflection, and crack branching. The form of the R-curve (i.e., short-range or long-range) was found to be dependent on the nature of the dominant toughening mechanism, which in turn was determined by the size and chemical composition of the zones.

Duplex ceramic microstructures have also shown considerable promise in nontransformation-toughened systems: Al_2O_3–c-ZrO_2,[31] Al_2O_3–Al_2TiO_5,[32] and Al_2O_3–$3Al_2O_3 \cdot 2SiO_2$.[33] The indentation–strength data, with the respective microstructures for the alumina–mullite system are illustrated in Fig. 4. The greatest degree of flaw tolerance is shown by the alumina–aluminum titanate composites, which is also the system where the degree of thermal mismatch is the highest. This situation may not always be the most desirable, however, because a very high thermal mismatch can give rise to microcracking if the microstructure is scaled up beyond a certain limit.[32] This illustrates, therefore, the need for microstructural tailoring if optimum properties are to be achieved. In that respect, the alumina–mullite system may be the more optimum choice.

From the processing standpoint, the challenge is to develop more effective methods for controlling the density and dispersion of the heterogeneities, whether in the form of spray-dried agglomerates or by other methods. One problem associated with the quest for enhanced flaw tolerance is that it is usually associated with reduced strength at small flaw sizes. The challenge is to optimize strength in the presence of both small and large flaws. Tape casting of multilayer structures may serve as a means of achieving an optimum microstructure as described in the following section on laminar composites.

(2) *Laminar Composites*

In this section, we describe four examples of the novel use of laminar composites to achieve unique mechanical properties. Other good examples are found in the literature.[34,35]

The first example is a laminar composite designed to exhibit high strength over a large range of flaw sizes. The concept is to fabricate a trilaminate composite consisting of outer layers of a strong material, with a flaw-tolerant inner layer, and to tailor the surface layer thickness to obtain the optimum strength versus flaw size response, as shown schemati-

cally in Fig. 5. The feasibility of this approach has been demonstrated in the alumina–aluminum titanate system. Russo *et al.*[34] used tape casting to fabricate trilaminates with a surface layer consisting of a homogeneous mixture of alumina–20% aluminum titanate (A-AT20), and a more-flaw-tolerant inner layer of inhomogeneous A-AT20. They demonstrated that, at an optimum surface layer thickness (of approximately 100 μm), the high strength of the homogeneous material was maintained at small flaw sizes, and the strength of the inhomogeneous material was preserved at large flaw sizes (see Fig. 6). A fracture mechanics framework for the composite response as a function of the surface layer thickness and bulk properties is under development.[35] The possibility exists to achieve dramatic property improvements in other ceramic systems using this trilaminate approach.

The second example concerns the use of a laminar design to promote toughening in ceria–zirconia (Ce-TZP). Fracture toughness values in the range of 10 to 20 MPa · m$^{1/2}$ have been reported for Ce-TZP that undergoes transformation toughening.[36–39] The transformation zones in these materials tend to extend far ahead of the crack (a distance of 10 to 20 times the zone width). This "runaway" transformation causes the fracture toughness to be much lower than optimum. Marshall[38] estimated that the fracture toughness could be doubled if the transformation zone was restricted to approximately the zone width, which is the case for magnesia-partially-stabilized zirconia. Marshall *et al.*[40] proposed to control the frontal zone in Ce-TZP by introducing obstructive layers of mixtures of 50% alumina and 50% Ce-TZP. They used a colloidal method to fabricate single-layer and multilayer structures with layer thicknesses in the range of 10 to 100 μm. These workers were able to demonstrate that the layers were effective in arresting the transformation. They also showed that the transformation zone spread laterally along the regions adjacent to the layers (Fig. 7). This unexpected lateral spreading of the transformation zone was calculated to result in a further increase in fracture toughness of approximately 50%. Marshall *et al.* predicted that zone spreading and the suppression of the frontal zone could increase the fracture toughness in Ce-TZP laminar composites from 20 to 48 MPa · m$^{1/2}$. They claimed that the potential exists for such composites to exhibit fracture toughnesses substantially higher than observed in any other ceramic material.

The third example exploits weak interfaces deliberately introduced into laminar composites as a means for increasing toughness by deflecting a growing crack. Clegg *et al.*[41] recently demonstrated the feasibility of this approach with laminar composites of silicon carbide and graphite. The composites were made by mixing α-silicon carbide powder (doped with boron) with a concentrated polymer solution in a high-shear mixer. The resulting plastic mass was rolled into 200-μm-thick sheets. After the sheets were dried, they were coated with a graphite layer, laminated, and sintered. The final thicknesses of the silicon carbide and graphite layers were 150 and 8 μm, respectively. Load–deflection curves for the laminated and monolithic materials are shown in Fig. 8. The monolith failed catastrophically, as expected. Its strength, fracture toughness, and work to fracture were computed to be 500 MPa, 3.6 MPa · m$^{1/2}$, and 28 J · m^{-2}, respectively. The laminated material began to fail at the same stress intensity as the monolith; however, its failure was gradual. As soon as the crack reached an interface, it was deflected along it, preventing catastrophic failure (Fig. 9). An apparent fracture toughness for the laminate was calculated from the peak load (which continued to increase after the first layer in the composite fractured) to be 15 MPa · m$^{1/2}$. The work to fracture for the laminated material was calculated from the area under the stress–strain curve to be 4625 J · m^{-2}, which is comparable to that for wood. Thus, laminating the material increased

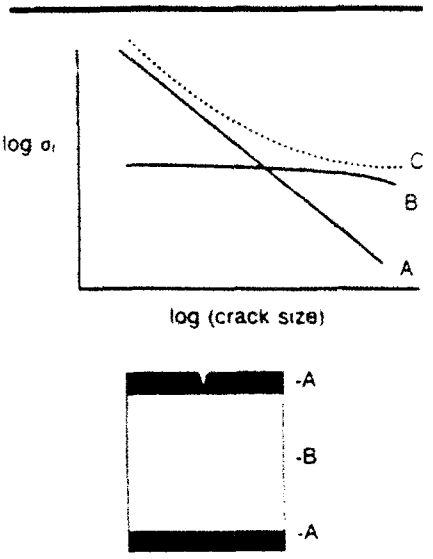

Fig. 5. Schematic diagram illustrating (C) composite response for a trilaminate structure consisting of a (A) strong (flaw-sensitive) surface layer and a (B) flaw-tolerant inner layer

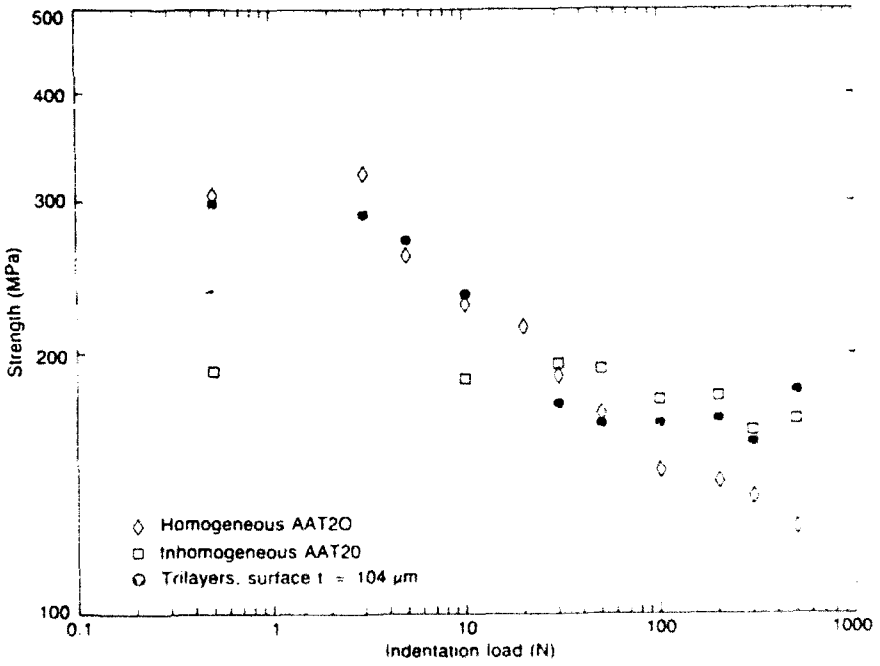

Fig. 6. Indentation strength response of the alumina + 20 vol% aluminum titanate trilayer composites and base materials. Trilayer composites display the high strength of the body material (inhomogeneous) for large flaws, as well as the high strength of the surface layer material (homogeneous) for small flaws. Data points at the extreme left represent breaks from natural flaws (unindented). (Courtesy C. Russo.)

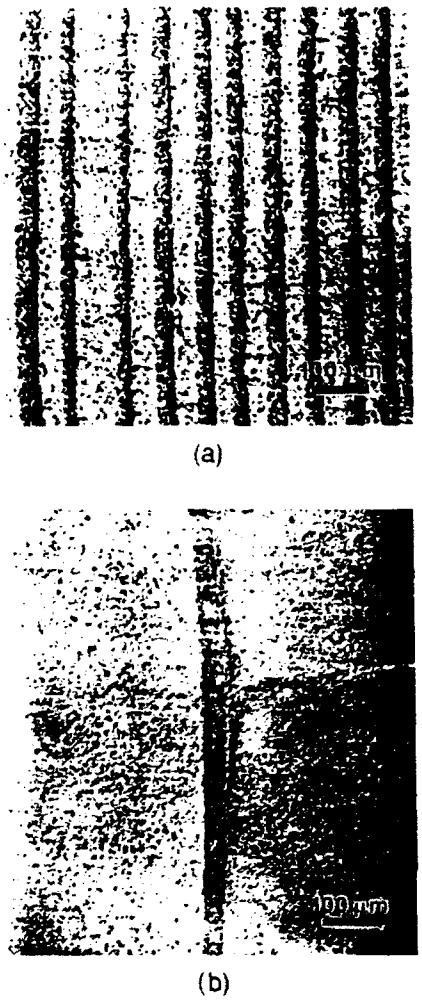

Fig. 7. (a) Optical micrograph of multilayered structure with alternating Ce-TZP and alumina–Ce-TZP layers 35 μm thick. (Courtesy D. B. Marshall.) (b) Crack interacting with alumina–Ce-TZP layer in Ce-TZP producing lateral spreading of transformation zone along the interface. (Courtesy D. B. Marshall.)

the work to fracture by a factor of over 100. Clegg *et al.* point out that their new method is an inexpensive and simple way to make tough ceramics of a variety of shapes.

Halloran *et al.*[42] have developed an alternate method for fabricating unique microstructures of sintered silicon carbide and graphite and other materials. The new approach, originally developed by Coblenz,[43] involves extruding a mixture of powder and binder to form a soft "green fiber." The fiber is then coated with another material (such as graphite in the case of silicon carbide fibers, or aluminum titanate with alumina fibers). The coated fibers are then arranged in the desired architecture (compacted felt or uniaxial) and compacted in a warm press. The green fibers deform during compaction, collapsing the void space between the fibers and laminating the fibers to make a monolithic green body. The green ceramic has a fabric of polycrystalline cells (fiber remnants) and cell boundaries (coating remnants). The green fibrous monolith then undergoes a conventional binder burnout, followed by sintering or hot-pressing at elevated temperatures. The fired microstructure of a silicon carbide–graphite fibrous monolith is shown in Fig. 10. The mechanical properties of a silicon carbide–graphite fibrous monolith have not yet been evaluated. However, this new approach holds promise as a unique and simple way for tailoring the microstructure and mechanical properties of structural ceramics.

In the fourth example, Folsom *et al.*[44] have developed a novel laminar ceramic–polymer composite design applicable to ceramic-matrix composites. The composite consists of dense alumina sheets bonded between sheets of a tough carbon-fiber-reinforced epoxy prepreg material. The fiber-reinforced epoxy layers provide high toughness and flaw tolerance, whereas the ceramic sheets impart high strength, high stiffness, and abrasion resistance. An advantage of this system is its ease of fabrication. For example, Folsom *et al.* bonded together sheets of dense alumina and carbon-fiber-reinforced epoxy at 135°C under an applied compressive stress of 0.35 MPa for 1.5 h. Under these conditions, the epoxy cured and bonded well to the alumina. Figure 11 shows tensile stress–strain curves for a composite containing 18% prepreg and for the prepreg material alone. The stiffness and initial cracking stress are dominated by the ceramic matrix, whereas the notch sensitivity and the toughness (as measured by the area under the stress–strain curve) are far superior to those of the ceramic matrix. The extent to which these materials are flaw tolerant is illustrated by the path taken by a crack propagating from a notch in a compact tension specimen, as shown in Fig. 12. Because of large-scale bridging, the fibers do not fail, therefore, as the crack approaches the compressive side of the specimen, it curls around. Folsom *et al.* suggest that high-temperature laminar composites with similar mechanical characteristics can be fabricated by replacing the prepreg reinforcement with an alternate high-temperature composite, such as a fiber-reinforced glass-ceramic.

(3) Nanoparticle Dispersion Strengthening

Particle dispersion strengthening of ceramic materials is by no means new, and it has been widely exploited in metallic systems. Modest strengthening (up to ~50%) has been observed in certain glass systems reinforced with coarse (>10 μm) ceramic particles[45] and in alumina reinforced with titanium carbide or boron nitride particles <5 μm.[46] The strengthening in such systems has been attributed to a variety of causes, including limiting the size of Griffith flaws, increasing the elastic modulus, and increasing the toughness due to crack–particle interactions.[45,46] Until recently, there have been virtually no studies of the effect of ultrafine (<1 μm) particle dispersions on the strength of ceramics. A group of Japanese scientists led by Professor Niihara at Osaka University has recently reported that the strength of alumina and magnesia, both at room and elevated temperatures, can be dramatically improved by incorporating dispersions of ultrafine (100 to 300 nm) particles of silicon carbide.[47] They term such materials "nanocomposites." In one set of experiments, the room-temperature strength (three-point bending) of hot-pressed alumina (3-μm grain size) was increased from 350 (undoped) to 1000 MPa with the addition of 5 vol% of 0.2-μm silicon carbide particles. Even more impressive was the subsequent increase in strength to 1540 MPa, which occurred following

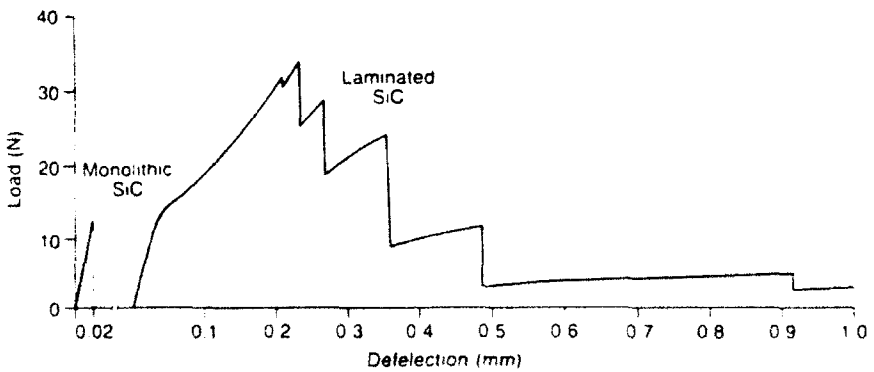

Fig. 8. Load–deflection curves for monolithic silicon carbide and laminated silicon carbide–graphite composites tested as notched specimens in three-point bending. (Courtesy W. J. Clegg.)

an annealing treatment of 2 h at 1350°C in air or argon (see Fig. 13). The aforementioned behavior has subsequently been confirmed by work conducted at Lehigh University,[48] where an identical annealing treatment was observed to result in an improvement in strength of 260 MPa for unindented samples. In addition to improved room-temperature mechanical behavior, Niihara and his coworkers have also demonstrated that the increases in strength achieved by silicon carbide particle additions are maintained at elevated temperatures (see Fig. 14).

To date, the mechanisms responsible for the impressive mechanical properties demonstrated by these novel "nanocomposites" are unknown. Niihara *et al.*[7,47] have suggested that residual stresses around the SiC particles lead to enhanced toughening and strengthening by a crack deflection mechanism. The difference in thermal expansion coefficient between silicon carbide (4.7×10^{-6} K^{-1}) and alumina (8.8×10^{-6} K^{-1}) would result in very high tangential tensile stresses (~2 GPa) in the alumina matrix. There is another school of thought, however, which questions whether the silicon carbide particles actually play a direct role in the reported strengthening. Instead, improvements in room-temperature strength could be argued to be due to improved surface condition and processing of the alumina matrix![48] In this regard, it is perhaps noteworthy that workers at Lehigh University have confirmed strengthening due to silicon carbide particle additions on unindented samples.[48] They observed four-point bend strengths of 560 MPa for undoped, hot-pressed alumina, 760 MPa for hot-pressed alumina and 5 vol% of 0.15-μm silicon carbide (unannealed), and 1000 MPa for hot pressed alumina and 5 vol% of 0.15-μm silicon carbide (annealed 2 h at 1300°C in argon). However, the effect for indented samples has been less dramatic than that reported by Niihara. Measurements of densification and grain growth in this system show that these processes are severely inhibited by the silicon carbide particles (Figs. 15 and 16). Clearly, this question of the role of nanoparticle dispersions in determining mechanical properties is highly complex, and more work is required to resolve this issue.

III. Microstructural Stability at Elevated Temperatures

(1) Grain-Growth Resistance of Interpenetrating Networks

There is a need for materials that can withstand long periods at elevated temperatures without grain growth. For example, in fiber-reinforced ceramic-matrix composites, grain growth within the fiber destroys the effectiveness

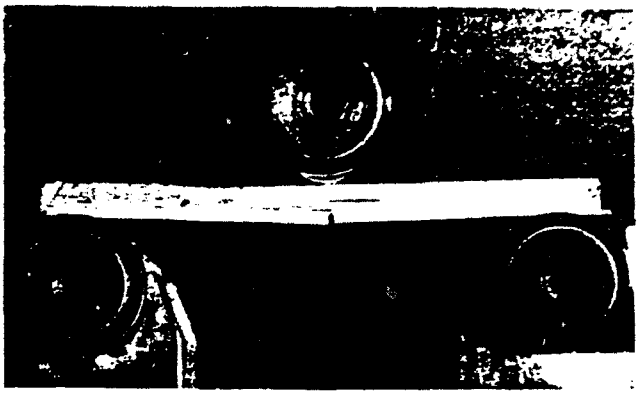

Fig. 9. Laminated bar of silicon carbide–graphite in three-point bend showing delamination along interface. (Courtesy W. J. Clegg.)

Fig. 10. Silicon carbide–graphite fibrous monolith. Light boundaries are graphite layers. (Courtesy J. Halloran.)

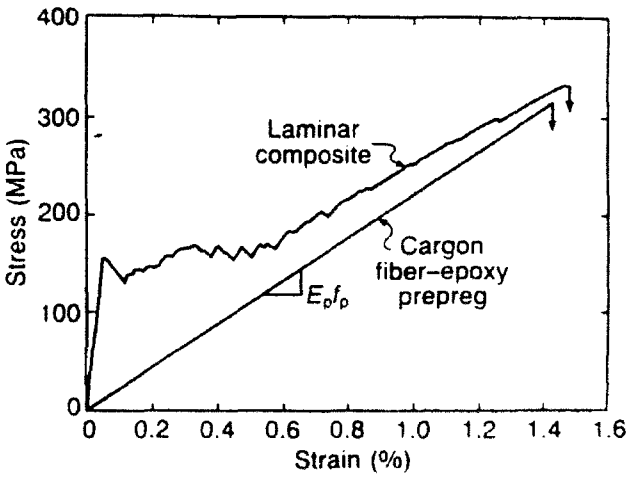

Fig. 11. Tensile stress–strain curve for an alumina–epoxy prepreg laminar composite containing 18% prepreg. (Courtesy C. A. Folsom, F. W. Zok, and F. F. Lange.)

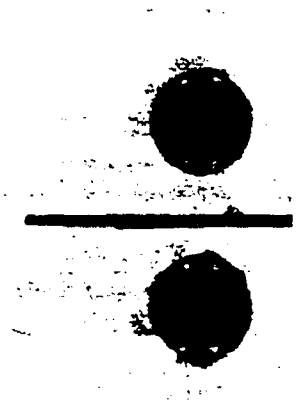

Fig. 12. Crack propagation in an alumina–epoxy prepreg compact tension specimen. Note crack path reversal. (Courtesy C. A. Folsom, F. W. Zok, and F. F. Lange.)

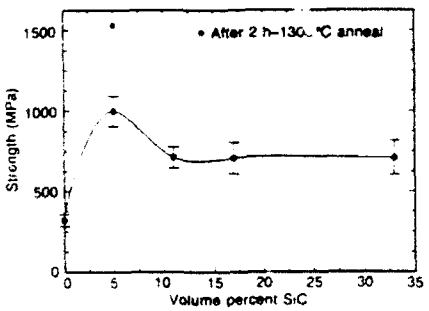

Fig. 13. Fracture strength versus silicon carbide content for alumina–silicon carbide nanocomposites. (Courtesy K. Niihara.)

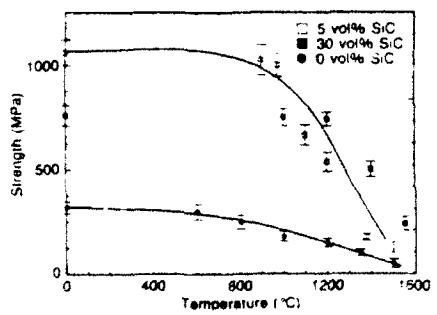

Fig. 14. Fracture strength of alumina–silicon carbide nanocomposites as a function of temperature. (Courtesy K. Niihara.)

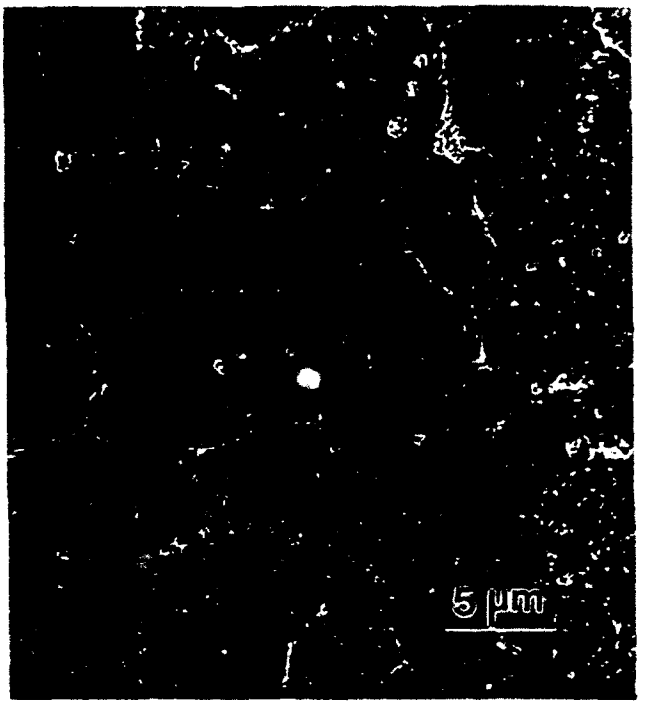

Fig. 15. SEM micrograph of polished and etched alumina and 5 vol% of 0.15-μm silicon carbide particles. Note uniform distribution of fine silicon carbide particles within grains. (Courtesy L. Stearns and J. Zhao.)

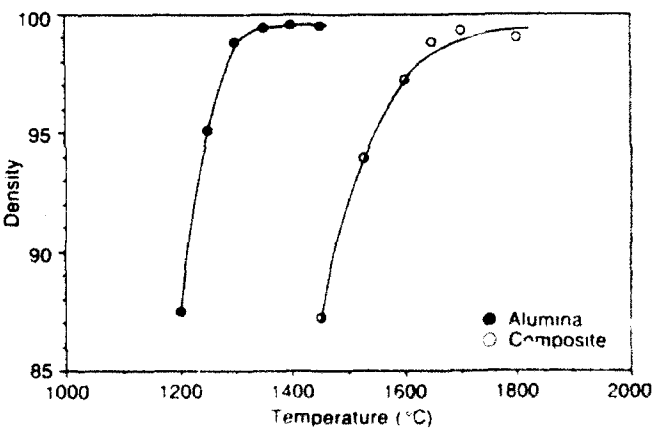

Fig. 16. Density as a function of firing temperature for pure alumina and alumina and 5 vol% of 0.15-μm silicon carbide. (Courtesy L. Stearns and J. Zhao.)

of the reinforcement (see Fig. 17). Conventional approaches for inhibiting grain growth, such as solid-solution additives or minor amounts of a discrete second phase, are limited in their effectiveness.[49] A potentially more useful approach is to develop an interpenetrating mixture of two or more phases.[50] This is demonstrated for the alumina–cubic-zirconia system in Fig. 18, which shows the grain-growth rate constants $K_{Al_2O_3}$ and K_{ZrO_2} for the constituent phases (defined by the equation $d^3 - d_0^3 = Kt$, where d is grain size and t is time) as a function of volume fraction. There is a marked decrease in the grain-growth rates in the region where both phases are interconnected (>20 vol%). The alumina–mullite and alumina–yttrium aluminum garnet (YAG) systems show similar behavior.[14,51] At high volume fractions (>20 vol%), coarsening is expected to be severely inhibited because it is limited by long-range interdiffusion rather than by the single-atom jump distances across a boundary. Also, one might expect more restraint in systems of limited mutual solubility (as in the case for alumina–cubic-zirconia). A model developed for describing simultaneous grain growth of both phases in $\alpha-\beta$ titanium alloys[52] is in reasonable agreement with the observed grain-growth kinetics for alumina–cubic-zirconia. An outstanding question is whether an interpenetrating two-phase mixture is inherently more stable because of the mutual topological constraint of the two phases. Depending on the dihedral angle and the grain coordination around a second-phase grain, a driving force for "anticoarsening" can be set up to drive the structure to an equilibrium of equal-sized grains.[50,53] This results from the case where grains have either negative curvature due to high coordination numbers or low dihedral angle. The latter case is shown schematically in Fig. 19. The experimental verification of the existence of anticoarsening might lead to its exploration for practical applications.

(2) Indentation Creep Resistance of Interpenetrating Networks

Hot hardness and indentation creep[54-58] (the increase in indent size with time under a given load) are convenient measures of the ability of a material to withstand damage under sustained load at high temperature. Examples of the hardness and indentation-creep behavior for fully dense, ~2-μm alumina–cubic-zirconia and alumina–YAG systems are presented in Fig. 20, where AZ50 and AY50 represent the interpenetrating compositions with 50 vol% second phase. The results for these two interpenetrating networks show both similar and dissimilar behaviors.

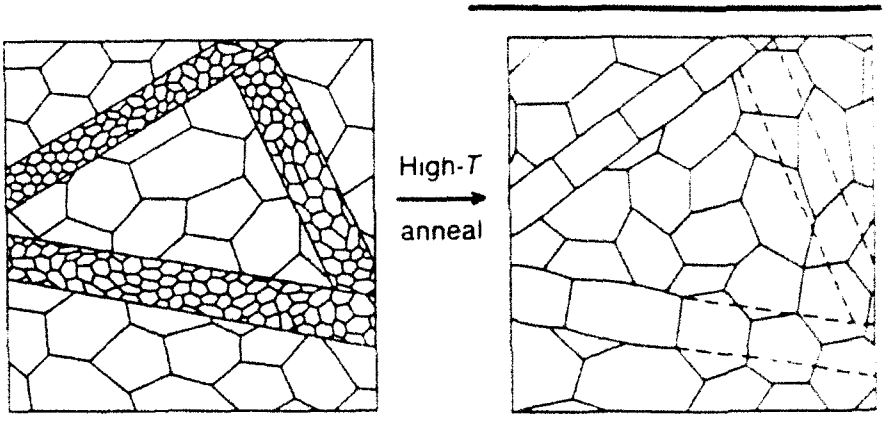

Fig. 17. Schematic diagram to illustrate that grain growth within fiber reinforcement can be detrimental to mechanical properties.

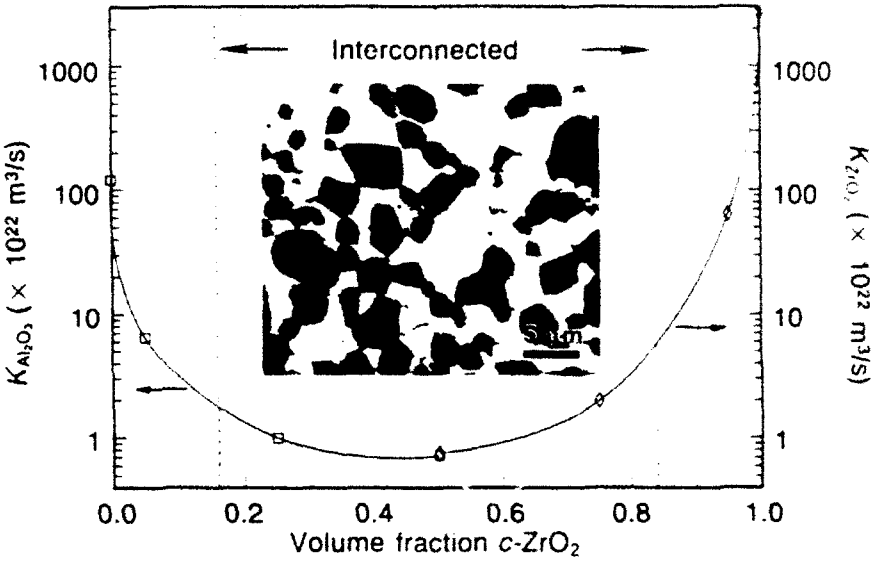

Fig. 18. Influence of an interpenetrating microstructure on the grain-growth rate constants in the alumina–cubic-zirconia system. (Courtesy J. D. French.)

The similarity is that, for both systems, the interpenetrating compositions exhibit a rate of hardness decay which corresponds closely to that of the softer phase. However, the harder phase must play a role, since the composite hardness is greater than that of the softer phase. An interpenetrating network could be more effective under nominally compressive loading than for tensile loading. Uniaxial creep studies are underway to evaluate this possibility.

The dissimilar behavior concerns the relationship between the interpenetrating composition and the harder phase for short and long dwell times. On one hand, for the alumina–YAG system, the interpenetrating composition, AY50, approaches the hardness of YAG at short times (~2 s) but falls at a faster rate than YAG. On the other hand, for the alumina–cubic-zirconia system, the short-time hardness of alumina is significantly higher than for AZ50, but it decays at a

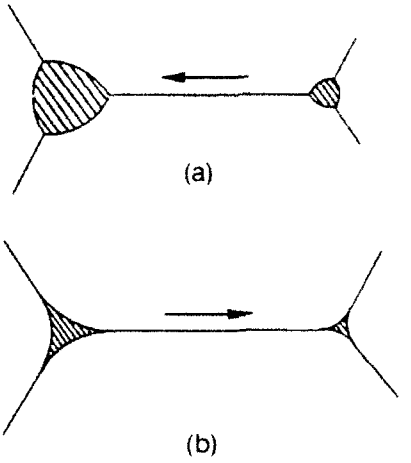

Fig. 19. Illustration of the effect of dihedral angle on the driving force for coarsening: (a) high dihedral angle–classical coarsening and (b) low dihedral angle–anticoarsening.

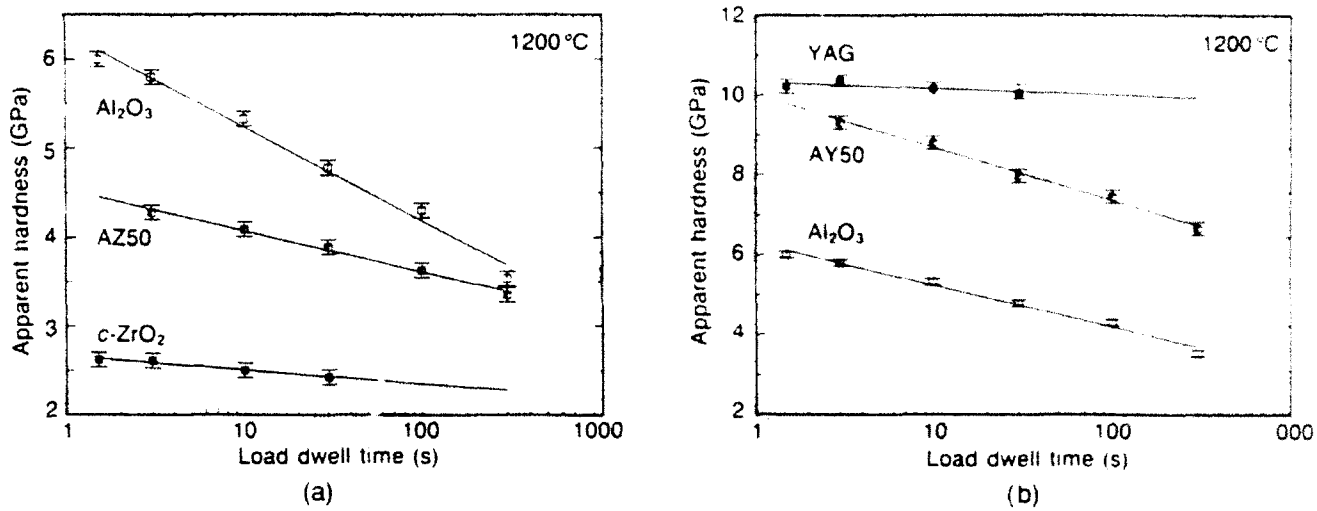

Fig. 20. (a) Indentation creep (apparent hardness versus load dwell time) of AZ50, alumina, and cubic-zirconia. (Courtesy J. D. French.) (b) Indentation creep of AY50, alumina, and YAG. (Courtesy J. D. French.)

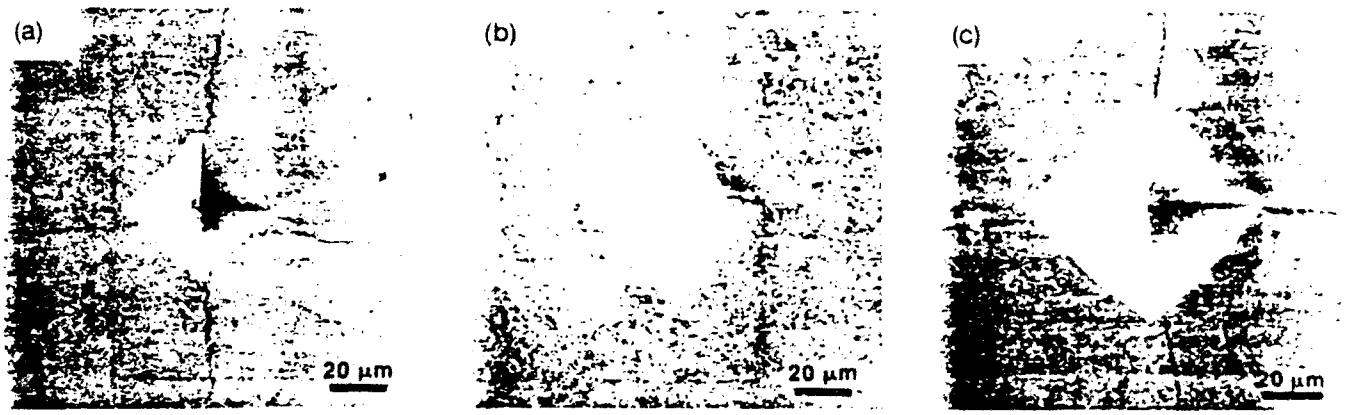

Fig. 21. Indentation sites in (a) alumina, (b) AZ50, and (c) cubic-zirconia indented at 1200°C, 10-N load, and 2 s. Note that the AZ50 material is not cracked, whereas the alumina and cubic-zirconia materials are cracked under similar indentation conditions. (Courtesy J. D. French.)

sufficiently rapid rate that both compositions are nearly equivalent after 300 s. The difference in damage between AZ50, alumina, and cubic-zirconia is apparent from a comparison of the indentation sites for these materials (Fig. 21). In this case, both alumina and cubic-zirconia are cracked after being indented by a 10-N load at 1200°C (dwell time of ~2 s), whereas AZ50 shows no evidence of cracking.

The behaviors of both the alumina–cubic-zirconia and alumina–YAG interpenetrating networks suggest that there could be unique benefits from the use of multiphase networks at high volume fraction. However, the fact that both systems can behave somewhat differently underscores the need for correlating hot hardness and indentation creep with other indexes of high-temperature performance. Thus, parameters, such as rupture life and minimum creep rate, must be evaluated to predict performance in the complex service environment for structural ceramics.

IV. Summary

Some of the more important conclusions of this article are reiterated below.

(1) A design concept for the fabrication of microstructures with controlled heterogeneity and internal residual stress has been developed for producing flaw tolerance in advanced structural ceramics.

(2) Dramatic property improvements have resulted from the designed incorporation of spray-dried agglomerates into two-phase ceramic matrices. This provides a simple and cost-effective fabrication route for ceramics.

(3) Ceramic-processing science does not yet provide first principles capable of predicting how chemical factors affect the development of grain morphology. This is an important topic for future basic research.

Panel B. Microstructural Design

Microstructural design based on the concepts for toughening in nontransforming ceramics.

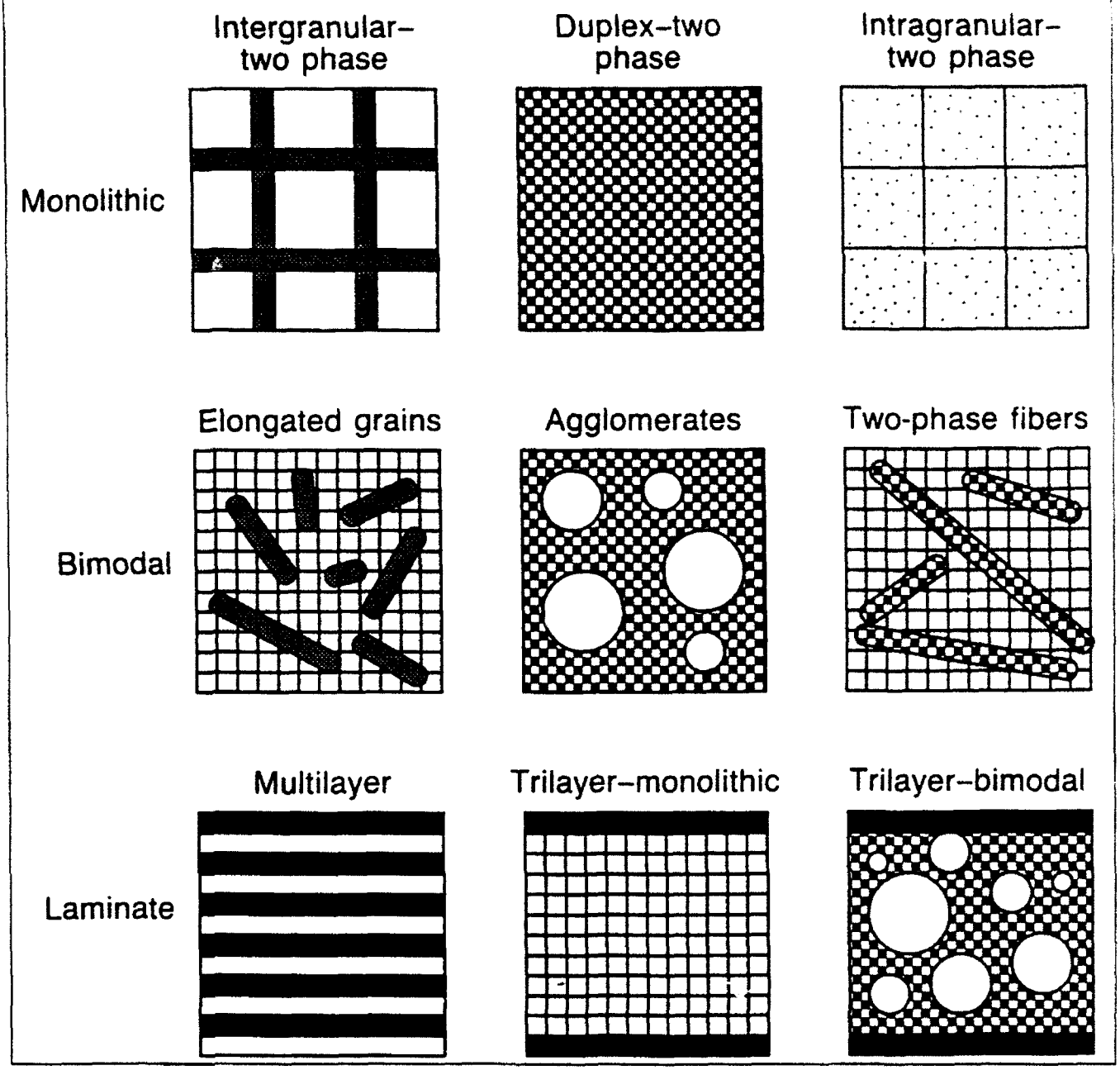

(4) Novel laminar designs are capable of producing ceramics with exceptionally high strength and toughness. Laminar composites should be given serious consideration for engineering ceramic applications.

(5) It has been confirmed that the strength of hot-pressed alumina can be increased dramatically by incorporating a small amount of submicrometer-sized particles of silicon carbide. This so-called "nanocomposite" approach needs to be analyzed further and extended to other ceramic systems.

(6) The high-temperature mechanical properties of alumina–cubic-zirconia and alumina–yttrium aluminum garnet interpenetrating phase networks suggest that there could be unique benefits (in terms of improved resistance to creep and cracking) from the use of multiphase networks at high volume fraction.

Acknowledgments: This work represents part of an ongoing collaborative effort between Lehigh University and the National Institute of Standards and Technology (NIST). Contributions from J. D. French, N. P. Padture, C. J. Russo, M. D. Stuart,

L. Stearns, and J. Zhao at Lehigh University; B. R. Lawn, S. J. Bennison, and S. M. Wiederhorn at NIST; D. B. Marshall at Rockwell Science Center; W. J. Clegg at Cambridge University, U.K.; F. F. Lange at University of California at Santa Barbara; J. Halloran at University of Michigan; K. Niihara at Osaka University, Japan; R. F. Cook at IBM Yorktown Heights; and C. W. Li at Allied-Signal Corp. are gratefully acknowledged.

References

[1]W. H. Rhodes, "Agglomerate and Particle Size Effects on the Sintering of Yttria-Stabilized Zirconia," *J. Am. Ceram. Soc.*, **64**, 19–22 (1981).

[2]*Ceramic Powder Science*, Ceramic Transactions, Vol. 1, Edited by G. L. Messing, E. R. Fuller, and H. Hausner, American Ceramic Society, Westerville, OH, 1988.

[3]F. F. Lange, "Powder Processing Science and Technology for Increased Reliability," *J. Am. Ceram. Soc.*, **72**, 3 (1989).

[4]T. S. Yeh and M. D. Sacks, "Low-Temperature Sintering of Alumina," *J. Am. Ceram. Soc.*, **71**, 841 (1988).

[5]R. F. Cook, B. R. Lawn, and C. J. Fairbanks, "Microstructure–Strength Properties in Ceramics. I. Effect of Crack Size on Toughness," *J. Am. Ceram. Soc.*, **68**, 604 (1985).

[6]S. J. Bennison and B. R. Lawn, "Flaw Tolerance in Ceramics with Rising Crack-Resistance Characteristics," *J. Mater. Sci.*, **24**, 3169 (1989).

[7](a) K. Niihara, "New Design Concept of Structural Ceramics—Ceramic Nanocomposites," *J. Ceram. Soc. Jpn.*, **99** [10] 974 (1991). (b) P. D. Ownby and J. Liu, "Nano-Diamond-Enhanced Silicon Carbide Matrix Composites," *Ceram. Eng. Sci. Proc.*, **12** [7–8] 1345 (1991).

[8]R. Knehans and R. Steinbrech, "Memory Effect of Crack Resistance During Slow Crack Growth in Notched Al_2O_3 Bend Specimens," *J. Mater. Sci. Lett.*, **1**, 327–29 (1982).

[9]P. L. Swanson, C. J. Fairbanks, B. R. Lawn, Y. W. Mai, and B. J. Hockey, "Crack-Interface Grain Bridging as a Fracture Resistance Mechanism in Ceramics: I. Experimental Study on Alumina," *J. Am. Ceram. Soc.*, **4**, 279–89 (1987).

[10]N. Ramachandran and D. K. Shetty, "Rising Crack-Growth-Resistance (*R*-Curve) Behavior of Toughened Alumina and Silicon Nitride," *J. Am. Ceram. Soc.*, **74**, 2634 (1991).

[11]P. Becher, E. R. Fuller, and P. Angelini, "Matrix-Grain-Bridging Contributions to the Toughness of Whisker-Reinforced Ceramics," *J. Am. Ceram. Soc.*, **74**, 2131 (1991).

[12]A. G. Evans, "Perspective on the Development of High-Toughness Ceramics," *J. Am. Ceram. Soc.*, **73**, 187–206 (1990).

[13]P. F. Becher, "Microstructural Design of Toughened Ceramics," *J. Am. Ceram. Soc.*, **74** [2] 255–69 (1991).

[14]F. F. Lange, "Relation between Strength, Fracture Energy, and Microstructure of Hot-Pressed Silicon Nitride," *J. Am. Ceram. Soc.*, **56**, 518–22 (1973).

[15]P. F. Becher, C. M. Hsueh, P. Angelini, and T. N. Tiegs, "Toughening Behavior in Whisker-Reinforced Ceramic-Matrix Composites," *J. Am. Ceram. Soc.*, **71** [12] 1050–61 (1988).

[16]M. M. Lewis, "Microstructural Engineering of Ceramics for High-Temperature Application"; pp. 713–30 in *Fracture Mechanics of Ceramics*, Vol. 7. Edited by R. C. Bradt, A. G. Evans, D. P. H. Hasselman, and F. F. Lange. Plenum, New York, 1986.

[17]S. J. Bennison and B. R. Lawn, "Role of Interfacial Grain-Bridging Sliding Friction in the Crack-Resistance and Strength Properties of Nontransforming Ceramics," *Acta Metall.*, **37**, 2659 (1989).

[18]P. Chantikul, S. J. Bennison, and B. R. Lawn, "Role of Grain Size in the Strength and *R*-Curve Properties of Alumina," *J. Am. Ceram. Soc.*, **73**, 2419 (1990).

[19]C. W. Li and J. Yamanis, "Super-Tough Si$_3$N$_4$ with *R*-Curve Behavior," *Ceram. Eng. Sci. Proc.*, **10**, 632 (1989).

[20]K. T. Faber, T. Iwagoshi, and A. Ghosh, "Toughening by Stress-Induced Microcracking in Two-Phase Ceramics," *J. Am. Ceram. Soc.*, **71** [9] C-399–C-401 (1988).

[21]K. T. Faber, W.-H. Gu, H. Cai, R. A. Winholtz, and D. J. Magley, "Fracture Properties of SiC-Based Particulate Composites"; pp. 3–17 in *Toughening Mechanisms in Quasi-Brittle Materials*. Edited by S. P. Shah. Kluwer Academic Publications, Dordrecht, Netherlands, 1991.

[22]J. Liu and P. D. Ownby, "Enhanced Mechanical Properties of Alumina by Dispersed Titanium Diboride Particulate Inclusions," *J. Am. Ceram. Soc.*, **74** [1] 241–43 (1991).

[23]M. Tava, S. Havashi, A. S. Kobayashi, and H. S. Yoon, "Toughening of a Particulate-Reinforced Ceramic-Matrix Composite by Thermal Residual Stress," *J. Am. Ceram. Soc.*, **73** [5] 1382–91 (1990).

[24](a) N. Padture, S. J. Bennison, J. Runyan, J. Rodel, H. M. Chan, and B. R. Lawn, "Flaw-Tolerant Alumina–Aluminum Titanate Composites"; pp. 715–21 in Ceramic Transactions, Vol. 19, *Advanced Composite Materials*. Edited by K. M. Nair. American Ceramic Society, Westerville, OH, 1991. (b) N. Padture, "Crack Resistance and Strength Properties of Some Alumina-Based Ceramics with Tailored Microstructures", Ph.D. Thesis, Lehigh University, Bethlehem, PA, 1991.

[25](a) M. Stuart, "Characterization and Mechanical Behavior of the Alumina–Mullite System", M.S. Thesis, Lehigh University, Bethlehem, PA, 1991. (b) M. Stuart, M. P. Harmer, H. M. Chan, and G. A. Miller; unpublished work.

[26]N. Padture and H. M. Chan, "Improved Flaw Tolerance in Alumina–1 vol% Anorthite via Crystallization of the Intergranular Glass," *J. Am. Ceram. Soc.*, **75** [7] 1870–75 (1992).

[27]N. Claussen, "Microstructural Design of Zirconia-Toughened Ceramics (ZTC)", pp. 325–51 in Advances of Ceramics, Vol. 12, *Science and Technology of Zirconia II*. Edited by N. Claussen, M. Rühle, and A. H. Heuer. American Ceramic Society, Columbus, OH, 1984.

[28]H. E. Lutz, N. Claussen, and M. V. Swain, "K^R-Curve Behavior of Duplex Ceramics," *J. Am. Ceram. Soc.*, **74** [1] 11–18 (1991).

[29]H. E. Lutz and N. Claussen, "Duplex Ceramics I. Stress Calculations, Fabrication, and Microstructure," *J. Eur. Ceram. Soc.*, **7**, 209–18 (1991).

[30]H. E. Lutz and N. Claussen, "Duplex Ceramics II. Strength and Toughness," *J. Eur. Ceram. Soc.*, **7**, 219–26 (1991).

[31]J. D. French, "Microstructural Evolution and Mechanical Properties in Dual-Phase, Interpenetrating Ceramic Microstructures: The Al_2O_3–*c*-ZrO_2 System", M.S. Thesis, Lehigh University, Bethlehem, PA, 1990.

[32]P. Boch, T. Chartier, and M. Huttepain, "Tape Casting of Al_2O_3/ZrO_2 Laminated Composites," *J. Am. Ceram. Soc.*, **69**, C-191 (1986).

[33]J. J. Hansen, R. A. Cutler, D. K. Shetty, and A. Virkar, "Indentation Fracture Response and Damage Resistance of Al_2O_3–ZrO_2 Composites Strengthened by Transformation-Induced Residual Stresses," *J. Am. Ceram. Soc.*, **71**, C-501 (1988).

[34]C. J. Russo, M. P. Harmer, H. M. Chan, and G. A. Miller, "Design of a Laminated Ceramic Composite for Improved Strength and Toughness", presented at 93rd Annual Meeting of the American Ceramic Society, Cincinnati, OH, May 2, 1991.

(Ceramic Matrix Composites Symposium, Paper No. 110-SVI-91).

[35]C. Russo, M. P. Harmer, H. M. Chan, and G. A. Miller: unpublished work.

[36]R. M. J. Hannink and M. V. Swain, "Metastability of Martensitic Transformation in a 12 mol% Ceria–Zirconia Alloy: Deformation and Fracture Observations," *J. Am. Ceram. Soc.*, **72**, 90 (1989).

[37]C. S. Yu and D. K. Shetty, "Transformation Zone, Shape, Size, and Crack-Growth Resistance (*R*-Curve) Behavior of Ceria-Partially-Stabilized Zirconia Polycrystals," *J. Am. Ceram. Soc.*, **72**, 921–28 (1989).

[38]D. B. Marshall, "Crack Shielding in Ceria-Partially-Stabilized Zirconia," *J. Am. Ceram. Soc.*, **73**, 3119 (1990).

[39]K. E. Tsukuma and M. Shimada, "Strength, Fracture Toughness, and Vickers Hardness of CeO_2-Stabilized Tetragonal Zirconia Polycrystals (Ce-TZP)," *J. Mater. Sci.*, **20**, 1178 (1985).

[40]D. B. Marshall, J. J. Ratto, and F. F. Lange, "Enhanced Fracture Toughness in Layered Microcomposites of Ce-ZrO_2," *J. Am. Ceram. Soc.*, **74**, 2979 (1991).

[41]W. J. Clegg, K. Kendall, N. McN. Alford, T. W. Button, and J. D. Birchall, "A Simple Way to Make Tough Ceramics," *Nature (London)*, **347**, 455–57 (1990).

[42](a) S. D. Nunn, S. Baskaran, D. Popovic, and J. W. Halloran, "Fibrous Monolithic Ceramics", unpublished work. (b) S. D. Nunn and J. W. Halloran, "Microstructural Design for Improved Toughness in Structural Ceramic Materials", presented at the 16th Annual Conference and Exposition on Composites and Advanced Ceramics of the American Ceramic Society, Cocoa Beach, FL, 1992.

[43]W. S. Coblenz, "Fibrous Monolithic Ceramics and Method for Production," U.S. Pat. No. 4 772 524, Sept. 20, 1988.

[44]C. A. Folsom, F. W. Zok, F. F. Lange, and D. B. Marshall, "The Mechanical Behavior of a Laminar Ceramic Composite," *J. Am. Ceram. Soc.*, in press.

[45]I. W. Donald, "Methods for Improving the Mechanical Properties of Oxide Glasses," *J. Mater. Sci.*, **24**, 4177 (1989).

[46]R. W. Rice, "Toughening in Ceramic Particulate and Whisker Composites," *Ceram. Eng. Sci. Proc.*, **11**, 667, 1990.

[47]K. Niihara and A. Nakahira, "Strengthening of Oxide Ceramics by SiC and Si_3N_4 Dispersions", p. 919 in *Ceramic Materials and Components for Engines*. Edited by V. J. Tennery. American Ceramic Society, Westerville, OH, 1989.

[48]J. Zhao, L. Stearns, R. Cook, M. P. Harmer, H. M. Chan, and G. A. Miller, "The Mechanical Properties of Alumina Containing Sub-Micron SiC Particles"; presented at the 94th Annual Meeting of the American Ceramic Society, Minneapolis, MN, April 15, 1992 (Tailoring of Multi-Phase Ceramics for Optimum Mechanical Properties Symposium, Paper No. 38-SX-92).

[49]M. P. Harmer, H. M. Chan, and D. M. Smyth, "Compositional Control of Ceramic Microstructures: An Overview," *Mater. Res. Soc. Symp. Proc.*, **60**, 125 (1986).

[50]J. D. French, M. P. Harmer, H. M. Chan, and G. A. Miller, "Coarsening-Resistant Dual-Phase Interpenetrating Microstructures," *J. Am. Ceram. Soc.*, **73**, 2508 (1990).

[51]J. D. French, H. M. Chan, M. P. Harmer, and G. A. Miller: unpublished work.

[52]G. Grewal and S. Ankem, "Modeling Matrix Grain Growth in the Presence of Growing Second-Phase Particles in Two-Phase Alloys," *Acta Metall. Mater.*, **38**, 1607 (1990).

[53]J. W. Cahn, "Stability, Microstructural Evolution, Grain Growth, and Coarsening in a Two-Dimensional Two-Phase Microstructure," *Acta Metall. Mater.*, **39** [10] 2189–99 (1991).

[54]W. B. Li, J. L. Henshall, R. M. Cooper, and K. E. Easterling, "The Mechanisms of Indentation Creep," *Acta Metall. Mater.*, **39**, 3099 (1991).

[55]J. H. Westbrook and P. J. Jorgensen, "Indentation Creep of Solids," *Trans. Metall. Soc. AIME*, **230**, 425–28 (1965).

[56]A. G. Atkins, A. Silverio, and D. Tabor, "Indentation Hardness and the Creep of Solids," *J. Inst. Met.*, **94**, 369–78 (1966).

[57]W. W. Walker, "Indentation Creep at Low Homologous Temperatures"; pp. 259–73 in *The Science of Hardness Testing and its Research Applications*. Edited by J. W. Westbrook and H. Conrad. American Society for Metals, Metals Park, OH, 1973.

[58]E. C. Yu and J. C. M. Li, "Impression Creep of LiF Single Crystals," *Philos. Mag.*, **36**, 811–25 (1977).

Martin P. Harmer is the Alcoa Professor of Materials Science and Engineering and Director of the Materials Research Center at Lehigh University. His work has been concerned mainly with the science of sintering, microstructure and properties of complex ferroelectric oxides, and tailoring of multiphase ceramics for optimum mechanical properties. Dr. Harmer received his Ph.D. and B.Sc. (first class honors) in ceramics from Leeds University in England. He spent a year at University of California at Berkeley as a visiting research scientist before coming to Lehigh. Dr. Harmer is a former presidential Young Investigator Award winner, a recipient of Lehigh University's 1990 Libsch Award for "outstanding achievement and distinction in research," a member of the American Ceramic Society, and an Associate Editor of the *Journal*. His work has resulted in approximately 90 publications.

Helen M. Chan is an Associate Professor in the Department of Materials Science and Engineering at Lehigh University and Director of the Ceramics Research Laboratory of the Materials Research Center. Her research interests include the study of localized deformation and crack nucleation processes, and the role of microstructure in determining the strength and toughness of ceramic composites. Dr. Chan received her Ph.D. and B.Sc. (first class honors) from Imperial College of Science and Technology (London University). She spent 18 months as a visiting scientist in the Mechanical Properties Group (Ceramics Division) at the National Institute of Science and Technology before joining the faculty at Lehigh. Dr. Chan has received the American Ceramic Society Roland B. Snow award on three separate occasions and, in 1990, was awarded the Lehigh University Alfred Noble Robinson award for "outstanding performance and unusual promise of professional achievement."

Gary A. Miller is Director of the Materials Liaison Program, Associate Director of the Materials Research Center, and Adjunct Professor of Materials Science and Engineering at Lehigh University. His work has been concerned with mechanical behavior and reliability or durability of all types of materials, including steel, solder, polymer composites, and tailored multiphase ceramics. Dr. Miller received S.B., S.M., and Sc.D. degrees from the Massachusetts Institute of Technology. Before coming to Lehigh, he worked at the Homer Research Laboratories of Bethlehem Steel on fatigue and fracture for 19 years. He is a member of Sigma Xi and has published about 40 papers.

Section 1.2

MECHANICAL BEHAVIOR OF Al_2O_3-SiC "NANOCOMPOSITES"

by

J. Zhao, L. C. Stearns, M. P. Harmer, H. M. Chan,
G. A. Miller, and R. F. Cook

Published in Journal of the American Ceramic Society,
Volume 76, page 503 (1993).

Mechanical Behavior of Al_2O_3-SiC "Nanocomposites"

Junhong Zhao, Laura C. Stearns, Martin P. Harmer, Helen M. Chan, and Gary A. Miller, Department of Materials Science and Engineering and The Materials Research Center, Lehigh University, Bethlehem, PA 18015.

Robert F. Cook, IBM Thomas J. Watson Research Center, Yorktown Heights, NY 10598.

Abstract

The fracture behavior of Al_2O_3 containing 5 vol% 0.15 μm SiC particles was investigated using indentation techniques. A significant increase in strength was achieved by the addition of SiC particles to the base Al_2O_3. Specifically, the strength increased from 560 MPa for Al_2O_3 to 760 MPa for the composite samples (average values for unindented hot-pressed bars tested in four-point bending). After annealing for 2 hours at 1300°C, the average strength of the composite samples increased to about 1000 MPa. Toughness was estimated using indentation-strength data. While there was a slight increase in toughness, the increase was not sufficient to account for the increase in the unindented strength on SiC particle addition. It is suggested that the observed strengthening and apparent toughening were due to a machining-induced compressive surface stress. (Key words: Alumina, Silicon Carbide, Strength, Toughness, Nanocomposite.)

1. Introduction

There is a growing interest in a class of materials known as "nanocomposites," in which ceramic matrices are reinforced with

sub-micrometer ceramic particles. Perhaps the most significant results have been reported by Niihara et al. [1-4], where strengths of over 1 GPa were achieved in Al_2O_3 containing 5 vol% 0.3 μm SiC particles. Further, a simple thermal treatment was reported to have increased the strength to over 1.5 GPa [3,4]. The underlying strengthening mechanism, as well as the reason for the enhancement after annealing, at present remain unclear. The toughness of the Al_2O_3 was also shown to increase as a result of the SiC additions, from 3.25 MPa $m^{1/2}$ to 4.70 MPa $m^{1/2}$. While many toughening mechanisms, including crack deflection and microcrack toughening, have been suggested [1-4], the mechanism behind these enhancements is unknown.

In a previous paper [5], we studied the system of Al_2O_3 containing 5 vol% 0.15 μm SiC particles from a processing and microstructural point of view. Preliminary mechanical testing revealed that strengths were quite sensitive to the method used to process the materials (for example, a uniform dispersion of SiC particles in the Al_2O_3 matrix was crucial to the attainment of high strengths). Using the processing techniques found to be successful in that work, we now present more detailed results on the mechanical properties of this system. The motivation behind the present study is to understand the mechanisms behind the strengthening and toughening reported by Niihara et al. [1-4].

In order to assess the mechanical properties as accurately as possible, comprehensive indentation-crack-length and indentation-strength measurements were made. The advantage of these techniques

is that they are able to provide an assessment of the mechanical properties at the correct microstructural length-scale. Also, the combination of these two methods permits strength, toughness, and intrinsic flaw distributions to be estimated separately. The materials tested in the present study were pure Al_2O_3, and Al_2O_3 containing 5 vol% 0.15 μm SiC particles, including samples which had undergone an annealing treatment.

2. Experimental Procedure

2.1 Materials

Ultra high-purity α-Al_2O_3* (99.995%) with a mean particle size of 0.2 μm was used in this investigation and the β-SiC powder** had a mean particle size of 0.15 μm. 5 vol% SiC particles were added to the Al_2O_3 starting powder, and the mixture was ultrasonically dispersed and then ball-milled in methanol. The slurry was slowly dried to produce a powder uniform in color which contained only soft agglomerates (easily broken up with a teflon rod). Powder processing was carried out in a clean room environment. Further details of the processing have been reported in an earlier paper [5].

Specimens were prepared for mechanical testing using two methods; hot-pressing and pressureless sintering. For hot-pressing, the starting powder (Al_2O_3 or Al_2O_3 containing 5 vol% SiC) was calcined in air at 600°C for 10 hours in order to burn out any residual organics from powder processing. It was then placed into a 76.2 mm diameter graphite die which was lined with graphite foil

and a boron nitride coating. The specimens were pressed at 50 MPa in flowing nitrogen, at 1400°C for 30 minutes for Al_2O_3 and 1640°C for 60 minutes for the composite. The top and bottom surfaces of each disc were removed to eliminate any reaction layer, and the discs were machined[5] to produce bars which were approximately 3 mm x 4.4 mm.

For pressureless sintering, disc specimens of the starting powder were uniaxially cold-pressed at 42 MPa, isostatically cold-pressed at 350 MPa, and calcined in air at 600°C for 10 hours. Sintering was conducted in flowing nitrogen at 1450°C for 2 hours for Al_2O_3 and at 1775°C for 4 hours for the composite samples to produce materials of similar density [5]. For calcining and sintering, the discs were surrounded by Al_2O_3 powder (Al_2O_3 specimens) or SiC powder (composite specimens) in a covered Al_2O_3 crucible. The sintered discs were approximately 25 mm in diameter and 2.8 mm thick. Both hot-pressing and pressureless sintering were carried out in a graphite-lined furnace using reducing atmospheres in order to minimize oxidation of the SiC.

All bars and discs were ground flat on one side and were ground and polished to a 6 μm diamond finish on the other side for mechanical testing. These processes were carried out industrially for the bars, while the discs were prepared in the laboratory. The bars were beveled parallel to their lengths in order to eliminate edge flaws. Some bars were annealed in argon at 1300°C for 2 hours before testing in order to test the hypothesis that heat treatment changes the mechanical properties.

For given polishing conditions, the composite specimens (bars or discs) exhibited a higher quality surface finish - even after shorter polishing times - than the Al_2O_3 specimens. Specifically, grain pullout occurred in the Al_2O_3 samples during polishing, while it was not a problem in the composite samples. A possible explanation for the lack of grain pullout (and hence better polished surfaces) in the composites is as follows. The SiC particles altered the morphology of the grain boundaries from straight in pure Al_2O_3 to wavy in the composite. A restraining force generated by the interlocked, wavy boundaries could prevent the easy intergranular fracture required for grain pullout, thereby providing a better, quicker polished surface for the composite.

Density measurements were made using the Archimedes technique with an immersion medium of deionized water plus a wetting agent. For observation by scanning electron microscopy (SEM), the specimens were polished to a 1 μm diamond finish and then thermally etched for 1 hour to reveal the grain structure; 1350°C in air for Al_2O_3 and 1450°C in argon for the composite samples. The grain size was measured using the linear intercept method on polished sections. The average density, ρ, and grain size, G, for each material are given in Table I. The lower density of the sintered composite (SC) (as compared to the sintered Al_2O_3 (SA)) is due to the fact that the SiC particles significantly retard densification of the Al_2O_3 matrix [5], so that although the composites were sintered at a higher temperature, they were still less dense than the sintered Al_2O_3 samples (this was overcome by hot-pressing so

that the hot-pressed composites, HC-A and HC-U, were over 99% dense). Also, the sintered composites exhibited a slightly larger grain size because they were sintered at a higher temperature than the other samples. Specimens for transmission electron microscopy (TEM) were prepared by grinding, dimpling, and ion beam thinning.

Figure 1 shows typical microstructures from polished sections of hot-pressed bars of the Al_2O_3 and the composite. It is apparent from these SEM and TEM micrographs that the SiC particles were well-distributed in the Al_2O_3 matrix, and that they were present at the grain boundaries as well as within the grains. The average inter-particle spacing was calculated to be 0.33 μm. While this may seem an underestimate when looking at the micrographs, it must be remembered that this represents an *average* distance - some of the particles are agglomerated (on a very fine scale), so that many of the particles are spaced much further than 0.33 μm apart. (SEM and TEM observations showed that the microstructures of the sintered discs were very similar to those of the hot-pressed bars of Figure 1).

*Sumitomo AKP-53, Osaka, Japan.

**Performance Ceramics, Co., Peninsula, OH.

$Insaco Inc., Quakertown, PA.

2.2. Mechanical Testing

Indentations were made on the polished faces of the specimens using a Vickers diamond pyramid at peak contact loads in the range

2 to 200 N. The indentations were made in ambient air, and silicone oil was placed immediately on the impression in order to prevent water from reaching the crack tips before strength measurements were made. For strength testing, the indentations were centered on the prospective tensile faces of the specimens.

The pressureless-sintered discs were broken in biaxial flexure using a 2.47 mm radius flat with the specimen loaded on a three-ball support of radius 9.37 mm [6]. The hot-pressed bars were tested in four point bending, using a fixture with an inner span of 12.55 mm and an outer span of 31.80 mm. All testing was performed using a piezoelectric load cell and failure times were less than 20 ms, such that the measured strengths were "inert." All samples were inspected after testing to ensure that failure initiated from the indentation. Unindented samples were also broken in order to assess the intrinsic strength. Strengths were calculated from outer fiber stresses using standard plate and beam theory [7].

Crack lengths for toughness assessment were measured in air using a darkfield technique in an optical microscope [8]. The system included a digital pad which facilitated the precise measurement of the crack lengths. Measurements were made within 15 minutes of indenting.

3. Theory

The indentation impression diagonal is related to the hardness (the supported contact stress) by the following relation:

$$H = P / 2a^2 \qquad (1)$$

where H is the hardness, P is the contact load, and a is the impression semi-diagonal. A $P^{1/2}$ dependence for a, indicating constant hardness, was verified for all materials before applying this relation to the data.

The surface trace of the half-penny crack is related to the toughness, T, by the following expression [9]:

$$T = \xi \ (E/H)^{1/2} \ (P/c^{3/2}) \qquad (2)$$

where E is Young's modulus and c is the crack length, measured from the center of the contact impression. ξ is a material-independent, dimensionless calibration constant which characterizes the geometry of the deformation field. The value assigned to ξ was 0.022 [10,11], rather than 0.016 [9], compensating for the difference in equilibrium crack lengths, and thus toughness, between systems in moist air and inert conditions.

Toughness can also be estimated from indentation-strength data, using the relation [12]:

$$T = \eta \ (E/H)^{1/8} \ (\sigma_m \ P^{1/3})^{3/4} \qquad (3)$$

where σ_m is the inert strength and $\eta = 0.52$ is a material-independent constant calibrated from tests on a range of ceramic materials [13]. The Young's modulus for all Al_2O_3 and composite

samples was taken to be 393 GPa [14], based on the assumption that the 5 vol% of SiC ($E_{SiC} \approx 435$ MPa [14]) particles did not significantly alter the elastic properties.

Similar to the data for hardness determination, the correct power-law dependencies for both the crack lengths and strengths on P (i.e. $c \propto P^{2/3}$ and $\sigma_m \propto P^{-1/3}$ respectively), were ascertained before Equations (2) and (3) were used to estimate toughness.

4. Results

4.1. Indentation Dimensions

Figure 2 shows well-formed 100 N contact impressions in Al_2O_3 and the composite. The surface traces of the cracks emanating from the corners of the impressions are quite straight, indicating very little microstructural interaction. Some lateral cracking was observed at loads of about 100 N and above, as evidenced by the slight surface uplift in Figure 2(a). It should be noted that unannealed hot-pressed Al_2O_3 samples were not tested because these samples showed a high degree of lateral cracking and chipping when indented, thus rendering estimates of ξ and η in Equations (2) and (3) uncertain [15,16]. This effect was not severe for the composite samples so that both unannealed and annealed samples were tested and compared.

Figure 3 (a-e) shows the impression semi-diagonal, a, and the crack length, c, as a function of indentation load, P, for the five materials tested: hot-pressed, annealed Al_2O_3 (HA); hot-pressed, annealed composite (HC-A); hot-pressed, unannealed composite (HC-

U); sintered Al_2O_3 (SA); sintered composite (SC). The symbols snow the means and standard deviations of measurements from at least four indentations at each load. (The error bars for the impression semi-diagonal data are smaller than the symbol size). The solid lines represent best fits to the data in accordance with Equations (1) and (2). The full range of indentation loads was used to fit the data for impression semi-diagonal, but in order to avoid lateral crack effects [15], only the load range 5-20 N was used to fit the crack length data. It was determined that a is proportional to $P^{1/2}$, indicating that the hardness is constant over the full indentation load range. Similarly, a $P^{2/3}$ dependence of c over the full load range was verified, which indicates constant toughness and little lateral crack influence on the half-penny cracks [15]. Table I gives the hardness, H, and $P/c^{3/2}$ parameters for the five materials. Toughness estimates from these $P/c^{3/2}$ values and Equation (2) are slightly lower than previous estimates [1-4].

4.2. Indentation-Strength Data

Figure 4 (a-e) shows the inert strength as a function of indentation load for the five materials. The symbols represent measurements from 4-6 breaks at each load, and the solid lines show best-fit $P^{-1/3}$ responses to the data over the indentation load range 5-20 N, in accordance with Equation (3). At larger indentation loads, the data displayed a tendency to lie above the $P^{-1/3}$ line extrapolated from lower loads, indicating a significant contribution from lateral crack effects [16] (particularly HA, HC-

A, and SC). Also, the 2 N data were omitted from the best fits in order to eliminate any possible effects due to interaction between the indentation cracks and the microstructure [13,17]. The $\sigma_m P^{1/3}$ parameter, representing the best-fit lines, is given in Table I. Using Equation (3), toughness, T, was estimated from these data, and the values are given in Table I. The indentation-strength responses for the SA and HA materials are in excellent agreement with those on similar Al_2O_3 materials with a wide range of grain sizes [17]. No indentation-strength responses have been reported for the composite materials.

The hatched bands in Figure 4 indicate the intrinsic strength levels of the samples. These bands give the standard deviation limits of at least six strength tests for unindented samples, and the strengths, σ_o, are given in Table I. From these data, it is possible to estimate an intrinsic flaw size, c_o, from the load P_o, for the samples using the equations:

$$P_o = \{[\sigma_m P^{1/3}]/\sigma_o\}^3 \quad (4)$$

$$c_o = (P_o/[P/c^{3/2}])^{2/3} \quad (5)$$

$$c_o = (T/\psi\sigma_o)^2 \quad (6)$$

where ψ is a geometrical constant = 1.24 [13]. Equations (5) and (6) are lower and upper bounds to the intrinsic crack lengths with and without residual stress fields, respectively. The P_o values

and crack length bounds are given in Table I. Note that the estimated intrinsic defect sizes (c_o) were larger than the grain sizes.

The σ_o and P_o values for the SA and HA materials in Table I agree with those that can be estimated from the previous Al_2O_3 study [17]. The *trends* of the c_o values for all materials are in agreement with upper bound estimates reported for this system [1,2,4]; a decrease in c_o on addition of SiC, and a further decrease after annealing. The reported numerical values of c_o were in the range 3-28 μm, which agrees with the 5-17 μm range here. However, the use of different toughness estimates (from indentation crack lengths) and crack geometry parameter (ψ - 1.8) precludes further comparison.

Figure 5 shows the fracture surfaces of Al_2O_3 and the composite. The Al_2O_3 exhibited predominantly intergranular fracture [some transgranular was apparent, e.g. the grain in the upper right corner of Figure 5(a)], while the composite showed completely transgranular fracture, similar to previous observation [1,3,4]. It was observed that the cracks circumvented the SiC particles rather than propagating through them, as evident by the many intact particles seen on the fracture surface and the impressions left by particles that are presumably on the matching surface. The significant difference in fracture morphology was not expected from the indentation traces in Figure 2, which showed similar behavior for both materials.

5. Discussion

The results reported here support the contention that small additions of sub-micrometer particles may enhance the mechanical properties of ceramics. However, the wide range of experimental conditions used here revealed two new observations: (1) The composite materials are stronger and tougher than Al_2O_3, but only when the specimens are prepared by hot-pressing. (2) For these hot-pressed composites, the intrinsic strengths increase after annealing, while the apparent toughness decreases. Based on these observations, the following develops a hypothesis for the mechanism underlying the enhancement of the fracture properties.

The data in Table I show that it is possible to achieve apparent toughening in this system. This toughening was only observed for the hot-pressed composite which was unannealed (HC-U), although the annealed composite (HC-A) did show some toughening compared to the other three materials (HA, SA, and SC). These latter three materials all showed similar toughness values. This implies that the increased toughness of the hot-pressed composite samples over the sintered composite samples derived from the way in which these samples were treated, rather than from the hot-pressing *per se* (otherwise the SA and HA materials would also show a difference in toughness). The only difference in specimen preparation between the the hot-pressed and sintered materials was that the test surfaces of the hot-pressed bars were industrially ground, while the test surfaces of the sintered discs were hand-

ground in the laboratory.

It is likely that this machining operation introduced significant compressive surface stress into the hot-pressed materials to a depth of tens of micrometers [18,19]. Such surface treatments have been observed to cause apparent toughening in other systems [10,20], and we hypothesize that a similar toughening mechanism is acting in this case. The unannealed composite material (HC-U) contained the largest compressive surface stress (it exhibited the highest toughness), and although this stress was diminished on annealing (HC-A), there was still some toughening over the other materials. The lower toughness of the HA material resulted from the complete removal of residual stress during annealing. This difference in extent of surface stress removal during annealing is explained as follows. Stress relief relies on the same bulk and grain boundary diffusional processes that control densification. It has previously been observed [5] that these fine SiC particles significantly retard densification in Al_2O_3, and therefore it follows that surface stress relief would also be more difficult in the composite material. Thus, only partial stress relaxation occurs, and some apparent toughening results in the composite materials.

Strength depends on both material toughness and the dominant flaw size in a specimen. The similar strengths of the HA, SA, and SC materials, along with the similar toughnesses, suggest that the dominant intrinsic flaws in the specimens were similar, although representing extremes of different flaw-size distributions. Figure

6 is a schematic of the flaw-size distributions assumed to exist in the various samples, consistent with the strength data. The sintered materials have broad flaw-size distributions dominated by remnant porosity from the sintering process. The HA material has a narrow distribution, associated with machining and polishing damage, although the largest flaw coincides with the largest flaw of the sintered materials. This is consistent with the observation that the polished surfaces of the hot-pressed Al_2O_3 samples were inferior to those of the composite samples.

Although the toughnesses of the HC-A and HC-U materials were larger than the other three materials, the increases were not consistent with the increases in intrinsic strength. For example, the highest strengths were observed in the HC-A material, which only exhibited intermediate toughness. This inconsistency can be resolved by assuming a flaw-size distribution with a smaller mean for the HC-U material, which is further reduced on annealing, as shown in Figure 6. A consequence of using an annealing temperature which is sufficient to allow stress relief (by bulk and grain boundary diffusion) is that significant surface diffusion will occur to heal any surface flaws. It is also possible, of course, that the compressive surface stress may aid in the driving force for surface rearrangement. These hypotheses are summarized in Figure 7; annealing the ground specimens has the double effect of diminishing the compressive surface layer while also healing the surface flaws. The indentation strengths are an indication of the material toughness, which is dependent on the surface stress.

Thus, the indented strengths decrease on annealing. The intrinsic strengths are a reflection of both the toughness and the flaw-size distributions. The intrinsic strengths increase on annealing because the reduction in intrinsic flaw size more than compensates for the decrease in toughness.

In light of the previous discussion, in which the apparent toughening derives from compressive stress incorporation, the fracture mode change seen in Figure 5 is quite surprising. Usually such dramatic changes in fracture morphology are associated with significant differences in mechanical properties, especially toughness [21,22]. Clearly the addition of the SiC particles forced a transgranular mode in the composite, which would normally correspond to an increase in toughness. The large thermal expansion mismatch between the SiC particles ($\alpha \approx 4.7 \times 10^{-6}$ /°C) and the Al_2O_3 matrix ($\alpha \approx 8.8 \times 10^{-6}$ /°C) is expected to have created regions of tension between the particles. A crack path which follows these regions of tension would give rise to a material of lower toughness [23]. However, in this case, this decrease in toughness is compensated by the increase in toughness resulting from the transgranular fracture path. Thus, while the fracture mode completely changes, there was no net significant difference in the toughness.

A partial explanation for early belief [1-4] that the observed strengthening was a material effect lies in the fact that previous discussions were based on microstructural toughening arguments derived from indentation crack length measurements alone. The

$P/c^{3/2}$ data in Table I show a factor of two increase in apparent toughness from HA to HC-U, which is not consistent with either the indentation-strength data or the intrinsic strength measurements. Thus, the use of the indentation-crack length technique exclusively in the assessment of toughness can be misleading. Estimation of toughness using the strength-indentation method is less misleading for the following reasons. First, indentation crack lengths increase with time after indentation in reactive environments (i.e. moist air). Hence, the apparent toughness will vary accordingly, even if the calibration constant for that environment is known. Second, the measured inert strength is less dependent on the details of the elastic-plastic indentation contact (quantified by the model-dependent geometry paramter χ) than is the indentation crack length (i.e. $\sigma \propto \chi^{-1/3}$ while $c_o \propto \chi^{2/3}$).

A clear implication of this work is that surface stresses introduced by machining may be extremely effective in producing strong and tough materials. Experiments to test this hypothesis would include explicit measurement of surface stresses introduced by various machining processes and the precise effect of annealing on both stress relaxation and surface flaw populations. An area for future development is materials which possess the following three special characteristics: (1) easily fabricated (i.e. pressureless sintering) (2) susceptible to the generation of large compressive stresses on machining (3) can be annealed to reduce surface flaws without diminishing the compressive surface stress.

6. Conclusions

(1) It is possible to obtain high strengths in Al_2O_3-SiC composites, but only for samples which have been surface-ground and then annealed.

(2) The strengthening and toughening observed in these samples are believed to derive almost exclusively from compressive surface stresses introduced by the grinding process. The addition of the SiC particles does **not** affect the intrinsic material toughness.

(3) Annealing the composite specimens has the double effect of diminishing the compressive surface stress while also healing the surface flaws.

(4) This study reinforces the need to consider all aspects of the fracture process, including toughness, strength, and intrinsic flaw distributions, before deducing any mechanism for an observed strength response.

Acknowledgements

The authors are grateful to S. J. Bennison for assistance in preparation of the hot-pressed samples and for helpful discussions. This research was supported by the Air Force Office of Scientific Research under contract AFOSR-87-0396 and the National Science Foundation under grant DMR-8821686.

Table I. Indentation parameters of the Al_2O_3 and Al_2O_3 - SiC materials.

Parameter	Material				
	HA	HC-A	HC-U	SA	SC
ρ (%)	99.5	99.9	99.9	99 .3	98.3
G (μm)	4.8	4.2	4.2	3.2	5.4
H (GPa)	19.1 ± 2.2	20.4 ± 1.2	21.2 ± 1.3	20.3 ± 1.0	19.2 ± 0.9
$P/c^{3/2}$ (MPa $m^{1/2}$)	22 ± 3	31 ± 3	43 ± 5	41 ± 4	31 ± 4
$\sigma_m P^{1/3}$ (MPa $N^{1/3}$)	591 ± 24	703 ± 23	810 ± 37	611 ± 19	545 ±17
T (MPa $m^{1/2}$)	2.9 ± 0.1	3.3 ± 0.1	3.6 ± 0.1	2.9 ± 0.1	2.7 ± 0.1
σ_o (MPa)	559 ± 51	1001 ±102	760 ± 28	569 ± 72	586 ± 72
P_o (N)	1.18 ± 0.35	0.35 ± 0.11	1.21 ± 0.21	1.24 ± 0.48	0.80 ± 0.31
c_o (μm)	14.0 - 17.3	5.0 - 6.9	9.3 -14.7	9.7 -17.2	8.7 -13.9

References

[1]. K. Niihara and A. Nakahira, "Strengthening of Oxide Ceramics by SiC and Si_3N_4 Dispersions," pp. 919-926 in Proceedings of the Third International Symposium on Ceramic Materials & Components for Engines, The American Ceramic Society, Westerville, OH (1988).

[2]. K. Niihara, A. Nakahira, G. Sasaki, and M. Hirabayashi, "Development of Strong Al_2O_3/SiC Composites," pp. 124-134 in Proceedings of the International Meeting on Advanced Materials, Vol. 4, The Materials Research Society, Japan (1989).

[3]. K. Niihara and A. Nakahira, "Particulate Strengthened Oxide Nanocomposites," pp. 637-664 in Advanced Structural Inorganic Composites, Edited by P. Vincenzini, Elsevier Sci. Pub. (1990).

[4]. K. Niihara, "New Design Concept of Structural Ceramics-Ceramic Nanocomposites," The Centennial Issue of the Ceramic Society of Japan, **99** [10] 974-982 (1991).

[5]. L. C. Stearns, J. Zhao, and M. P. Harmer, "Processing and Microstructure Development in Al_2O_3-SiC 'Nanocomposites'," in press.

[6]. D. B. Marshall, "An Improved Biaxial Flexure Test for Ceramics," Am. Ceram. Soc. Bull., **59** [5] 551-553 (1980).

[7]. R. J. Roark and W. C. Young, Formulas for Stress and Strain, 5th Edition, McGraw-Hill, Japan (1983).

[8]. D. Johnson-Walls, M. D. Drory, A. G. Evans, D. B. Marshall, and K. T. Faber, "Evaluation of Reliability of Brittle Components by Thermal Stress Testing," J. Am. Ceram. Soc., **68** [7] 363-367 (1985).

[9]. G. R. Anstis, P. Chantikul, B. R. Lawn, and D. B. Marshall, "A Critical Evaluation of Indentation Techniques for Measuring Fracture Toughness: I, Direct Crack Measurements," J. Am. Ceram. Soc., **64** [9] 533-538 (1981).

[10]. R. F. Cook, Strength Characterisation of Ceramics Using Controlled Indentation Flaws, Ph. D. Thesis, University of New South Wales, Australia (1985).

[11]. R. F. Cook, "Influence of Crack Velocity Thresholds on Stabilized Nonequilibrium Fracture," J. Appl. Phys., **65** [5] 1902-1910 (1989).

[12]. P. Chantikul, G. R. Anstis, B. R. Lawn, and D. B. Marshall, "A Critical Evaluation of Indentation Techniques for Measuring Fracture Toughness: II, Strength Method," J. Am. Ceram. Soc., **64**

[9] 539-543 (1981).

[13]. R. F. Cook, C. J. Fairbanks, B. R. Lawn, and Y-W. Mai, "Crack Resistance by Interfacial Bridging: Its Role in Determining Strength Characteristics," J. Mater. Res., **2** [3] 345-355 (1987).

[14]. R. F. Cook and G. M. Pharr, "Mechanical Properties of Ceramics" in Materials Science and Technology, Edited by R. W. Cahn, T. Haasen, and E. G. Kramer, V. C. H. Publishers, Germany, in press.

[15]. R. F. Cook, M. R. Pascucci, and W. H. Rhodes, "Lateral Cracks and Microstructural Effects in the Indentation Fracture of Yttria," J. Am. Ceram. Soc., **73** [7] 1873-1878 (1990).

[16]. R. F. Cook and D. H. Roach, "The Effect of Lateral Crack Growth on the Strength of Contact Flaws in Brittle Materials," J. Mater. Res. **1** [4] 589-600 (1986).

[17]. P. Chantikul, S. J. Bennison, and B. R. Lawn, "Role of Grain Size in the Strength and R-curve Properties of Alumina," J. Am. Ceram. Soc., **73** [8] 2419-2427 (1990).

[18]. J. Lankford and D. L. Davidson, "Characterization of Surface Damage in Ceramics Using Selected Area Electron Channeling," pp. 395-405 in The Science of Ceramic Machining and Surface Finishing II, Edited by B. J. Hockey and R. W. Rice, U.S. Government Printing Office, Washington, D.C. (1979).

[19]. F. F. Lange, M. R. James, and D. J. Green, "Determination of Residual Surface Stresses Caused by Grinding in Polycrystalline Al_2O_3," J. Am. Ceram. Soc., [2] C-16-C-17 (1983).

[20]. R. F. Cook, B. R. Lawn, T. P. Dabbs, and P. Chantikul, "Effect of Machining Damage on the Strength of a Glass-Ceramic," J. Am. Ceram. Soc., **64** [9] C-121-C122 (1981).

[21]. R. L. Stewart, M. Iwasa, and R. C. Bradt, "Room-Temperature K_{Ic} Values for Single-Crystal and Polycrystalline $MgAl_2O_4$," J. Am. Ceram. Soc., **64** [2] C-22-C-23 (1981).

[22]. R. F. Cook, "Segregation Effects in the Fracture of Brittle Materials: Ca-Al_2O_3," Acta Metall. Mater., **38** [6] 1083-1100 (1990).

[23]. S. J. Bennison and B. R. Lawn, "Role of Interfacial Grain-Bridging Sliding Friction in the Crack-Resistance and Strength Properties of Nontransforming Ceramics," Acta Metall., **37** [10] 2659-2671 (1989).

Figure Captions

Figure 1. (a) SEM micrograph showing polished section of Al_2O_3. (b) SEM micrograph showing polished section of Al_2O_3 containing 5 vol% SiC particles. Arrow indicates SiC particles. Note the wavy nature of the grain boundaries in the composite. (c) TEM micrograph showing the distribution of SiC particles on the Al_2O_3 grain boundaries as well as in the grains. Arrows indicate SiC particles.

Figure 2. Optical micrographs showing 100 N contact impressions in sintered discs of (a) Al_2O_3 and (b) composite.

Figure 3. Crack length, c, and indentation semi-diagonal, a, as a function of indentation load, P, for the five materials tested; (a) Al_2O_3, (b) annealed composite, (c) unannealed composite, (d) sintered Al_2O_3, and (e) sintered composite.

Figure 4. Inert strength, σ_m, as a function of indentation load, P, for the five materials tested; (a) Al_2O_3, (b) annealed composite, (c) unannealed composite, (d) sintered Al_2O_3, and (e) sintered composite.

Figure 5. SEM micrographs showing the fracture surfaces of (a) Al_2O_3 and (b) composite.

Figure 6. Schematic diagram of flaw probability vs. flaw size for the five materials tested, showing the flaw size distributions proposed to exist based on the strength data.

Figure 7. Plot of inert strength, σ_m, as a function of indentation load, P, for hot-pressed, annealed composite (HCA) and hot-pressed unannealed composite (HCU). The schematic drawings show the hypothesized effect of annealing on the specimen surface; the residual stress layer is diminished while the defect size is also reduced.

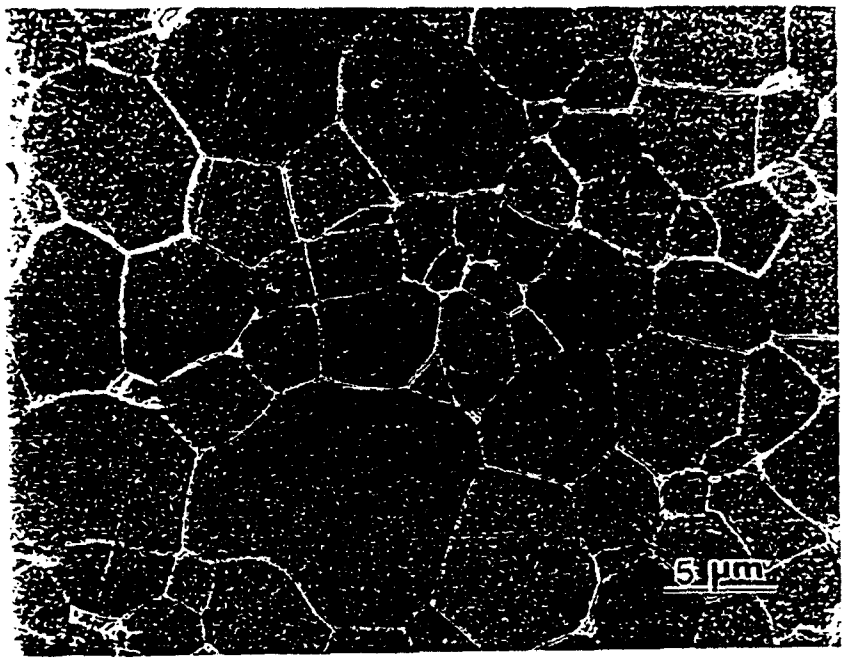

(a)

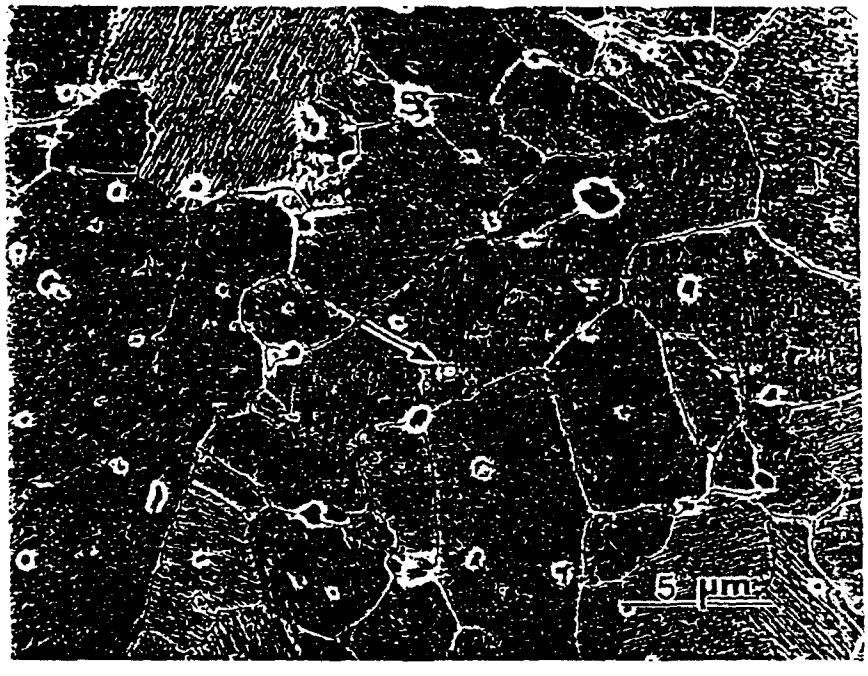

(b)

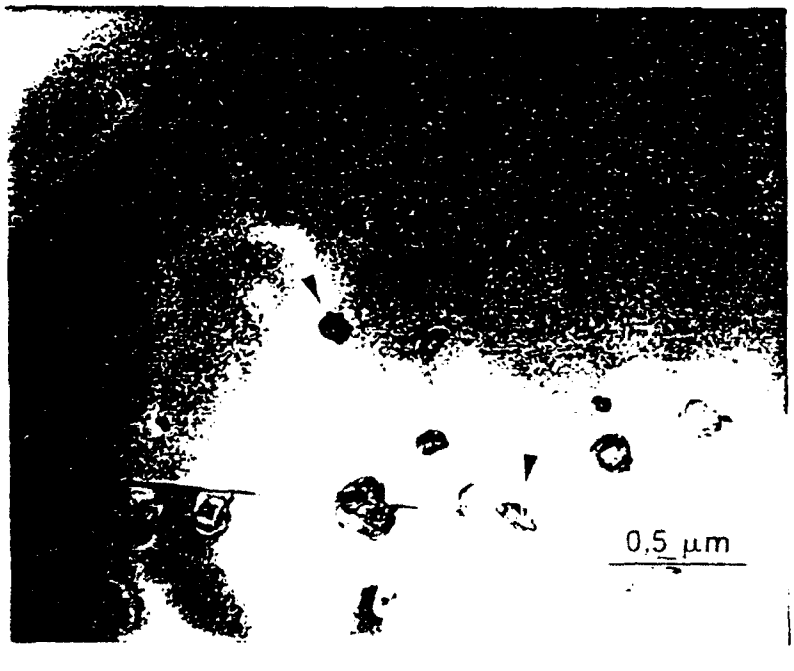

(c)

Fig 1

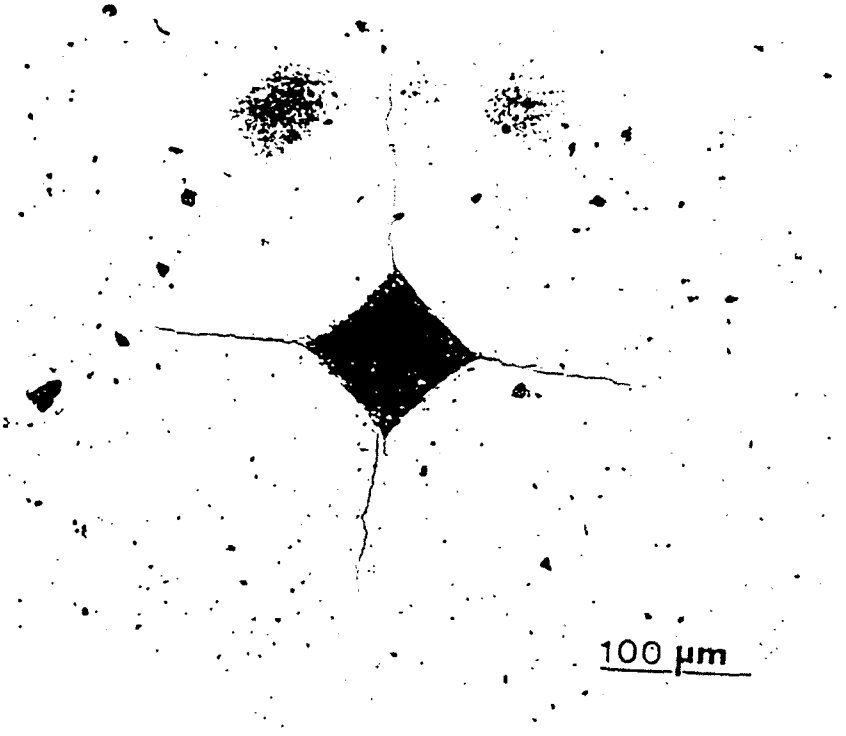

(a)

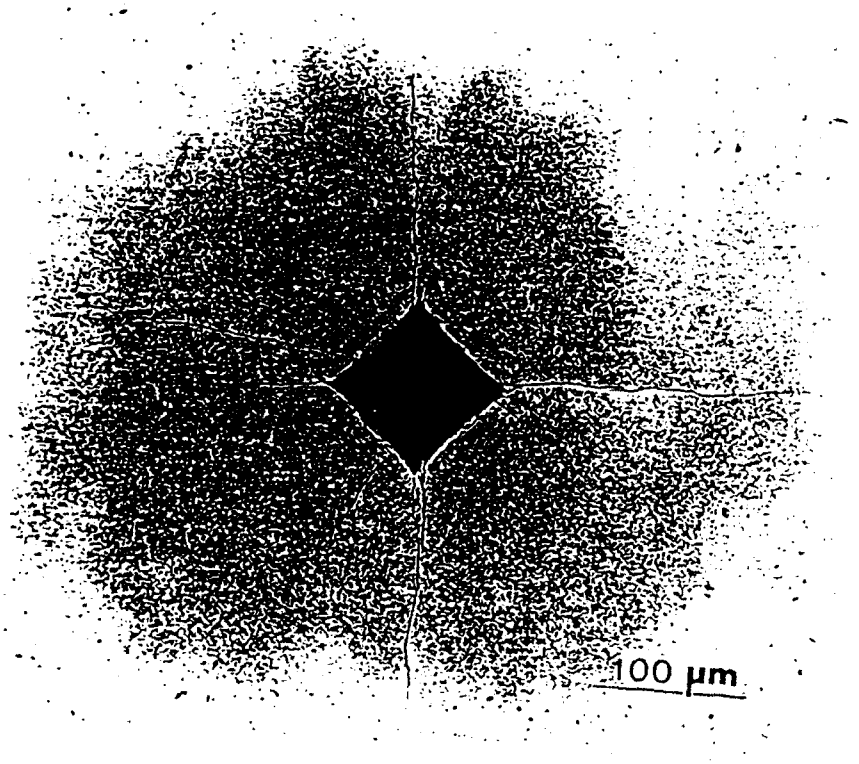

(b)

Fig. 2

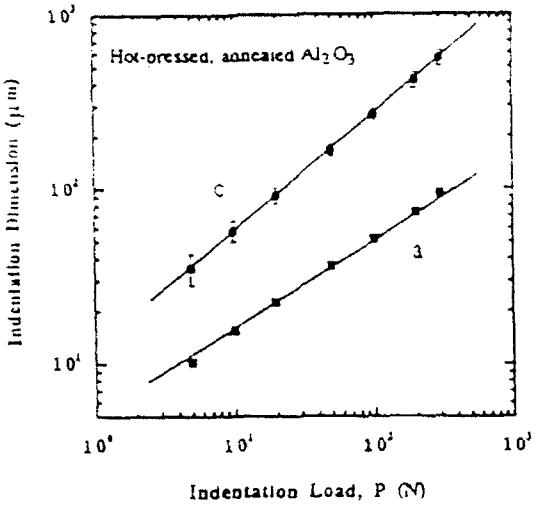
Hot-pressed, annealed Al_2O_3
Indentation Dimension (μm)
Indentation Load, P (N)
c
a

(a)

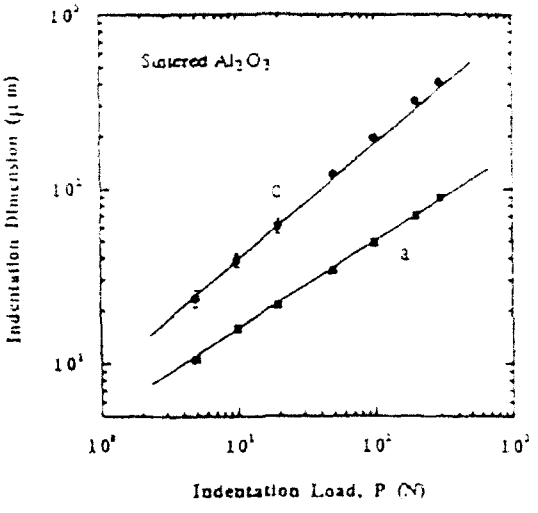
Sintered Al_2O_3
Indentation Dimension (μm)
Indentation Load, P (N)
c
a

(d)

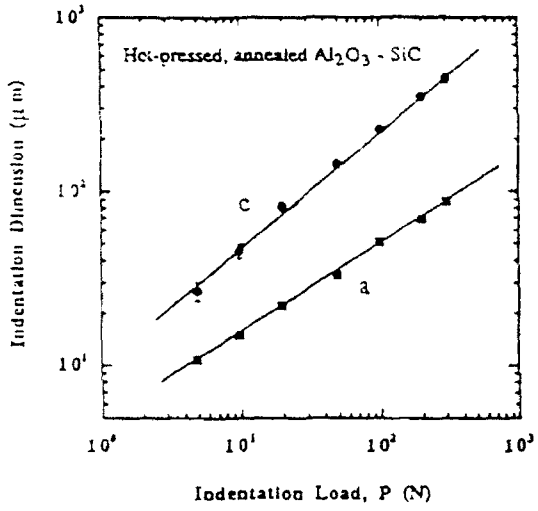
Hot-pressed, annealed Al_2O_3 - SiC
Indentation Dimension (μm)
Indentation Load, P (N)
c
a

(b)

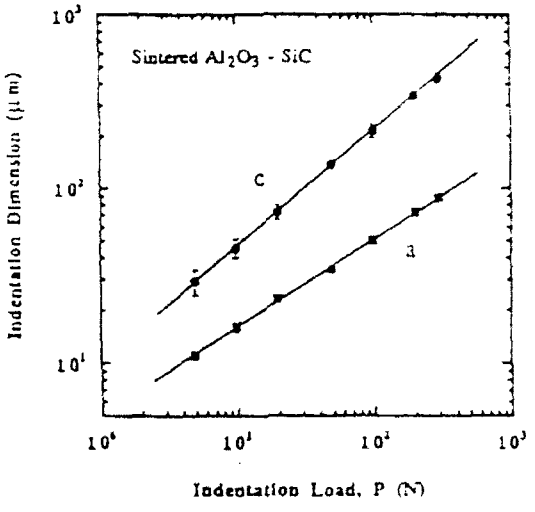
Sintered Al_2O_3 - SiC
Indentation Dimension (μm)
Indentation Load, P (N)
c
a

(e)

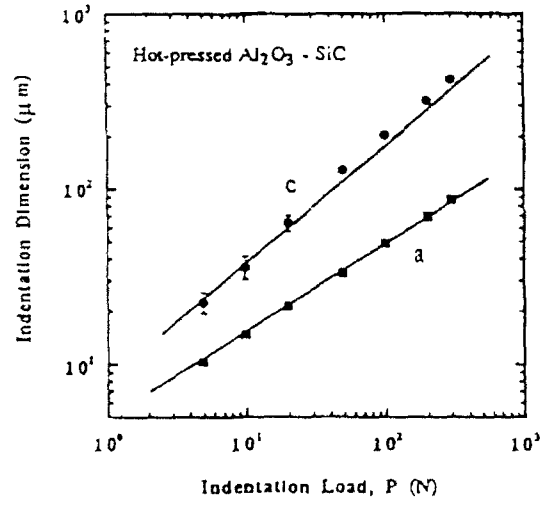
Hot-pressed Al_2O_3 - SiC
Indentation Dimension (μm)
Indentation Load, P (N)
c
a

(c)

Fig 3

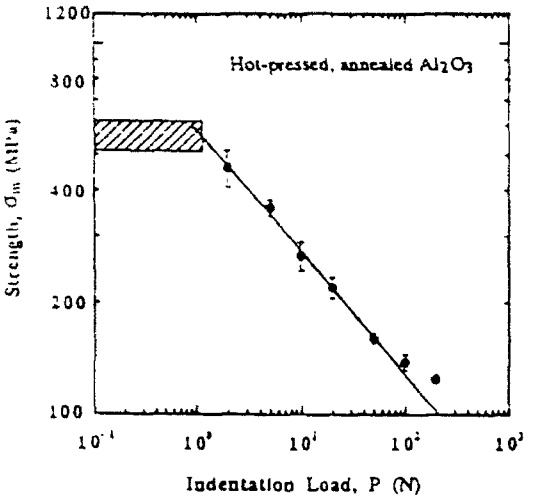
Hot-pressed, annealed Al_2O_3
Strength, σ_m (MPa)
1200
800
400
200
100
10^{-1}
10^{0}
10^{1}
10^{2}
10^{3}
Indentation Load, P (N)

(a)

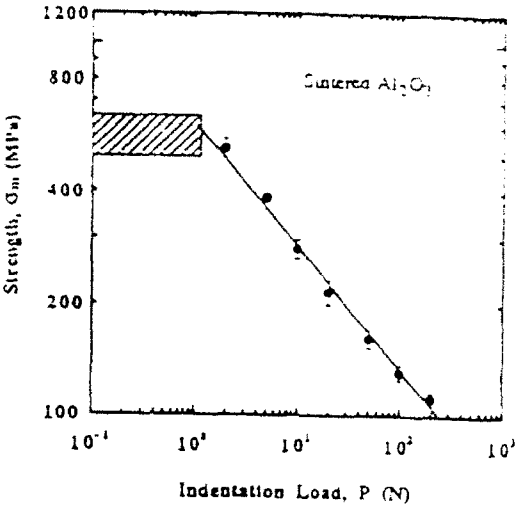
Sintered Al_2O_3
Strength, σ_m (MPa)
1200
800
400
200
100
10^{-1}
10^{0}
10^{1}
10^{2}
10^{3}
Indentation Load, P (N)

(d)

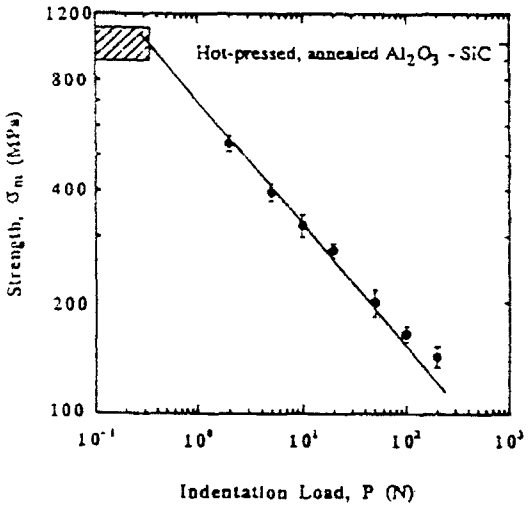
Hot-pressed, annealed Al_2O_3 - SiC
Strength, σ_m (MPa)
1200
800
400
200
100
10^{-1}
10^{0}
10^{1}
10^{2}
10^{3}
Indentation Load, P (N)

(b)

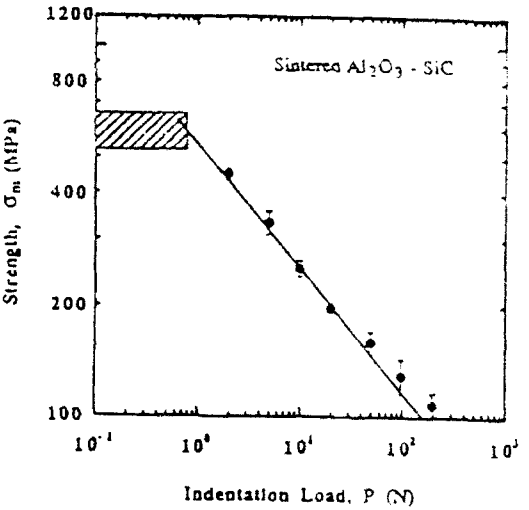
Sintered Al_2O_3 - SiC
Strength, σ_m (MPa)
1200
800
400
200
100
10^{-1}
10^{0}
10^{1}
10^{2}
10^{3}
Indentation Load, P (N)

(e)

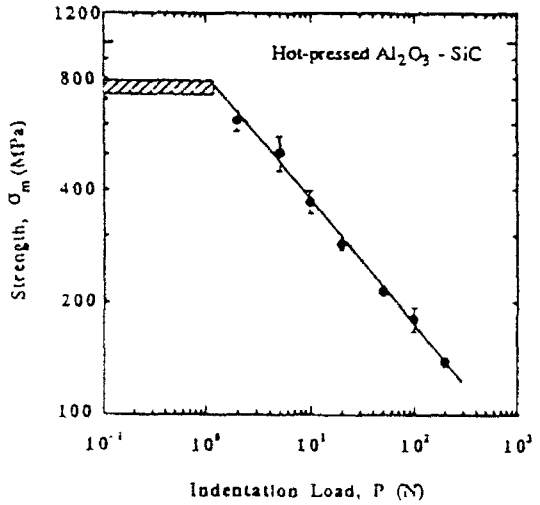
Hot-pressed Al_2O_3 - SiC
Strength, σ_m (MPa)
1200
800
400
200
100
10^{-1}
10^{0}
10^{1}
10^{2}
10^{3}
Indentation Load, P (N)

(c)

Fig 4

(a)

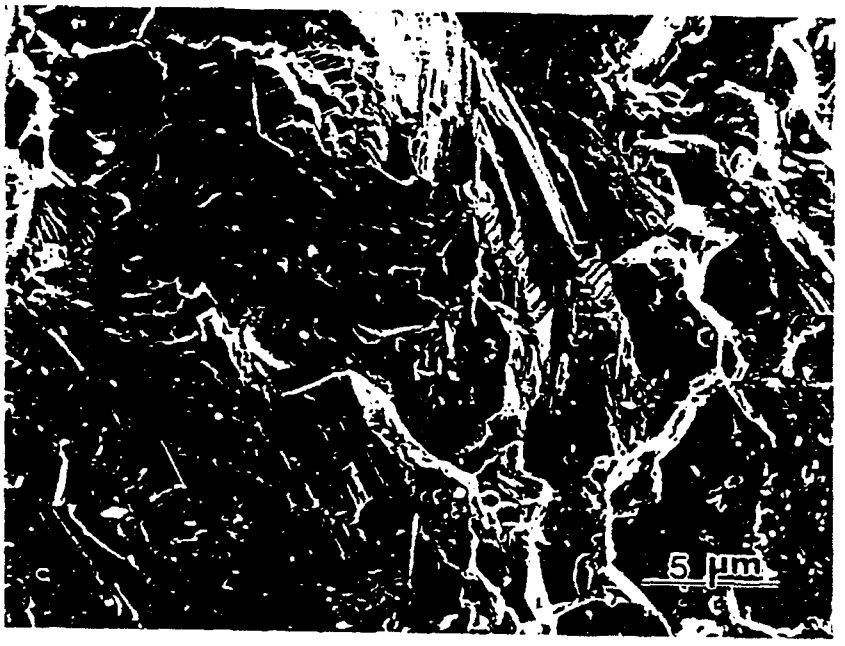

(b)

Fig 5

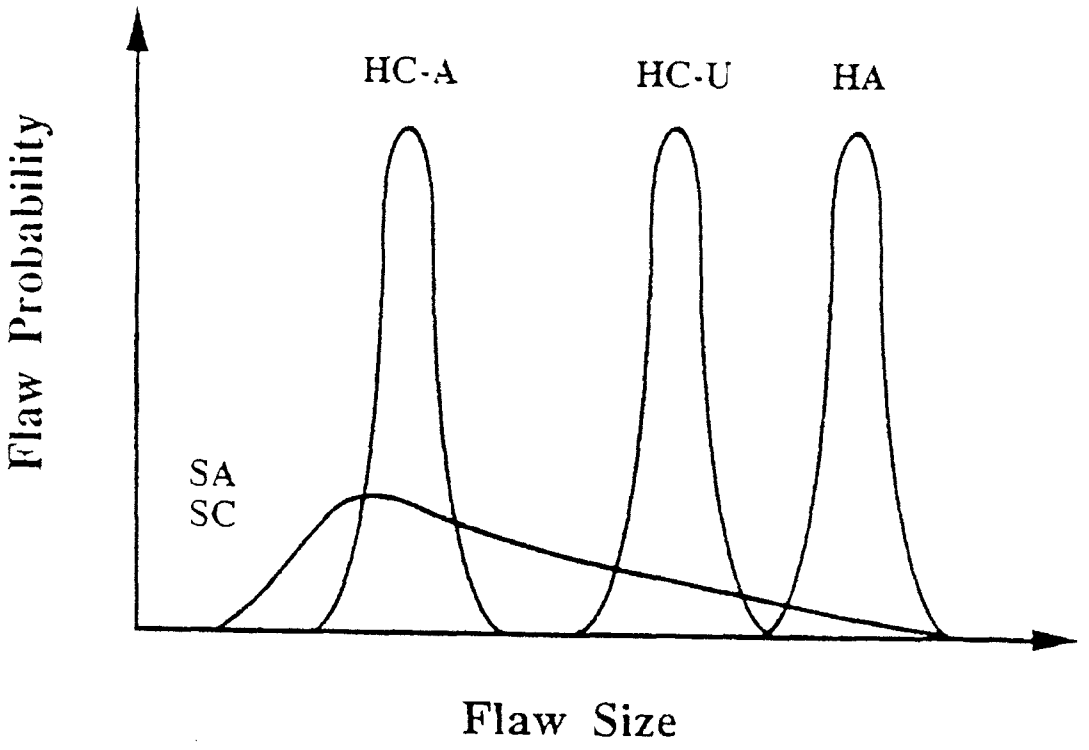

Fig. 6

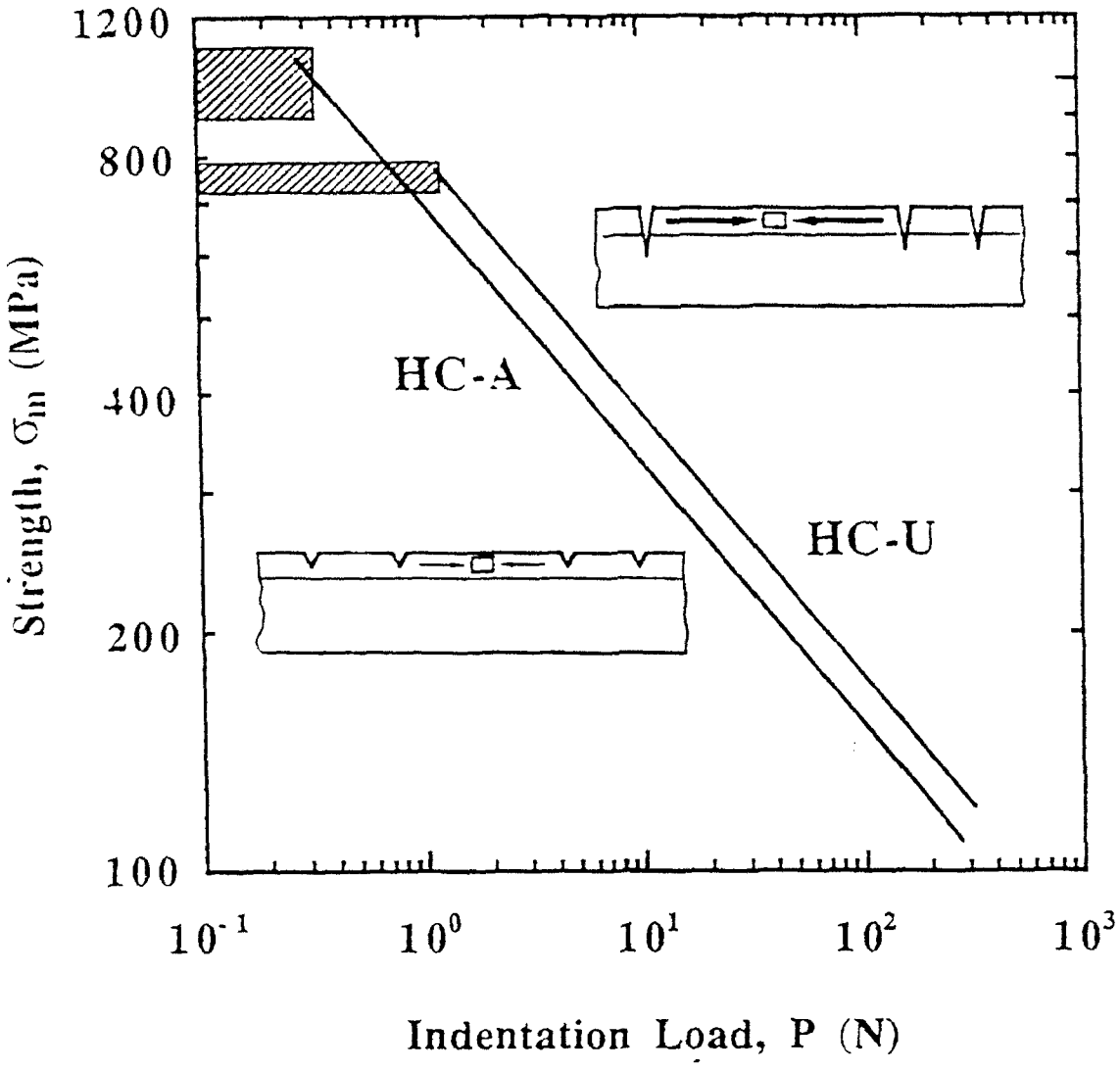
1200
800
400
200
100
Strength, σ_m (MPa)
HC-A
HC-U
10^{-1}
10^0
10^1
10^2
10^3
Indentation Load, P (N)

Fig 7

Section 1.3

PROCESSING AND MICROSTRUCTURE DEVELOPMENT IN Al_2O_3-SiC "NANOCOMPOSITES"

by

L. C. Stearns, J. Zhao, and M. P. Harmer

Published in the Journal of the European Ceramic Society, Volume 10, page 473 (1992)

Processing and Microstructure Development in Al_2O_3-SiC "Nanocomposites"

Laura C. Stearns, Junhong Zhao, and Martin P. Harmer, Department of Materials Science and Engineering and The Materials Research Center, Lehigh University, Bethlehem, PA 18015

Abstract

Composites consisting of Al_2O_3 + 5 vol% 0.15 μm SiC particles were prepared by pressureless sintering. The optimum conditions for achieving dense and uniform microstructures by conventional ceramic processing are given in detail. The SiC particles were found to strongly inhibit grain growth of the Al_2O_3 matrix. Densification was also significantly retarded by these ultra-fine particles, and possible explanations for this behavior are discussed.

Key words: Processing, Al_2O_3-SiC, Densification, Grain growth, Nanocomposite.

Introduction

It was recently reported by Niihara et al. [1-4] that the incorporation of small amounts (5-10 vol%) of "nano"-sized (0.3 μm diameter) SiC particles into an Al_2O_3 matrix could significantly enhance the strength compared to pure Al_2O_3. In fact, the unindented strengths were reported to increase from 350 MPa for Al_2O_3 to over 1 GPa for the 5 vol% SiC composite. Niihara et al. have provided relatively little detail on the processing procedures they used to produce such high strength samples, other than that they used conventional techniques such

as ball milling (various dispersants have been reported). Research in our group and elsewhere has shown that small differences in the processing procedure (such as drying schedule, dispersant used, etc.) can have a pronounced effect on the microstructure and properties of these materials. This caused us to experience some initial difficulties in reproducing the findings of Niihara et al., and we anticipate that other researchers will experience similar problems. The first objective of the present work, therefore, is to provide a detailed description of the experimental conditions we found to be favorable for producing "nanocomposite" powders which subsequently can be fabricated into high strength ceramics. It should be noted here that after homogeneous samples have been prepared using the methods outlined in this paper, surface preparation is also an important factor in the achievement of high strengths. (We have obtained four-point bend strengths greater than 1 GPa on samples machined and then annealed at 1300^{o}C in argon for two hours. The details of the mechanical behavior will be reported elsewhere [5]). Further, we have concentrated on using conventional processing techniques as a relatively simple, cost-effective method for producing large quantities of samples.

The second objective of this study is to present preliminary results on the effects of ultra-fine (0.15 μm) SiC particles on the sintering behavior of Al_2O_3. It has been previously reported that 4 μm SiC particles inhibit grain growth in Al_2O_3 [6]; however, the extent to which ultra-fine SiC particles influence

grain growth in Al_2O_3 has not been investigated. Also, there are no previous reports on the effect of such fine SiC particles on the densification kinetics of Al_2O_3. It is well known that larger inclusions, fibers, or whiskers of SiC constrain densification in Al_2O_3 [7-11]. However, ultra-fine SiC particles would not be expected to impose the same constraints on densification as those produced by these larger reinforcing phases. In certain metal systems, dispersions of second phase particles have been found to retard sintering [12]. However, in ceramic systems, small second phase particles have been observed to both enhance the overall densification rate (as in $BaTiO_3$ with Ba_2TiO_4 second phase particles [13]) and to retard it (as in Al_2O_3 with ZrO_2 second phase particles [14-16]). Thus, the effect of ultra-fine SiC particles on densification in Al_2O_3 is not easily predicted.

Experimental Procedure

Ultra high purity α - alumina (99.995%)* with a mean particle size of 0.2 μm and β - SiC powder** with a mean particle size of 0.15 μm were used in this study. The powders were kept in a clean room environment in a class 100 laminar flow hood, and whenever possible, any handling in the green state was performed in the clean room.

The starting powders were weighed in the appropriate amounts to yield a final volume fraction of 5 vol% SiC particles. In order to promote homogeneous mixing of the two powders, they were dispersed in an organic medium. (The use of an aqueous medium was abandoned due to the tendency of the slurry to form hard

agglomerates on drying). As several different organics have reportedly been used as dispersants for this system [1,3,17], sedimentation experiments were performed using hexane, acetone, ethanol, and methanol. The results are given in Figure 1. It is clear from this bar graph that hexane and acetone led to considerable flocculation. Methanol was chosen for processing because it produced the best dispersion, but for comparison, some samples were also prepared using hexane. For dispersion, the slurry was placed in a strong ultrasonic bath for 40 minutes. High purity ZrO_2 milling balls[$] were then added to the slurry, and it was milled for 48 hours to further promote homogeneous mixing of the Al_2O_3 and SiC. The slurry was poured into a teflon bowl in the laminar flow hood, and dried under an infrared heat lamp. The height of the lamp was adjusted so that the slurry dried over a period of 24 hours. The lamp was then removed and the slurry continued to dry in the hood for another 24 hours. Although seemingly trivial, these details are extremely important, as we found that drying for less time or under higher heat (lamp closer to slurry) led to hard agglomerates which could not be removed without compromising the purity of the powder. After slow drying under low heat, the powder was very uniform in color, and contained only soft agglomerates which were easily broken up using a Teflon[R] rod. Before pressing, the powder was crushed in 2-gram lots between pieces of weighing paper for further homogenization. The powder was then uniaxially pressed at 42 MPa into discs 1.44 cm in diameter using a high purity alumina punch and die set, and isostatically pressed at 350 MPa. Calcining was performed at 600°C for 10 hours in air. This

temperature was found to be low enough not to oxidize the SiC, but high enough to burn off any residual organics from powder processing. The samples were then sintered in flowing nitrogen at various temperatures for 2 hours. For calcining and sintering, the samples were surrounded by SiC powder in a covered alumina crucible.

For preparation of the Al_2O_3 samples, the Al_2O_3 powder was used without any special processing (i.e. dispersion, milling, crushing, etc.). Some Al_2O_3 samples were prepared by ball-milling, however, in order to check for any effects of ZrO_2 from the milling media on densification, as it has been reported that very small amounts of ZrO_2 can inhibit densification in Al_2O_3 [14]. No difference in densification behavior was observed between Al_2O_3 samples prepared by both methods, so it was concluded that there was no contribution from ZrO_2 contamination. Discs were uniaxially and isostatically pressed as described above, but a separate alumina die set was used to prevent cross-contamination. The samples were surrounded by alumina powder in a covered alumina crucible, and were calcined and sintered under the same conditions as the composite samples.

Sintered densities were measured using the Archimedes method with an immersion medium of deionized water plus a wetting agent. The theoretical density of the composite samples was calculated to be 3.948 g/cm^3, based on theoretical densities of Al_2O_3 and SiC of 3.986 g/cm^3 and 3.217 g/cm^3, respectively. For the grain growth experiments, some Al_2O_3 and composite samples were hot-pressed to full density (vacuum, 1400°C, 50 MPa, 1.5 hrs. for

Al_2O_3; nitrogen, 1640°C, 50 MPa, 1 hr. for the composite). These samples were then annealed in flowing nitrogen for various times at 1700°C. For microscopic observation, samples were polished using diamond paste to a 1 μm finish. The composite samples were thermally etched in argon at 1450°C for 1 hr. in order to reveal the grain boundaries. The Al_2O_3 samples used for microscopic observation were those which were sintered at 1450°C, and they were thermally etched in air at 1400°C for 2 hrs. The polished sections were examined using a high resolution scanning electron microscope (SEM). Grain size was measured using the linear intercept method with at least 400 intercepts for each measurement. Samples were prepared for observation by transmission electron microscopy (TEM) using grinding, dimpling, and ion beam thinning.

* Sumitomo AKP-53, Osaka, Japan.

** Performance Ceramics, Co., Peninsula, OH.

$ Tosoh Ceramics Division, Bridgewater, NJ.

Results and Discussion

Figure 2(a-c) shows microstructures of Al_2O_3 and the composite materials prepared using methanol. It is evident from Figures 2(b) and 2(c) that the SiC particles are well-distributed throughout the Al_2O_3 matrix. Also, note that the particles are present inside the grains as well as on the grain boundaries. The grain boundaries of the composite are somewhat wavy and irregular compared to the quite straight boundaries of the Al_2O_3 sample. For comparison, Figure 2(d) shows the microstructure of

the composite prepared using hexane, a poor dispersant. This sample was sintered at 1800°C for 2 hours, and reached a density of 92%, whereas the methanol-prepared sample was 99% dense after 2 hours at 1700°C. The hexane-prepared samples contained large voids, due to agglomeration of the SiC particles during mixing. Also, this microstructure shows a smaller grain size than the methanol-prepared sample, most likely due to considerable pore drag in the hexane-prepared sample, as it was only 92% dense.

Figure 3 shows a plot of grain size as a function of annealing time for Al_2O_3 and the composite (methanol-prepared). Here, zero annealing time corresponds to attainment of the setting temperature (1700°C). It is clear that the SiC particles significantly inhibited grain growth of the Al_2O_3 matrix. For instance, after 24 hours at 1700°C, the Al_2O_3 grains were about 20 μm in diameter, while the composite grain size was 4.78 μm after 24 hours. It is interesting to note that the grain size of the composite material is larger than would be predicted by particle pinning analyses [18-20]. For instance, the weakest pinning (largest limiting grain size) is given by Zener's original model [18], which predicts a limiting grain size for 5 vol% 0.15 μm particles as 2 μm. Further, the stronger pinning models [19,20] predict grain sizes an order of magnitude smaller than this.

The densification behavior is shown in Figure 4 for Al_2O_3 and the composite (methanol-prepared). It can be seen that the Al_2O_3 samples sintered to nearly full density at 1400°C. However, the composite samples reached only 87% theoretical density at this temperature. In fact a temperature of 1700°C was

necessary to achieve 99% density in these samples (for the same sintering time). From this data, it is clear that the presence of only 5 vol% SiC particles severely inhibits densification. According to classical sintering theory, a reduction in grain growth rate should lead to an indirect enhancement of densification (densification rate α 1/(grain size)^n, where n = 3 for lattice diffusion and n = 4 for grain boundary diffusion [21,22]). However, in this case it appears that the retardation of densification was so severe that it overcame the inhibition of grain growth to result in an overall reduction in the densification rate. Similar behavior has been observed in Al_2O_3 containing small amounts (up to 10 vol%) of ZrO_2 [15,16], but the mechanism for densification inhibition has not been determined. We suggest two possible explanations for the retardation of densification in the Al_2O_3-SiC system. First, consider that densification of Al_2O_3 is controlled by diffusion along the boundaries [22]. Due to the strong, directional bonding of both Al_2O_3 and SiC, diffusion at the Al_2O_3/SiC interface is expected to be slow. Consequently, the first possibility is that diffusion of atoms along the grain boundaries to the pores may be limited by the presence of SiC particles on those boundaries, and thus densification will also be slowed. For the second possibility, consider that matter must be removed uniformly from all regions of the boundary for uniform shrinkage. This requires that material be removed from the Al_2O_3/SiC interface if a particle is on the boundary. The process of removing Al^{+3} and O^{-2} ions from this interface may be more difficult than the

diffusion of these ions along the interface. Thus, this would cause a reduction in the densification rate. A full kinetics study is necessary to test these hypotheses.

Summary

A processing method which utilizes relatively conventional techniques has been developed for reproducibly fabricating Al_2O_3-SiC "nanocomposites." Dense microstructures with uniformly distributed SiC particles were obtained via pressureless sintering. As may have been expected, the SiC particles strongly inhibited grain growth of the Al_2O_3 matrix. The ultra-fine particles also significantly retarded overall densification, despite this beneficial influence on grain growth. Possible mechanisms for the densification inhibition have been discussed, but a full study of the kinetics is necessary to test these hypotheses.

Acknowledgements

We are grateful to K. Niihara for donating some of his samples for comparison with our measurements, and to A. M. Thompson for helpful discussions regarding this work. This research was supported by the National Science Foundation under grant DMR-8821686.

References

[1]. K. Niihara and A. Nakahira, "Strengthening of Oxide Ceramics by SiC and Si_3N_4 Dispersions," pp. 919-926 in Proceedings of the Third International Symposium on Ceramic Materials & Components for Engines, (Las Vegas) The American Ceramic Society, Westerville, OH (1988).

[2]. K. Niihara, A. Nakahira, G. Sasaki, and M. Hirabayashi, "Development of Strong Al_2O_3/SiC Composites," pp. 129-134 in Materials Research Society Symposium Proceedings on International Meeting on Advanced Materials, Vol. 4, Materials Research Society, Japan (1989).

[3]. K. Niihara and A. Nakahira, "Particulate Strengthened Oxide Nanocomposites," pp. 637-664 in Advanced Structural Inorganic Composites, Edited by P. Vincenzini, Elsevier Sci. Pub. (1990).

[4]. K. Niihara, "New Design Concept of Structural Ceramics: Ceramic Nanocomposites," The Centennial Memorial Issue of The Ceramic Society of Japan, **99** [10] 974-982 (1991).

[5]. J. Zhao, L. C. Stearns, M.P. Harmer, H. M. Chan, G. A. Miller, and R. F. Cook, in press.

[6]. F. F. Lange and N. Claussen, "Some Processing Requirements for Transformation Toughened Ceramics," pp. 493-507 in Ultrastructure Processing, Edited by Hench and Ulrich, The American Ceramic Society, Westerville, OH (1984).

[7]. T. N. Tiegs and P. F. Becher, "Sintered Al_2O_3-SiC Whisker

Composites," Am. Ceram. Soc. Bull., 66 [2] 339-342 (1987).

[8]. J. R. Porter, F. F. Lange, and A. H. Chokshi, "Processing and Creep Performance of SiC-Whisker-Reinforced Al_2O_3," Am. Ceram. Soc. Bull., 66 [2] 343-347 (1987).

[9]. C. P. Ostertag, "Technique for Measuring Stresses Which Occur During Sintering of a Fiber-Reinforced Ceramic Composite," J. Am. Ceram. Soc., 70 [12] C-355-C-357 (1987).

[10]. H. M. Jang, W. E. Rhine, and H. K. Bowen, "Densification of Alumina-Silicon Carbide Powder Composites: I, Effects of a Polymer Coating on Silicon Carbide Particles," J. Am. Ceram. Soc., 72 [6] 948-953 (1989).

[11]. H-W. Lee and M. D. Sacks, "Pressureless Sintering of SiC-Whisker-Reinforced Al_2O_3 Composites: I, Effect of Matrix Powder Surface Area," J. Am. Ceram. Soc., 73 [7] 1884-1893 (1990).

[12]. D. L. Johnson, "Particle Drag Retardation of Surface Smoothing and Sintering," J. Mater. Sci., 11 2312-2318 (1976).

[13]. Y-H. Hu, "Degradation Mechanisms and Microstructural Control in $BaTiO_3$," Ph. D. Thesis, Lehigh University (1985).

[14]. R. Majumdar, E. Gilbart, and R. J. Brook, "Kinetics of Densification of Alumina-Zirconia Ceramics," Br. Ceram. Trans. J., 85 [5] 156-160 (1986).

[15]. F. F. Lange, T. Yamaguchi, B. I. Davis, and P. E. D. Morgan, "Effect of ZrO_2 Inclusions on the Sinterability of Al_2O_3," J. Am. Ceram. Soc., 71 [6] 446-448 (1988).

[16]. J. Wang and R. Raj, "Activation Energy for the Sintering of Two-Phase Alumina/Zirconia Ceramics," J. Am. Ceram. Soc., 74 [8] 1959-1963 (1991).

[17]. K. Niihara, private communication.

[18]. C. Zener, as quoted by C. S. Smith, "Grains, Phases, and Interfaces: An Interpretation of Microstructure," Trans. Metall. Soc. AIME 175 15-51 (1949).

[19]. D. J. Srolovitz, M.P. Anderson, G. S. Grest, and P. S. Sahni, "Computer Simulation of Grain Growth - III. Influence of a Particle Dispersion," Acta Metall. 32 [9] 1429-1438 (1984).

[20]. M. Hillert, "Inhibition of Grain Growth by Second Phase Particles," Acta Metall. 36 [12] 3177-3181 (1988).

[21]. R. L. Coble, "Sintering Crystalline Solids, I; Intermediate and Final Stage Diffusion Models," J. Appl. Phys., 32 787-792 (1961).

[22]. J. Zhao and M. P. Harmer, "Sintering Kinetics for a Model Final-Stage Microstructure: A Study of Al_2O_3," Phil. Mag. Lett., 63 [1] 7-14 (1991).

Figure Captions

Figure 1. Volume fraction of powder sedimented in graduated cylinder as a function of organic used for dispersing. The solid content was 8 vol%, and measurement of vol% sedimented was taken every 24 hours - this data corresponds to the readings after 5 days.

Figure 2. **(a)** SEM micrograph of Al_2O_3 sintered at 1450^oC, **(b)** SEM micrograph of composite prepared using methanol, sintered at 1700^oC, (c) TEM micrograph of composite prepared using methanol (arrows indicate SiC particles), **(d)** SEM micrograph of composite prepared using hexane, sintered at 1800^oC. All samples were sintered in flowing nitrogen for 2 hours.

Figure 3. Grain size as a function of time for Al_2O_3 and the composite annealed at 1700^oC in flowing nitrogen.

Figure 4. Density as a function of temperature for Al_2O_3 and the composite. Sintering was conducted in flowing nitrogen for 2 hours.

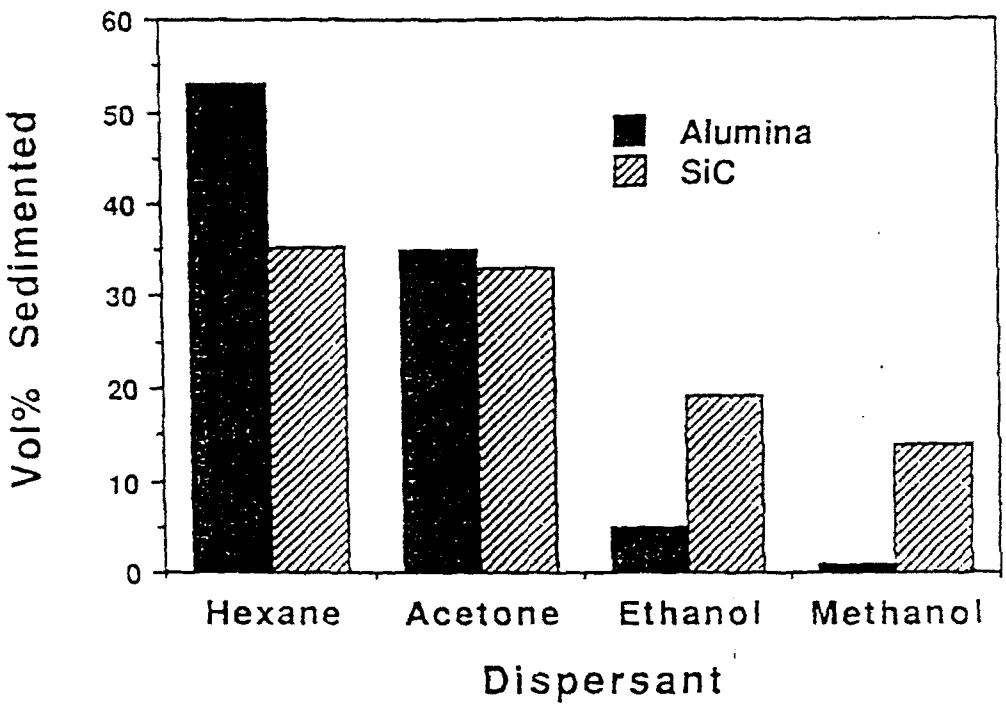
60
50
40
30
20
10
0
Vol% Sedimented
Alumina
SiC
Hexane
Acetone
Ethanol
Methanol
Dispersant

Fig. 1

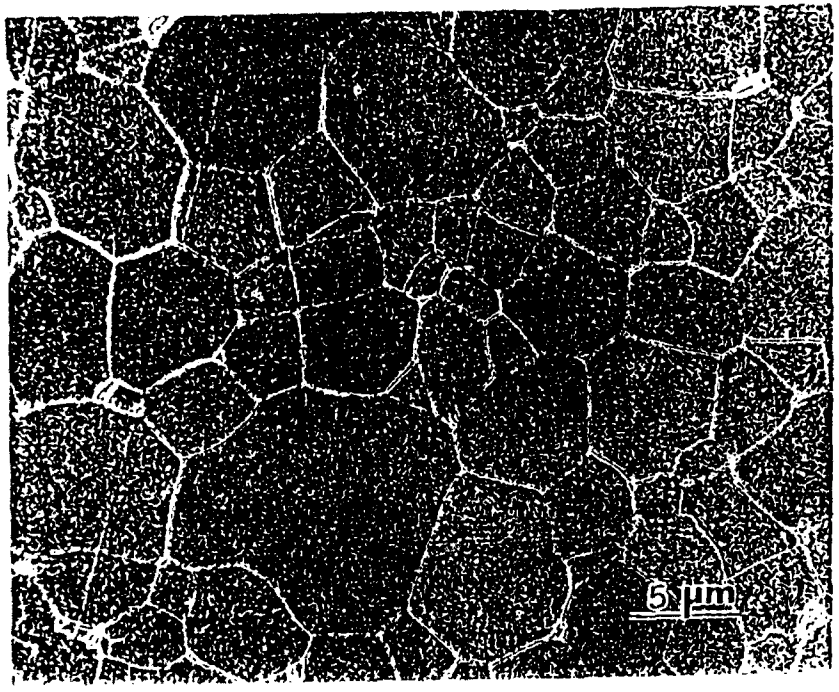

(a)

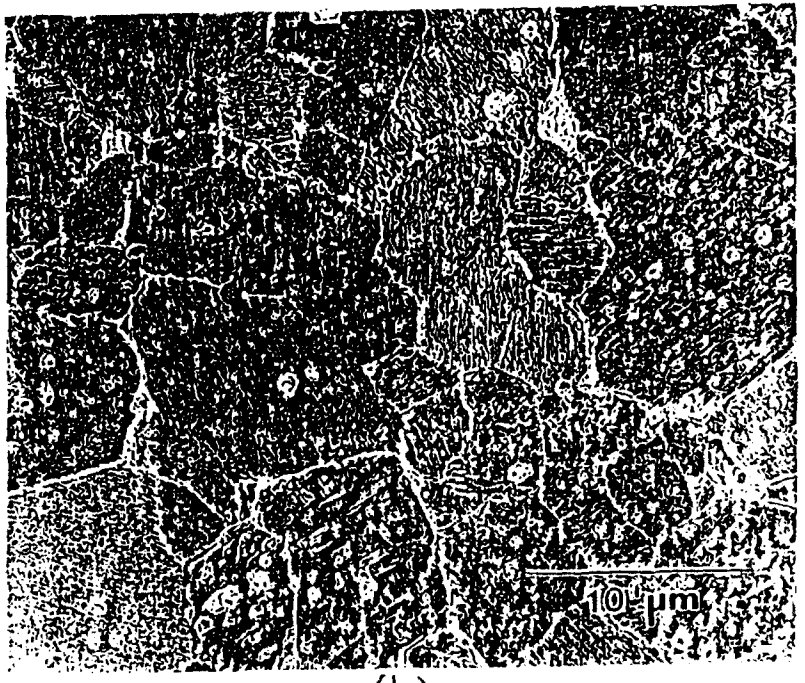

(b)

(c)

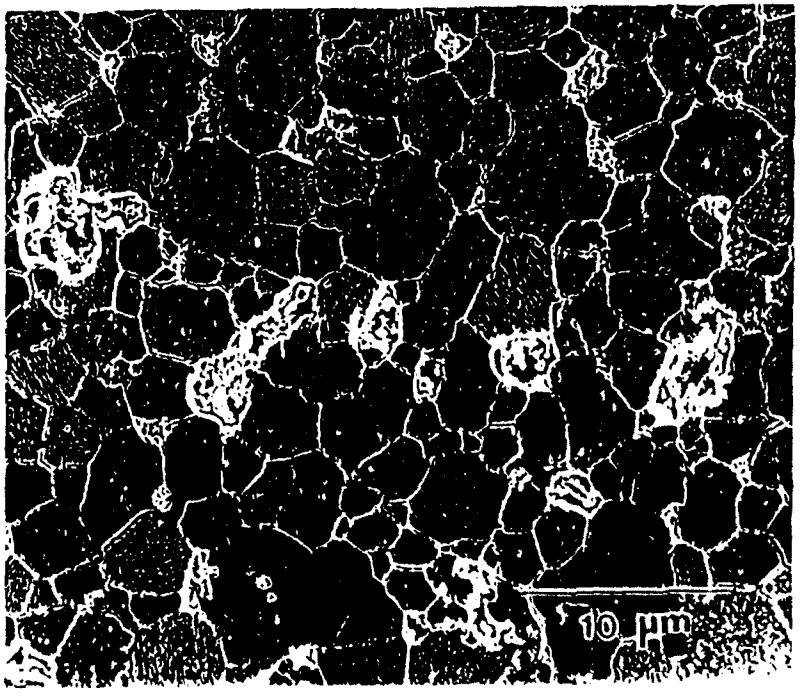

(d)

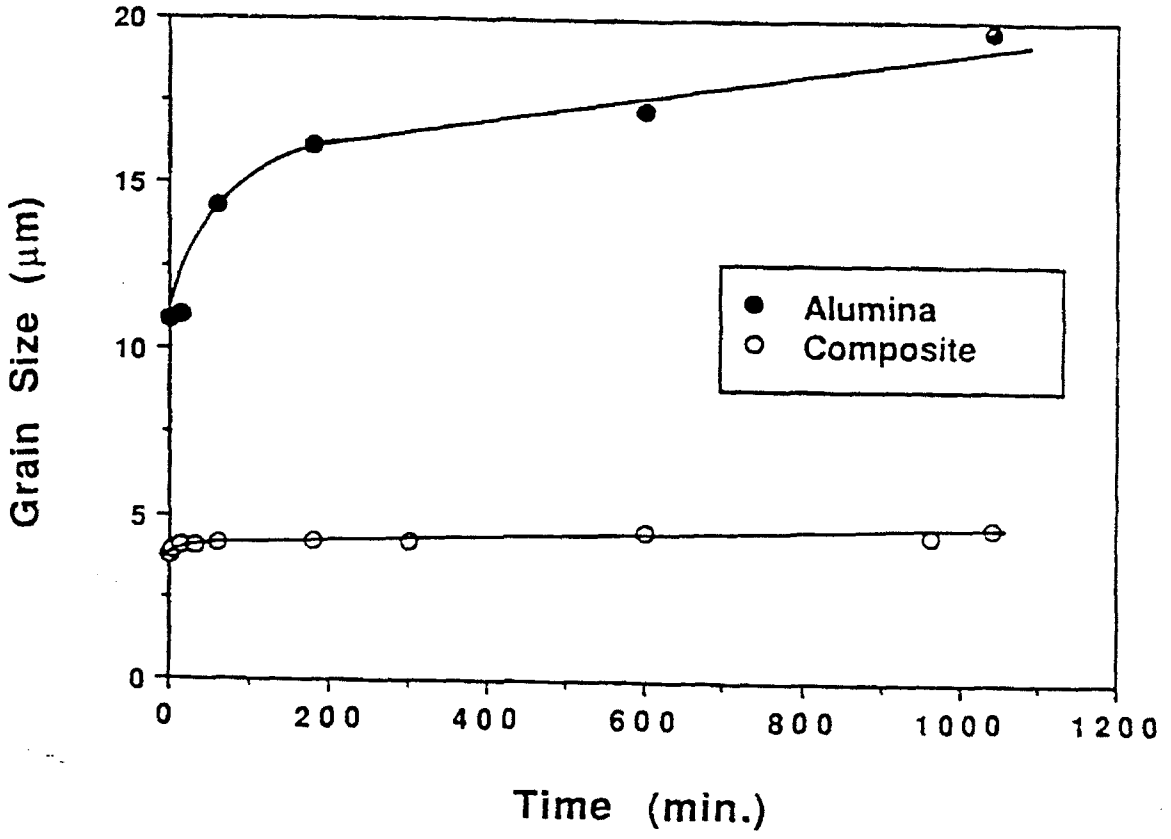
Grain Size (μm)
20
15
10
5
0
0
200
400
600
800
1000
1200
Time (min.)
Alumina
Composite

Fig. 3

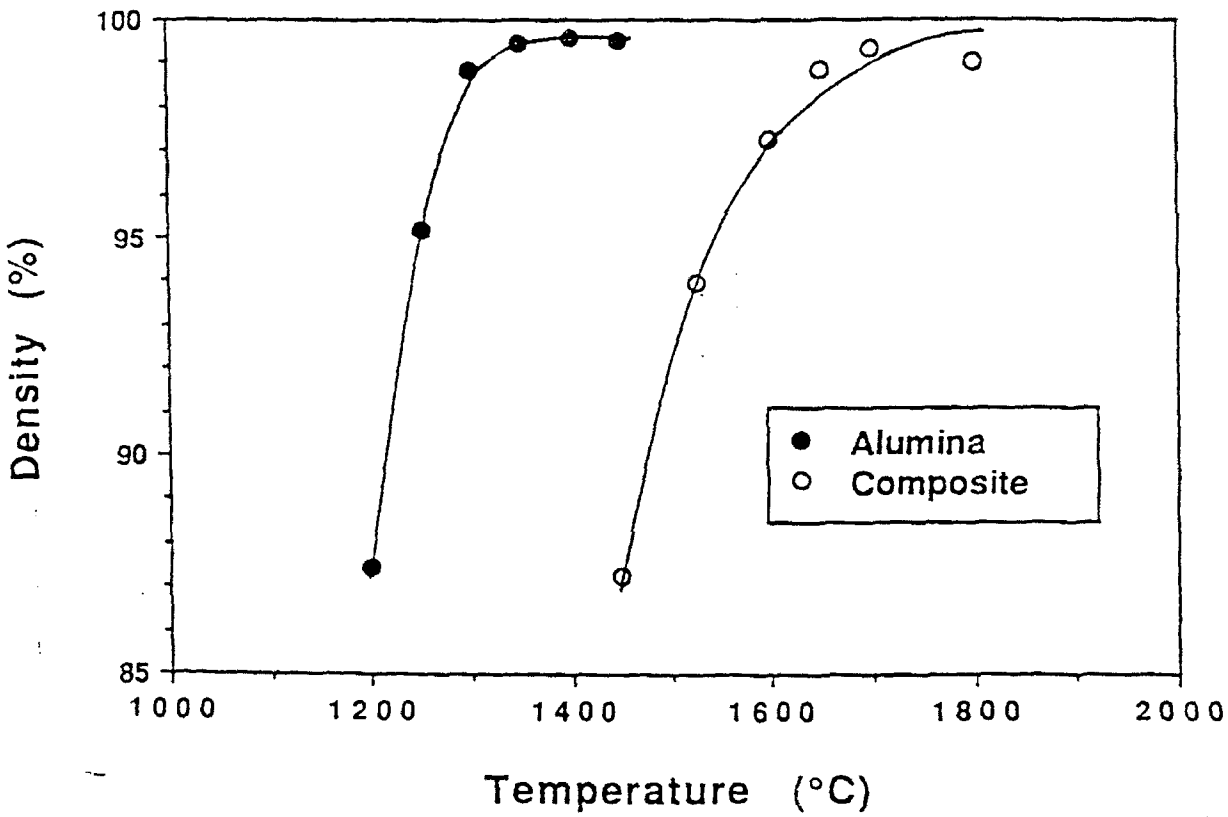
100
95
90
85
Density (%)
1000
1200
1400
1600
1800
2000
Temperature (°C)
Alumina
Composite

Fig. 4

Section 1.4

CRACK HEALING AND STRESS RELAXATION IN Al_2O_3-SiC "NANOCOMPOSITES"

by

A. Mark Thompson, H. M. Chan, and M. P. Harmer

Technical Progress Report

Crack Healing and Stress Relaxation in Al_2O_3-SiC "Nanocomposites"

A. Mark Thompson, H. M. Chan, and M. P. Harmer

I. Introduction

The mechanical properties of single phase ceramics can be significantly improved through the addition of sub-micron reinforcing particles. Niihara et al.,first reported that as little as 5 vol% of 0.3 μm SiC particles could increase the unindented strength of Al_2O_3 to over 1 GPa. An additional annealing treatment enhanced the unindented strength of the nanocomposite to 1.5 GPa[1-4]. In addition to these high strengths, it was reported that the toughness of alumina was improved from 3.25 MPa $m^{1/2}$ to 4.7 Mpa $m^{1/2}$ with the SiC additions.

Subsequent work by Zhao et al. confirmed the strengthening of alumina by SiC additions[5]. In their work, annealing for 2 hours at 1300°C increased the unindented strength of the nanocomposite to about 1 GPa. In contrast to Niihara's work, they found that the toughness increase was modest and not sufficient to account for the vast improvement in unindented strength. Instead, they proposed that the strengthening and apparent toughening arose from machining-induced compressive surface stresses. Their hypothesis is summarized in Figure 1.It is postulated that during grinding of the composite, compressive stresses and machining flaws are introduced into the surface. The compressive surface stresses raise the apparent toughness of the nanocomposite, as determined by the indentation-strength technique. The unindented strengths, thus, reflect both the material toughness and the dominant (machining) flaw size. Upon annealing, the residual surface stresses relax slightly by diffusional processes, and the machining flaws heal. Consequently, the apparent toughness diminishes slightly and the σ-P curve is translated to lower strengths. The flaw healing more than compensates for this reduction in toughness, and so the unindented strengths are improved significantly. In the case of Al_2O_3, it was proposed that the residual surface stresses were relaxed completely upon annealing so that no apparent toughening or strength increases were realized.

The purpose of the following work was to characterize the flaw healing and stress

relaxation behavior in Al_2O_3, and Al_2O_3 containing 5 vol% 0.15 μm SiC particles. Because machining flaws are difficult to observe, each material was characterized using single Vickers indentations. The indentation technique develops controlled flaws and can, therefore, act as a probe to compare the ability of machining flaws to heal in each material system.

In this approach, a Vickers diamond pyramid is loaded onto polished sections of each material. During loading, cracks emanate from the impression corners. Upon unloading these radial cracks grow under the residual tensile stress field. The cracks arrest when the residual stress intensity equals the material toughness. For a center-loaded, half-penny crack this condition is given by[6]

$$T = \frac{\chi P}{c^{3/2}} \tag{1}$$

where, T(c) is the material toughness, c is the equilibrium crack length, P is the peak indent load and χ is the residual stress parameter, a dimensionless coefficient which reflects the intensity of the residual Vickers elastic-plastic contact deformation field. The residual stress parameter in turn is given by

$$\chi = \xi \left(\frac{E}{H}\right)^{1/2} \tag{2}$$

where E is the Young's modulus, H is the hardness, and ξ is a material-independent calibration constant.

II. Experimental Procedure

Experiments were conducted using hot-pressed, mechanical testing bars supplied by Zhao, et al. The details of their fabrication are outlined elsewhere[7]. Two types of material were provided; undoped Al_2O_3, and Al_2O_3 containing 5 vol% 0.15 μm SiC particles. All samples had previously been annealed in argon for 2 hours at 1300°C, indented and then tested in four point bending. In order to remove the silicone oil remaining from the mechanical testing procedure, the polished surfaces of the bars were lightly polished with a 0.3 μm alumina slurry. The

samples were then given an acid washing procedure (aqua regia followed by HF acid) to remove further surface contamination.

The cleaned samples were indented using a Vickers diamond pyramid with peak contact loads ranging from 10-100N. Each bar was indented at numerous points along its length with sufficient space between indentations to avoid interaction of the stress fields surrounding the impressions. Three bars of each material were indented. Crack lengths were measured in air immediately after indenting using a scattered darkfield optical technique[8]. One bar of each material was then mounted into a clamped jig and imaged uncoated in an SEM. Crack length measurements were repeated immediately prior to annealing. The bars were placed in a covered alumina crucible and annealed in argon for 2 hours at 1300°C in a graphite-lined furnace. The atmosphere inside the furnace was sufficiently reducing to prevent significant oxidation of the SiC particles. Immediately after annealing the crack lengths were remeasured. The impressions were again imaged uncoated in the SEM.

III. Results

(i) Crack Length Measurements

The indentation crack lengths in both the Al_2O_3 and composite appeared to be relatively insensitive to the moisture in the laboratory atmosphere. Table 1 shows the crack length measurements made immediately after indenting and immediately prior to annealing. There was no significant increase in crack length in either material even though the samples had been left under normal laboratory conditions in excess of 300 hours. Therefore, it appears that there is relatively little sub-critical crack growth in these materials. Accordingly, it can be assumed that the crack lengths measured immediately prior to annealing represent the equilibrium crack lengths resulting from the indentation.

The indentation measurements of single samples of each material are shown in Figure 2(a),(b). Each crack length data point represents the average and standard deviation of three indents (twelve crack length measurements). The error bars for the indent semi-diagonals are smaller than the symbols. The solid and dashed lines represent best fits to the data using a power law function. The other two samples of each material showed virtually identical responses. In

both materials, the indentation diagonal was proportional to $P^{1/2}$, indicating that the hardness in each material was constant over the entire indentation range. Annealing did not significantly affect the indentation diagonal in either material. In accordance with equation (1), the crack lengths measured prior to annealing showed a $P^{2/3}$ dependence. This indicates that the toughness was constant over the indentation range, and that there was little interaction of lateral cracks with the half-penny median cracks[9].

The annealing step had a remarkably different effect on each material. In the case of alumina, the crack lengths appeared to grow slightly (see Figure 1(a)). However, this small increase was not statistically significant. The cracks in the composite sample appeared to heal substantially. Note that the reduction in crack length especially at low indentation loads exceeded the error in crack length measurement. It appears then, from the optical crack length measurements, that the flaws in the composite are able to heal while those in the Al_2O_3 are not.

(ii) SEM Observation of Radial Cracks

The polished surface of the composite material is shown in its unannealed condition in Figure 3(a). The acid washing procedure had the beneficial effect of revealing both the SiC particles and the matrix alumina grain boundaries. It can be seen that the SiC particles are well dispersed and generally isolated as individual sub-micron particles. Occasional SiC agglomerates are observed. The crack tip shown is one that emanated from a 10N indentation, and is characteristic of indentation cracks in this material. Note that the fracture path is quite flat and predominantly transgranular. These observations are consistent with previous work in this composite system[1-5]. The crack is visibly open along the majority of its length and the tip appears to arrest inside one of the alumina grains.

Upon annealing, the crack opening displacement decreases to the extent that the opposing fracture surfaces mate (see Figure 3(b)). It is difficult to determine the degree of diffusional bonding across the majority of this fracture plane. The crack tip, however, is not observable and has presumably diffusionally bonded. Note that the scale of this diffusive healing is only on the order of a 1-2 microns. This observation is in contrast to the optical crack length measurements which indicated that the 10N indentation crack lengths should heal by around 10-20 microns. This apparent disparity is addressed in the discussion section.

The polished surface of an Al_2O_3 sample is shown in Figure 4 both before (a) and after (b) annealing. Again, the acid washing procedure revealed the alumina grain boundaries. The crack shown in Figure 3(a) emanated from a 50 N impression. Note that the fracture path in this case is predominantly intergranular, and more tortuous than the corresponding crack in the composite sample. The crack is open along the majority of its length and appears to arrest along one of the grain boundaries (as indicated in Figure 4(a)). Upon annealing, the crack does not close as expected, but instead grows: the opening displacement increases as the crack penetrates further along grain boundaries (see Figure 4(b)). The extent of crack growth is only on the order of 5 μm, which is too small an increase to be identified by optical techniques.

IV. Discussion

(i) Limitations of Optical Crack Length Measurements

It is clear from the observations in the previous section that flaw healing cannot be characterized using optical techniques alone. It the case of the composite, the optical measurements indicated significant healing, while the SEM revealed only a small degree of diffusional bonding. This disparity arises because the resolution limits of the optical technique are governed by the crack opening displacement. When the displacement at the crack tip is small, the optical technique cannot resolve the correct position of the crack tip.

A further limitation of the optical technique is evident from the results for the undoped alumina. The small degree of crack growth observed by SEM was masked by the error in the crack length measurements. Therefore, while it is relatively simple and productive to measure crack lengths optically, these measurements must be complemented with higher magnification images of the crack tips.

(ii) Crack Healing Behavior

Healing of indentation cracks can occur in two processes: Either the crack diffusionally bonds in spite of the residual tensile stress field, or the residual stress field relaxes allowing the opposing fracture surfaces to mate. In the latter case, crack healing could be enhanced by further diffusional bonding of the closed crack. (This appears to be process taking place in the

composite system.) In either process, it is not expected that the crack will actually open during annealing, as observed in the undoped alumina. The difference in crack healing behavior between the two materials can be explained by considering the toughening mechanisms and fracture mode in each system.

The toughness of polycrystalline alumina is not, generally, single-valued. Instead, alumina exhibits R-curve behavior, a phenomenon in which the fracture resistance increases as the crack extends. For non-cubic ceramics which fail intergranularly, the principal mechanism for this rising fracture resistance has been shown to be grain-localized bridging behind the advancing crack tip[10,11]. The fracture resistance increases as work is done pulling out these interlocking grains against the frictional tractions constraining them. Consequently, the toughness of alumina is generally expressed as

$$T(c) = T_0 + T_\mu(c) \tag{3}$$

where T_0 is the intrinsic toughness, and T_μ is the microstructural toughening arising from the pullout of interlocking grains. Note that if the ceramic fails transgranularly, grain bridging is minimal and microstructural toughening is not realized ($T_\mu = 0$).

The frictional tractions which oppose the pullout of interlocking grains are believed to arise from the thermal expansion anisotropy of alumina[12-14]. As the ceramic cools from its fabrication temperature, thermal expansion mismatches between adjacent grains generate stresses across the grain boundaries. Although the magnitude of these stresses is relatively insensitive to the grain size, microstructural toughening is often limited to coarse-grained alumina because the large bridging grains are effective over a large crack opening displacement and, therefore, long crack wake. In fine-grained alumina, these frictional tractions may still be effective in inhibiting grain sliding over each other. With this in mind, the annealing response of each material can now be explained.

When the alumina is indented, the radial cracks extend to their equilibrium length according to equation (1). This equilibrium state is shown schematically in Figure 5(a). In this room temperature state, the toughness of the alumina is given by equation (3), where the microstructural toughening arises from the frictional tractions across grain boundaries. As the alumina is heated to the annealing temperature, the thermal expansion mismatch between adjacent

grains decreases and the fractional tractions diminish. Consequently, the toughness of the alumina is reduced slightly, and the radial crack extends (see Figure 5(b)). As the alumina is held at the annealing temperature, the residual stress field surrounding the impression slowly relaxes, thereby, reducing the driving force wedging open the radial crack (see Figure 5(c). Note, however, that the crack does not close upon relaxation of this driving force. The reason for this is two-fold: First, the fracture path in the alumina is tortuous. It may be difficult to mate two opposing surfaces with such a rough topography. Second, the frictional tractions may not have disappeared completely (see Figure 5(c)). Closing the crack would, therefore, require an additional driving force to act against these frictional tractions.

The flaw healing behavior of the composite samples is explained schematically in Figure 6. Because the composite failed transgranularly, it is believed that its toughness would be single-valued and would not vary with temperature. Consequently, the equilibrium crack length obtained after indenting would remain unchanged during heating to the annealing temperature (see Figure 6(a)). Subsequent relaxation of the residual stress field reduces the driving force opening the radial crack. In contrast to the alumina, the cracks in the composite are able to close (see Figure 6(b)). This difference in behavior can be attributed to the mode of failure. First, the fracture path was relatively flat. Closing of the crack would only require a small degree of fit between the opposing fracture surfaces. Second, the fracture path was predominantly transgranular. Grains on opposite surfaces of the crack would have the same orientation and, therefore, the same coefficients of thermal expansion. Frictional tractions at asperities would be minimized enabling the crack to close.

In summary, it appears that radial cracks extend in alumina because the microstructural toughening falls off more quickly than the residual-stress field relaxes. Once the residual stress field is relaxed, the cracks are prevented from closing because of the tortuous fracture path and the thermal expansion anisotropy. In the composite, the fracture path is flat and transgranular. Consequently, the cracks do not extend upon heating and are able to heal during annealing.

An implication of this work is that machining flaws in the two materials considered would react differently to the annealing step. It can be expected that machining flaws will heal in the composite samples. The response of the flaws in alumina is not as clear. It is quite possible that machining flaws may grow instead of healing during the annealing step. If this is the case, the

annealing step would have a more beneficial effect on the composite than on the alumina, which is consistent with the unindented strengths determined in previous work[5].

V. Conclusions

(1) Optical crack length measurements are not sufficient to characterize flaw healing behavior in ceramics. They must be complemented with high magnification observations of the crack tips.

(2) Indentation cracks do not necessarily heal during annealing. In the composite the cracks close whereas in the alumina the cracks open and extend.

(3) The difference in flaw healing behavior is attributed to the mechanism of toughening and fracture mode in each material.

(4) The implications of this study are that machining flaws in each material react differently to the annealing step. In the composite, these flaws may close, while in the alumina they remain open or grow.

References

(1) K. Niihara and A. Nakahira, "Strengthening of Oxide Ceramics by SiC and Si_3N_4 Dispersions," pp. 919-926 in Proceedings of the Third International Symposium on Ceramic Materials & Components for Engines, The American Ceramic Society, Westerville, OH (1988).

(2) K. Niihara, A. Nakahira, G. Sasaki, and M. Hirabayashi,"Development of Strong Al_2O_3 Composites," pp. 124-134 in Proceedings of the International Meeting on Advanced Materials, Vol. 4, The Materials Research Society, Japan (1989).

(3) K. Niihara and A. Nakahira, "Particulate Strengthened Oxide Nanocomposites," pp. 637-664 in Advanced Structural Inorganic Composites, Edited by P. Vincenzini, Elsevier Sci. Pub. (1990).

(4) K. Niihara, "New Design Concept of Structural Ceramics - Ceramic Nanocomposites- ," The Centennial Issue of the Ceramic Society of Japan, **99** [10] 974-982 (1991).

(5) J. Zhao, L. C. Stearns. M. P. Harmer, H. M. Chan, G. A. Miller and R. F. Cook, "Mechanical Behavior of Al_2O_3-SiC "Nanocomposites"," J. Am. Ceram. Soc., **76** [2] 503-10 (1993).

(6) G. R. Anstis, P. Chantikul, B. R. Lawn, and D. B. Marshall, "A Critical Evaluation of Indentation Techniques for Measuring Fracture Toughness: I, Direct Crack Measurements," J. Am. Ceram. Soc., **64** [9] 533-538 (1981)

(7) L. C. Stearns, J. Zhao, and M. P. Harmer, "Processing and Microstructure Development in Al_2O_3-SiC "Nanocomposites"," J. Eur. Ceram. Soc., **10** (1992) 473-477.

(8) D. Johnson-Walls, M. D. Drory, A. G. Evans, D. B. Marshall, and K. T. Faber, "Evaluation of Reliability of Brittle Components by Thermal Stress Testing," J. Am. Ceram. Soc., **68** [7] 363-67 (1985).

(9) R. F. Cook, M. R. Pascucci, and W. H. Rhodes, " Lateral Cracks and Microstructural Effects in the Indentation Fracture of Yttria," J. Am. Ceram. Soc., **73** [7] 1873-78 (1990).

(10) C. Fairbanks, B. R. Lawn, R. F. Cook and Y-W. Mai, " Microstructure and Strength of Ceramics," pp 23-37 in Fracture Mechanics of Ceramics Vol 8, Edited by R. C. Bradt, A. G. Evans, D. P. H. Hassleman and F. F. Lange, Plenum, New York (1986).

(11) P. L. Swanson, C. Fairbanks, Y-W Mai, B. R. Lawn and B. J. Hockey, " Crack-Interface Grain Bridging as a Fracture Resistance Mechanism in Ceramics: I, Experimental Study on Alumina," J. Am. Ceram. Soc., **78** [4] 279-89 (1987).

(12) A. G. Evans and Y. Fu, "Microstructural Residual Stresses," pp 137-153 in Fracture in Ceramic Materials, Edited by A. G. Evans, Noyes, New Jersey (1984).

(13) S. J. Bennison and B. R. Lawn, "Role of Interfacial Grain-Bridging Sliding Friction in the Crack-Resistance and Strength Properties of Nontransforming Ceramics," Acta Metall. **37** [10] 2659-2671 (1989).

(14) J. E. Blendell and R. L. Coble, "Measurement of Stress Due to Thermal Expansion Anisotropy in Al_2O_3," J. Am. Ceram. Soc., **65** [3] 174-178 (1982).

Indentation Load / N	c / μm (As indented)	c / μm (Immediately prior to annealing)	c / μm (Immediately after annealing)
10	58 ± 7	58 ± 6	62 ± 7
50	195 ± 26	191 ± 18	300 ± 40
100	291 ± 48	300 ± 40	315 ± 41

(a)

Indentation Load / N	c / μm (As indented)	c / μm (Immediately prior to annealing)	c / μm (Immediately after annealing)
10	52 ± 3	51 ± 4	39 ± 5
50	147 ± 13	147 ± 11	118 ± 12
100	239 ±13	239 ± 13	203 ± 15

(b)

Table 1: Indentation crack lengths for (a) undoped Al_2O_3, and (b) Al_2O_3/SiC, measured immediately after indenting, immediately prior to annealing, and immediately after annealing.

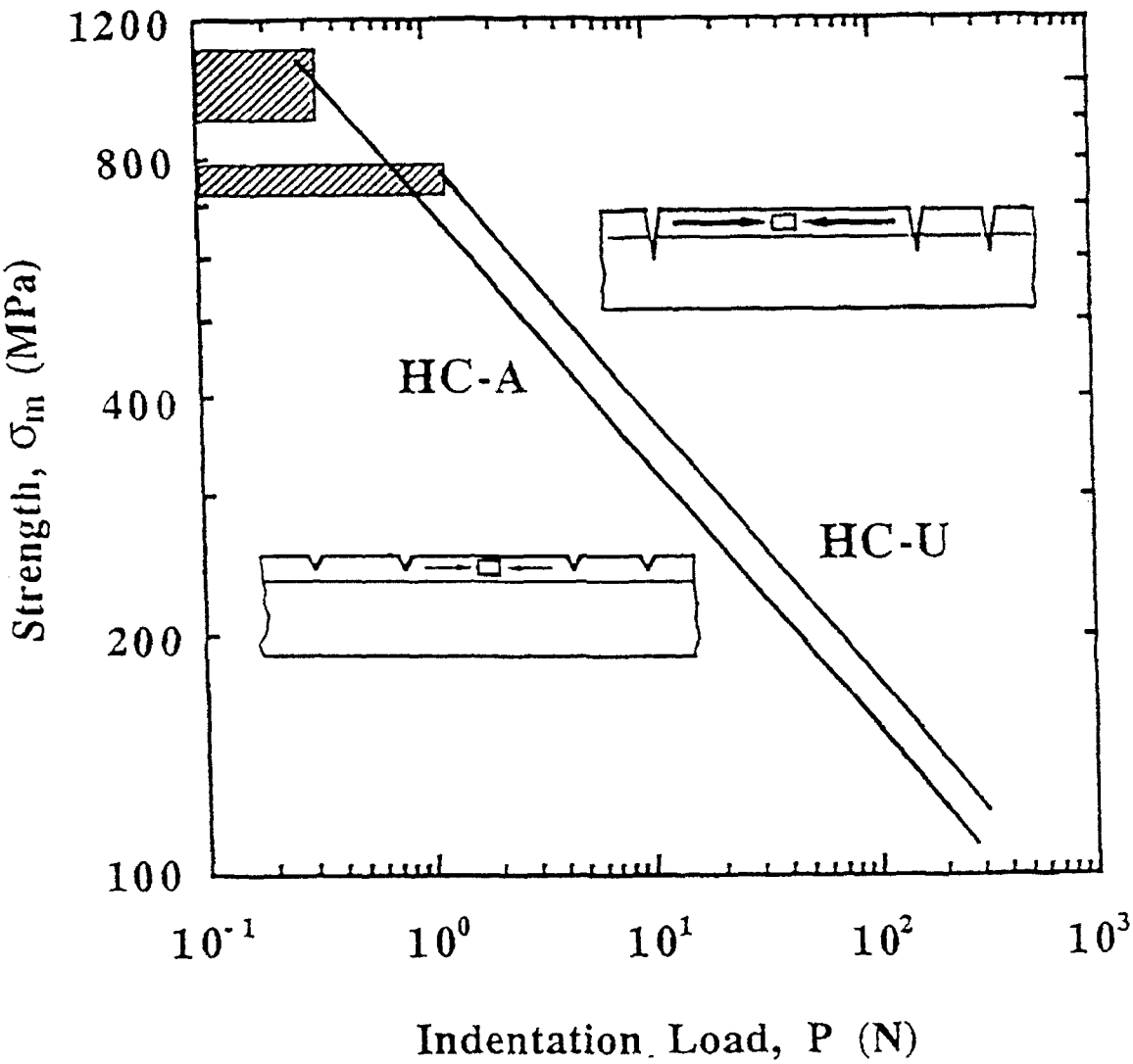

Figure 1: Plot of inert strength as a function of indentation load for hot-pressed, annealed composite (HC-A) and hot-pressed unannealed composite (HC-U). The schematic drawings show the proposed effect of annealing the specimen surface. The residual stress layer is relaxed and the flaw size is reduced. After Zhao, et al.[5]

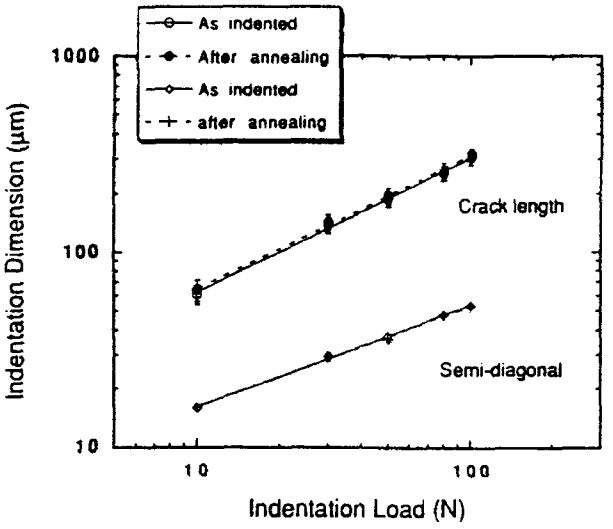

(a)

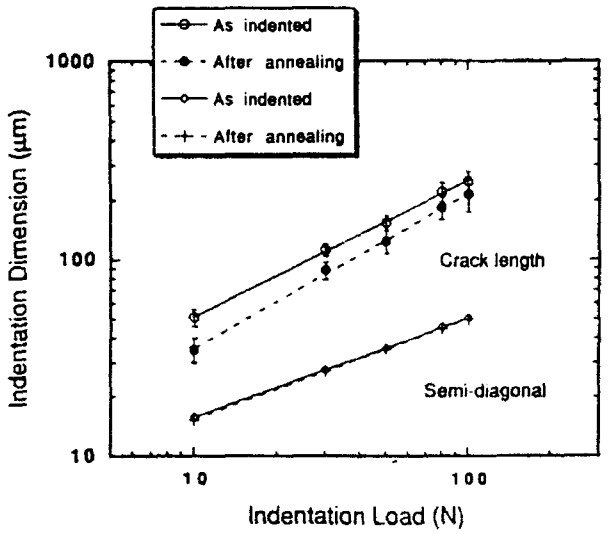

(b)

Figure 2: Crack length and indentation semi-diagonal as a function of indentation load for (a) undoped Al_2O_3 and (b) Al_2O_3 nanocomposite.

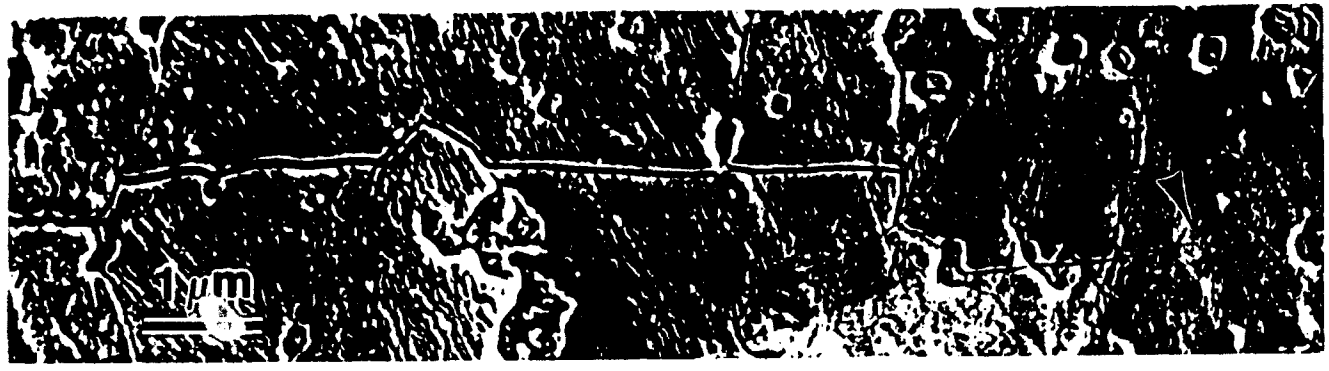

(a)

(b)

Figure 3: SEM images of an uncoated Al_2O_3/SiC composite sample (a) prior to, and (b) after annealing for 2 h at 1300°C in argon. The crack emanated from one corner of a 10N Vickers impression.

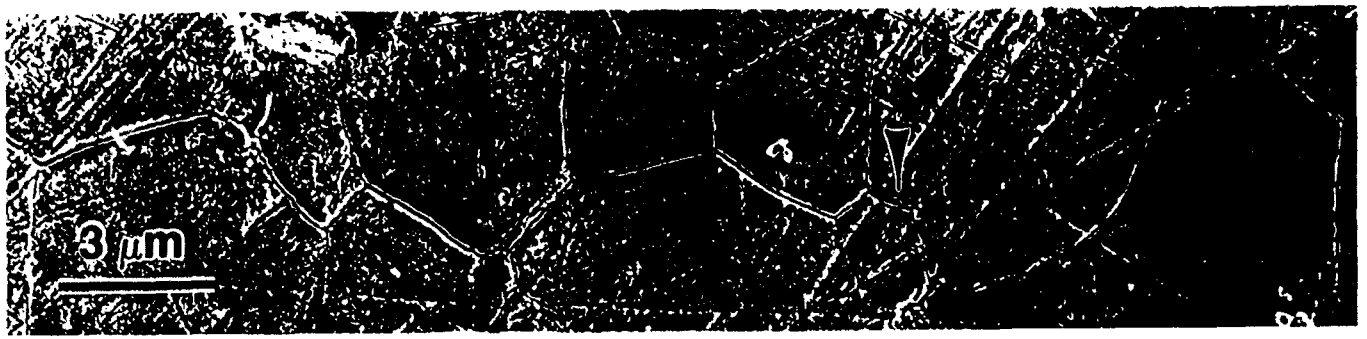

(a)

(b)

Figure 4: SEM images of an uncoated undoped Al_2O_3 sample (a) prior to, and (b) after annealing for 2 h at 1300°C in argon. The crack emanated from one corner of a 50N Vickers impression.

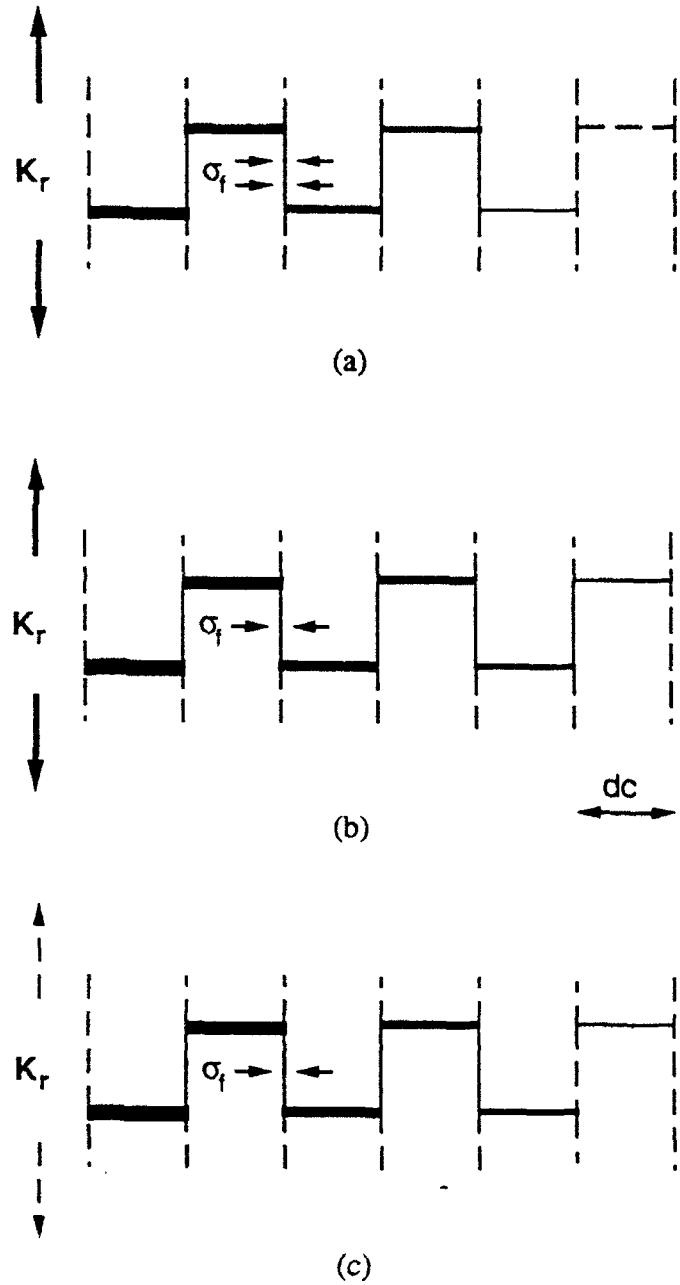

Figure 5: Schematic diagram depicting the crack tip in alumina (a) after indenting, (b) during heating to the annealing temperature, and (c) after soaking at the annealing temperature. K_r represents the residual stress intensity wedging open the crack, and σ_f represents the frictional tractions arising from the thermal expansion anisotropy.

Section 1.5

MICROSTRUCTURES OF Al_2O_3-SiC NANOCOMPOSITE

by

J. Fang, A. M. Thompson, I. Chou, M. P. Harmer, and H. M. Chan

Technical Progress Report

Microstructures of Al_2O_3-SiC Nanocomposite

J. Fang, A. M. Thompson, I. Chou, M. P. Harmer and H. M. Chan

I. Introduction

In recent years, there has been a growing interest in a group of nano-composite materials typified by Al_2O_3-SiC system [1-6]. It has been reported [1-4, 6] that addition of 5 vol.% 0.3 μm SiC not only remarkably increased the unindented strength, but also slightly improved toughness of hot-pressed alumina. A simple annealing step further increased the unindented strength of the composite [3, 4, 6]. In contrast, no beneficial effects of SiC particles were found in pressureless sintered alumina [6]. While mechanical behavior has been extensively studied, little microstructural investigation has been carried out.

The purposes of the present work are (1) to characterize the microstructures of the nanocomposite and (2) to evaluate surface compressive residual stress induced during machining. Coupled with the previous mechanical measurements, these observations might help us to understand mechanism(s) responsible for the beneficial effects of SiC.

II. Material and experimental

Materials used in the current study are hot-pressed Al_2O_3 and Al_2O_3+5 vol.% SiC. Details about preparation of the materials and mechanical properties have been reported elsewhere [5, 6].

Microstructures were examined using SEM and TEM equipped with an energy dispersive x-ray spectrometer (EDS). SEM samples were polished down to 1 μm using diamond paste on an auto polisher. They were thermally etched for 1 hour at 1400^0C in air for Al_2O_3 and at 1450^0C in Ar for the composite. TEM samples were prepared by grinding, dimpling and ion beam thinning.

Residual stress in the ground surface of each material was evaluated by X-ray diffraction technique. The ground surfaces were observed using SEM. The original polished surfaces were also examined using TEM. TEM foils were thinned using one ion Ar gun only to preserve the original polished surface.

III. Results and discussion

3.1 Microstructures of bulk materials

Addition of 5 vol.% SiC into Al_2O_3 significantly altered the morphology of microstructure. Pure Al_2O_3 exhibited a single-phase structure composed of equiaxed grains with straight grain boundaries (Fig. 1a). Al_2O_3-SiC composite contained many elongated grains and grain boundaries were wavy (Figs. 1b). These observations are consistent with previous work by Zhao et al. [6] Both SEM and TEM examinations showed that SiC particles situated both along grain boundaries and within the grains (Figs. 1b and 1c). It is apparent from Fig. 1c that SiC particles pinned the grain boundaries during grain growth, giving rise to the wavy boundaries. One possibility for the formation of elongated grain in the composite is that SiC particles were not present along all grain boundaries and therefore the boundaries without SiC particles grew much faster than those with particles.

3.2 Oxidation of SiC

Gadlla et al. [7] applied x-ray diffraction and weight loss measurement methods to investigate reactions in Al_2O_3-SiC system at high temperature. Their results have shown that SiC can be oxidized to form silica in flowing nitrogen above 1750^0C, which is similar to sintering condition in our material [6]. Thus, SiC particles are closely examined using TEM in the present work to ascertain the degree of surface oxidation.

Majority of SiC particles did not oxidize. However, particles occasionally were found in which oxidation was suspected. An example of such a particle is shown in Fig. 2. Since very slight contrast can be seen in region 2 (Fig. 2a), oxidation is suspected to occur in this region. Therefore, the matrix, the suspected region, and the surrounding SiC particle

were further investigated by convergent beam electron diffraction (CBED) (Fig. 2b to Fig. 2d) and EDS (Fig. 2e to Fig. 2g). Rings (Fig. 2c) and only Si peak (Fig. 2f) from EDS from the examined region suggest amorphous structure of silica. Note that this particle was the exception rather than the rule. It appears that the nanocomposite did not significantly oxidize during sintering.

3.3 Ground and polished surfaces

SEM micrographs of ground surfaces are shown in Fig. 3 for hot-pressed alumina and composite. The surfaces for these two materials appear very different. Pure alumina showed smooth grain boundary facets and very few smeared patches, indicating that most material had been removed by intergranular fracture. In contrast, the composite exhibited a mixture of transgranular fracture and smeared regions where striations run along grinding direction. Transition from predominately intergranular fracture to transgranular fracture upon the addition of 5 vol.% SiC is attributed to toughening of grain boundaries by SiC particles [6].

Residual stress on ground surfaces was measured by X-ray diffraction technique [8] and results were summarized in Table 1. While a slight amount of tensile residual stress was present in alumina, compressive surface stress in the composites was substantial. However, the difference in residual stress between unannealed and annealed composites could not be discerned because it is not large enough to be out of the band of scatter. Thus, it appears that a significant amount of compressive residual stress was induced during grinding process and that annealing relieved the residual stress in Al_2O_3 close enough to zero but not very much in the composite.

Fig. 4 shows TEM images of polished surfaces of unannealed and annealed hot-pressed composites. In the unannealed material, most of dislocations are limited to narrow linear bands, whereas the other area contains a low density of dislocations, as shown in Fig. 3a. The narrow bands of high dislocation density define the traces of the surfaces scratches produced by individual abrasive particles. Considerable dislocation motion and

rearrangement occurred during annealing, as illustrated in Fig. 3b. The movement of dislocations from the narrow bands led to a more uniform distribution of dislocations throughout the foil. Similar phenomena have been observed in unannealed and annealed polished surfaces of pure alumina [9, 10]. Usually, annealing reduces dislocation density and, hence, relieves residual stress. However, the pinning effect of SiC retard the reduction in dislocation density and thus still maintain high residual stress. These observations are consistent with x-ray residual stress measurements.

Table 1. Surface stress measurements

Specimen	Surface stress (MPa)	Nature of stress
unannealed HP composite	-141±87	compressive
	-72±24	
annealed HP composite	-221±75	compressive
	-153±52	
annealed HP alumina	67±41	tensile

IV. Conclusions

1. Monolithic Al_2O_3 consists of equiaxed grains with straight boundaries, whereas nanocomposite contains some elongated grains with wavy boundaries. The feature of wavy boundaries arise from the pinning effect of SiC.

2. Majority of SiC particles do not oxidize, even though oxidation occasionally occurs in some particles.

3. Addition of 5 vol.% SiC dramatically changes ground morphology from intergranular to a mixture of transgranular and smeared region. This change arises from mechanically interlocking of SiC particles.

4. Surface residual stress is induced during grinding and annealing almost relieves the residual stress in Al_2O_3 but not very much in composite.

5. In the composites, surface residual stress is connected with high density of dislocations and dislocation rearrangement occurs during annealing.

V. References

1. K. Niihara and A. Nakahira, "Strengthening of Oxide Ceramics by SiC and Si_3N_4 Dispersions", pp. 919-926 in Proc. of 3th Inter. Symp. of Ceramic Materials & Components for Engines, The American Ceramic Society, Westerville, OH (1988).
2. K. Niihara, A. Nakahira, G. Sasaki and M. Hirabayashi, "Development of Strong Al_2O_3/SiC Composites", pp. 124-134 in Proc. of the inter. Meeting on Advanced Materials, vol. 4, The Materials Research Society, Japan (1989).
3. K. Niihara and A. Nakahira, "Particulate Strengthened Oxide Nanocomposites", pp. 637-664 in Advanced Structural Inorganic Composites, Ed. by P. Vincenzini, Elsevier Sci, Pub. (1990).
4. K. Niihara, "New Design Concept of Structural Ceramics-Ceramic Nanocomposites,", the Centennial Issue of the Ceramic Society of Japan, 99 [10] 974-982 (1991).
5. L. C. Stearns, J. Zhao and M. P. Harmer, "Processing and Microstructure Development in Al_2O_3-SiC 'Nanocomposites' ", submitted to J. of European Ceramics.
6. J. Zhao, L. C. Stearns, M. P. Harmer, H. M. Chan, G. A. Miller and R. F. Cook, "Mechanical Behavior of Al_2O_3-SiC 'Nanocomposites' ", J. Am. Ceram. Soc. **76**, 503-510 (1993).
7. A. Gadalla, M. Elmasry and P. Kongkachuichay, "High Temperature Reactions within SiC-Al_2O_3 Composites", J. Mater. Res. **7**, 2585-2592, 1992.
8. F. F. Lange, M. R. James and D. J. Green, "Determination of Residual Surface Stresses Caused by Grinding in Polycrystalline Al_2O_3", J. Am. Ceram. Soc., [2] C-16-C-17 (1983).

9. B. J. Hockey, "Observations on Mechanically Abraded Aluminum Oxide Crystals by Transmission Electron Microscopy", pp. 333-339 in Proc. of the Science of Ceramic Machining and Surface Finishing, held Nov. 2-4, 1970.

10. B. J. Hockey, "Plastic Deformation of Aluminum Oxide by Indentation and Abrasion", J. Am, Ceram. Soc. **54**, 223-231 (1971).

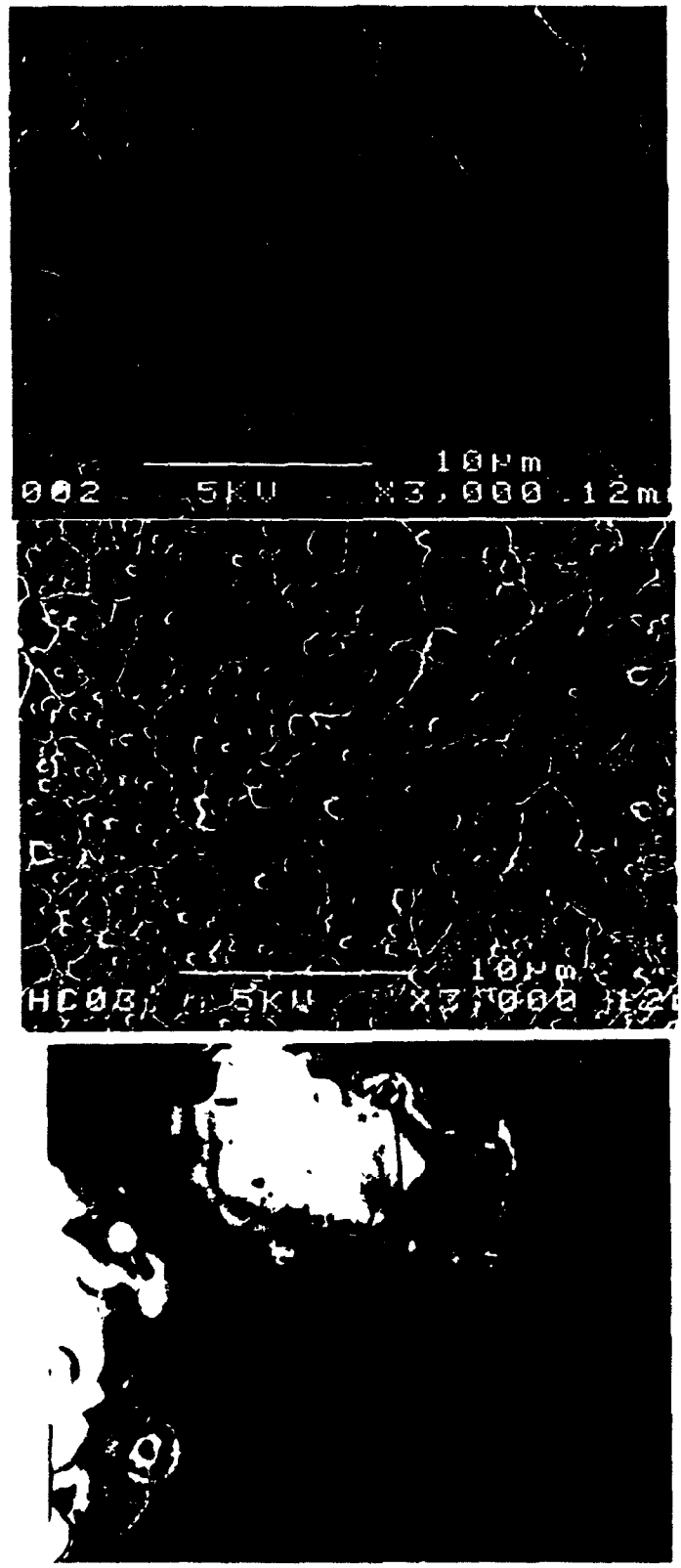

(a)

(b)

(c)

Fig. 1. SEM micrographs illustrating (a) eqiaxed grains with straight grain boundaries in Al_2O_3 and (b) elongated grains with wavy boundaries in composite. TEM image clearly showing SiC particles pinning grain boundaries in composite.

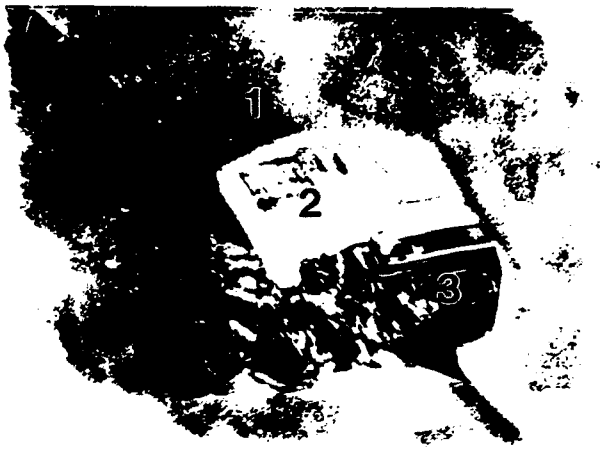

100 nm

(a)

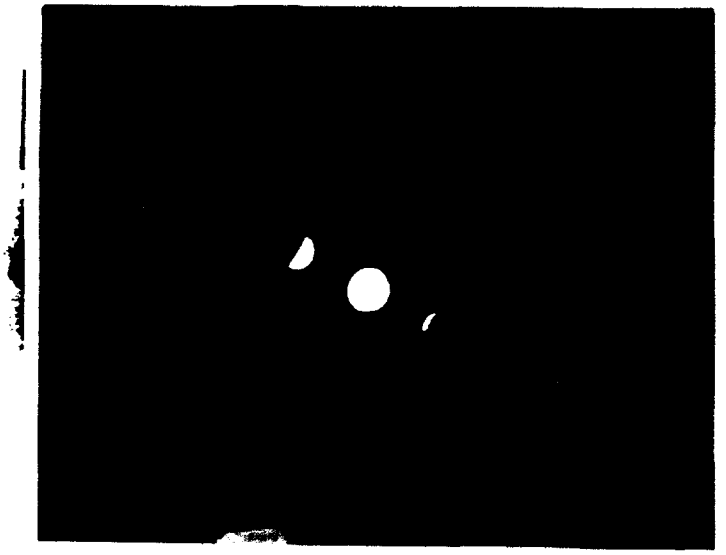

(b)

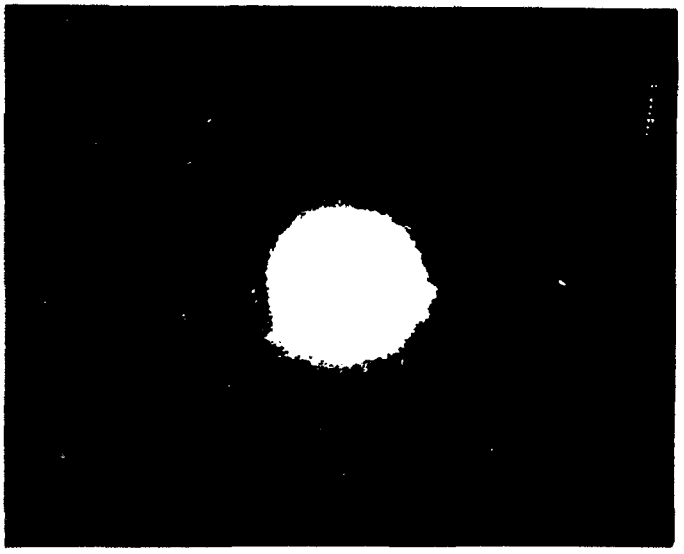

(c)

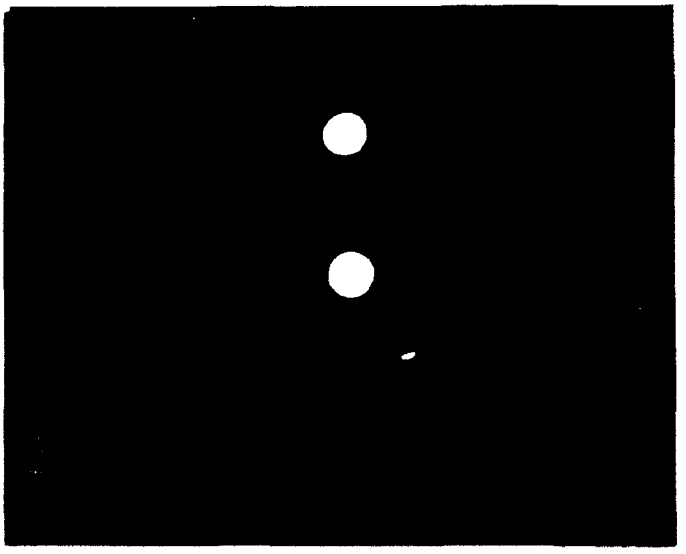

(d)

Fig. 2. TEM image of an SiC agglomerate (a). Fig. 2 (b) to (d) showing CBED pattern from regions 1 (matrix), 2 (oxidized SiC) and 3 (crystalline SiC). (Continued)

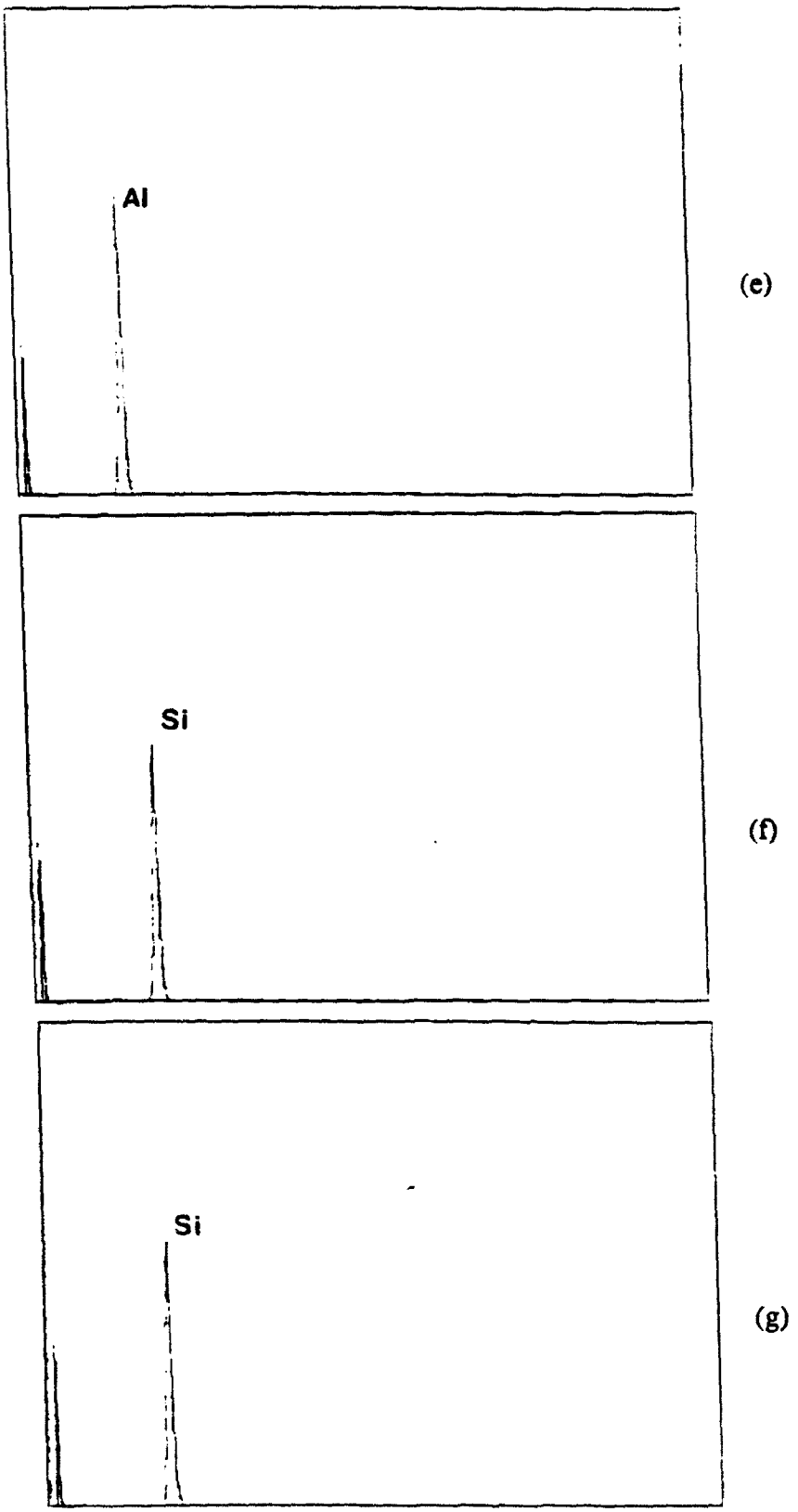

Fig. 2. (e) to (g) showing energy dispersive spectra from regions 1 (matrix), 2 (oxidized SiC) and 3 (crystalline SiC).

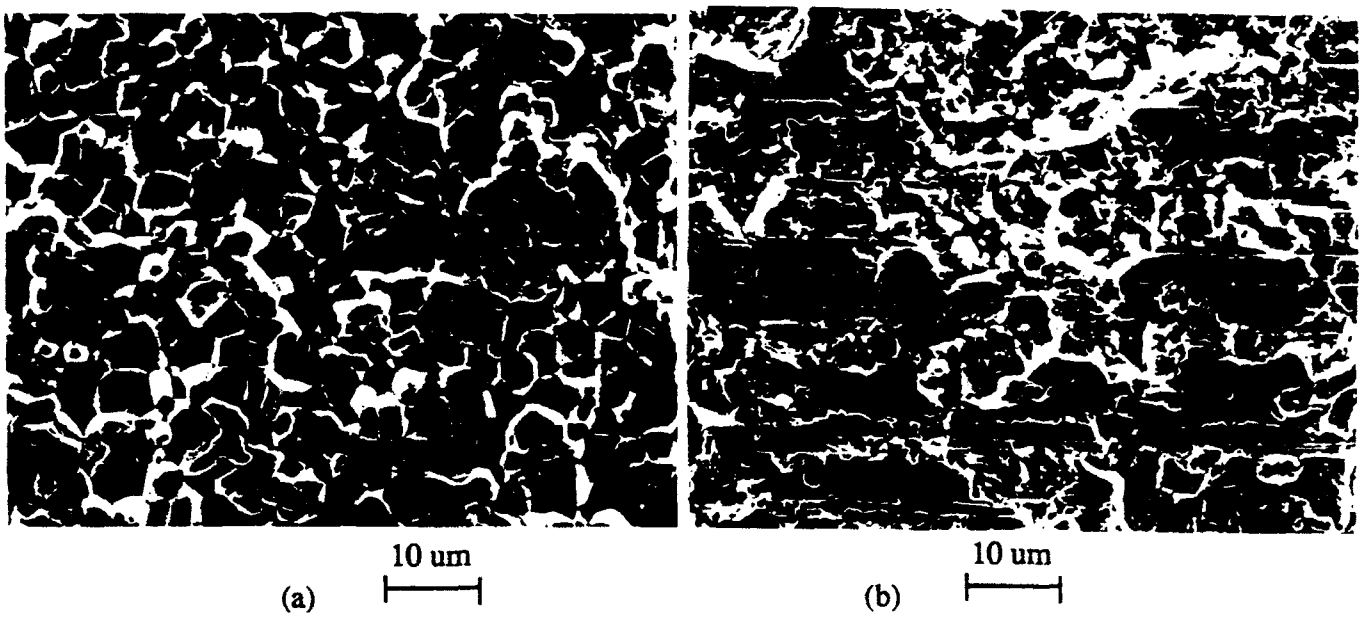

Fig. 3. SEM micrographs of ground surfaces of (a) Al_2O_3 and (b) Al_2O_3+5 vol.% SiC.

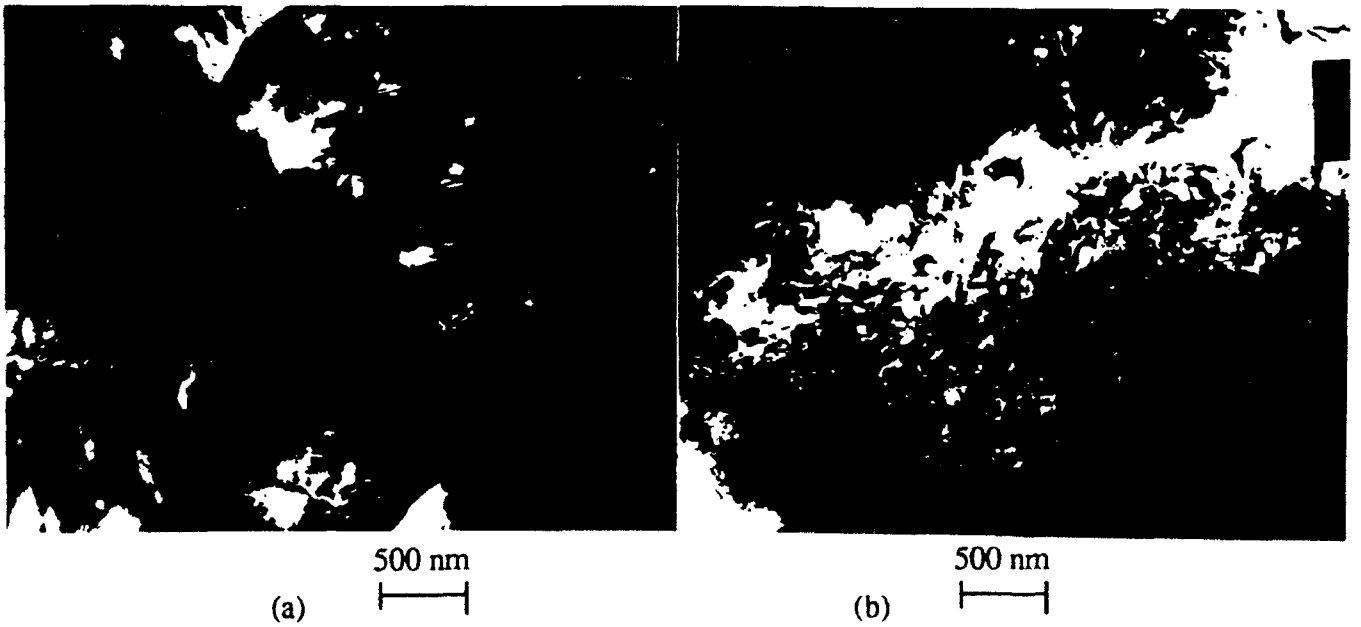

Fig. 4. TEM images of polished surfaces of unannealed and annealed composites.

Section 1.6

MECHANICAL PROPERTIES OF COARSE GRAIN "NANOCOMPOSITES"

by

I. A. Chou, A. M. Thompson, J. Fang, H. M. Chan and M. P. Harmer

Technical Progress Report

Mechanical Properties of Coarse Grain "Nanocomposites"

I. A. Chou, A. M. Thompson, J. Fang,
H. M. Chan and M. P. Harmer

I. Introduction

Alumina has high potential in structural applications. Unfortunately, it suffers from relatively low fracture toughness/strength and poor creep, fatigue and thermal shock resistance. Previous studies by Niihara et al. [1 - 4] have shown significant improvements in unindented fracture strength and toughness by incorporating ≈ 0.2 - 0.3 μm SiC particles into the alumina matrix. The maximum strength was achieved by hot pressing Al_2O_3 containing 5 vol% of SiC particles, followed by annealing at 1300 °C for 2 hours in argon or air. However, similar studies done by Zhao, et al. [5, 6] have discovered that the strength increment occurred only for hot - pressed composites but did not appear for sintered samples with the same composition. The sintered composites showed identical strength as sintered pure alumina materials. In addition, even though the strength of the hot-pressed composites increased upon annealing, toughness actually decreased. Consequently, Zhao, et al. proposed that the strengthening observed in the hot - pressed composites is derived from compressive surface stresses introduced by the grinding process rather than an increase in the intrinsic material toughness as suggested by Niihara.

The objective of the current research is to confirm the influence of machining induced residual stress on the strength and toughness on Al_2O_3 - SiC composites, to examine the effect of annealing on the residual stress, and to determine the mechanism of strengthening in the hot - pressed composites.

II. Experimental Procedures

Ultra high purity α - Al_2O_3 (99.995%, Sumitomo AKP - 53, Osaka, Japan) with a mean particle size of 0.2 μm and ß - SiC powder (Performance Ceramics Company, Peninsula, Ohio) with a mean particle size of 0.15 μm were used in this study. Five vol% of SiC was added to the Al_2O_3 starting powder and the mixture ultrasonically dispersed and ball milled in methanol. The slurry was then slowly dried to produce a uniform powder. Disk specimens were prepared by uniaxial cold pressing at 75 MPa plus isostatic cold pressing at 350 MPa. They were then calcined in air at 600 °C for 10 hours and sintered at 1775 °C in nitrogen for 4 hours. For both calcining and sintering, the disks were surrounded by SiC powder in a covered high purity Al2O3 crucible. Density measurements using Archimedes technique show almost fully densed samples with density ≥ 98.4% theoretical density. The dimension of the disks were approximately 21 mm diameter and 2.3 mm thickness.

The indentation strength test was used to examine the effect of grinding on the composites. One side of the disks was ground flat and the other side polished down to 6 μm. To introduce machining damage, the polished side was then ground at either 22 μm or 40 μm grit for 20 minutes at 135 N and 150 r.p.m. An indentation load of 20 N was used for all tests. It is chosen so that the radial cracks would be small enough to experience the full influence of the machining damage without being dominated by the machining flaws themselves [8, 9]. The indentations were all carried out by a Vickers diamond indentor, and the disks were broken in biaxial flexure with the specimen loaded on a three ball support. As a reference point, some disks were broken in the 6 μm polished condition without any machining damage.

III. Result and Discussion

Figure 1. is a SEM micrograph of the Al_2O_3 - 5 vol% SiC composite processed in this study without any machining damage. The SiC particles are evenly distributed in the matrix as well as along the grain boundaries. There is a wide range of grain size with some of the grains $\geq 60\ \mu m$. This is in contrast to previous studies [5, 6] in which the average grain size was $\approx 5.4\ \mu m$. Possible reasons for this larger grain size are (1) the chemistry of the starting powder may have been slightly different to that of the original study, or (2) the sintering conditions such as temperature or atmosphere may have been slightly altered.

Despite the difference in grain size, the strength behavior of the sintered composites used in this study is similar to the prior work as shown in Figure 2. The maximum strength difference is only ≈ 20 MPa. Similar studies made by Niihara [7] have also shown a lack of strength variation with the grain size for the Al_2O_3 -SiC composite. In contrast, undoped alumina shows a strong strength dependence in grain size [10, 11]. This difference in behavior for the two materials can be attributed to their difference in toughening mechanisms and fracture mode. The undoped alumina fractures intergranularly, and its microstructural toughening arises from grain bridging. The contribution of this microstructural toughening to the overall material toughness increases as the grains coarsen. In comparison, the fracture mode of the composite is trangranular [2, 5]. Therefore, toughening mechanisms such as grain bridging are not realized, and grain size has little effect on the strength behavior of the composite.

Preliminary investigation into the role of machining damage produced inconclusive results as shown in Table I:

Testing Surface Condition	Strength at 20 N Indentation Load (MPa)
Normal Polish	240 ± 9
22 μm ground	233 ± 22
40 μm ground	253 ± 22

Table I. Strength Data for Different Machining Condition

Even though the 40 μm ground samples showed an increase in strength, the result is statistically insignificant because of the large standard deviation. The variation in these results is presumed to be a consequence of non-uniform grinding condition. Further work will focus on (1) enhancing the degree of machining to produce a statistically significant change/improvement in strength, and (2) refining the machining technique in order to improve reproducibility.

IV. Conclusions

(1) The indentation strength behavior of Al_2O_3 - 5 vol% SiC nanocomposite is independent of grain size.

(2) Greater control of machining condition is required to evaluate the role of machining damage in the strength behavior of these materials.

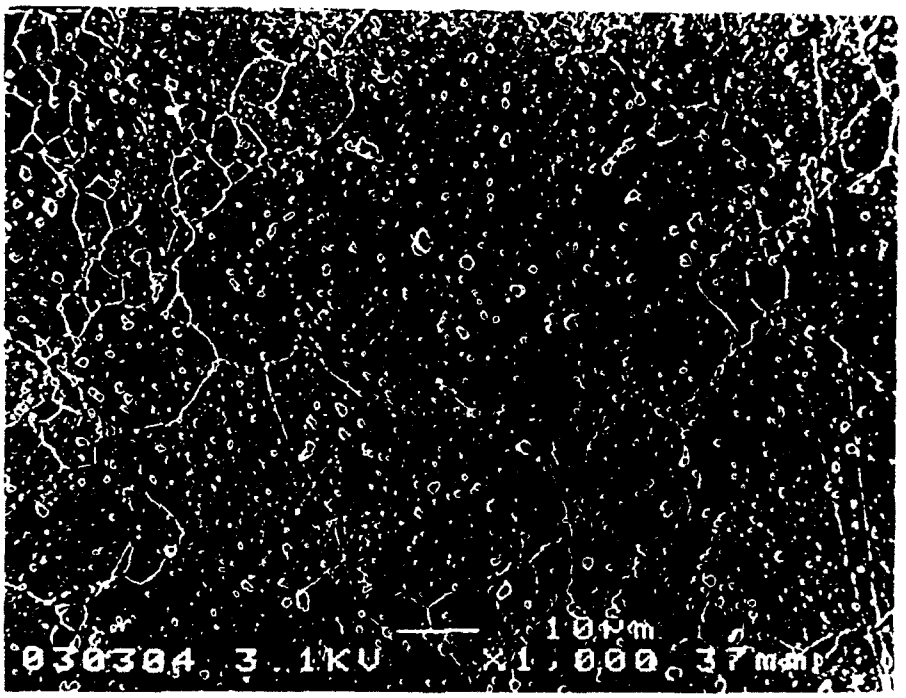

Figure 1. SEM micrograph of
Al_2O_3 - 5 vol% SiC composite

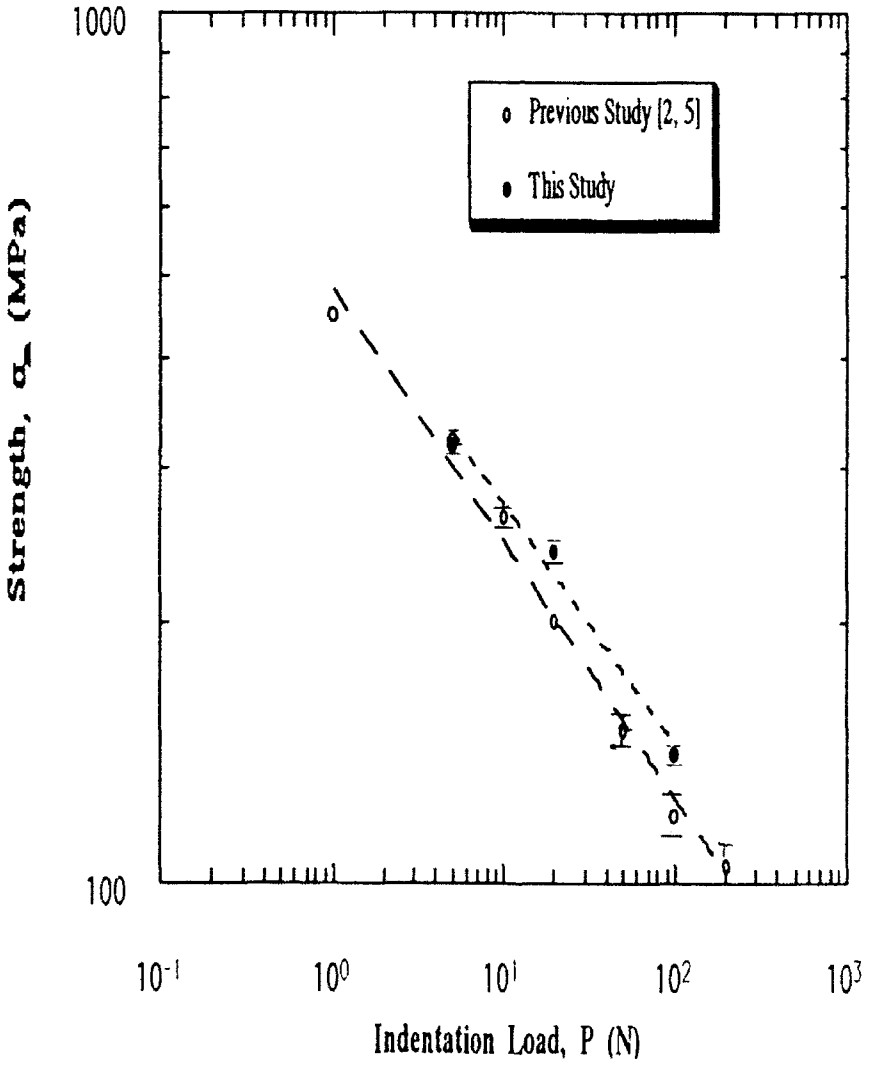

Figure 2. Strength versus indentation load for the Al2O3 - 5 vol% SiC composite

V. Reference

[1] K. Niihara and A. Nakahira, Proceeding of the Third International Symposium on Ceramic Materials & Components for Engines, the American Ceramic Society, Westerville, OH (1988), pp. 919 - 926.

[2] K. Niihara, A. Nakahira, G. Sasaki, and M. Hirabayashi, Proceedings of the International Meeting on Advanced Materials, Vol. 4, the Materials Research Society, Japan (1989), pp. 124 - 134.

[3] K. Niihara, the Centennial Issue of the Ceramic Society of Japan, vo. 99, no 10, pp. 974 - 982 (1991).

[4] K. Niihara and A. Nakahira, Advanced Structural Inorganic Composites, edited by P. Vincenzini, Elsevier Sci. Pub. (1990), pp. 637 - 664.

[5] J. Zhao, L. C. Stearns, M. P. Harmer, H. M. Chan, G. A. Miller, and R. F. Cook, Journal of the American Ceramic Society, no. 2, (1993).

[6] L. C. Stearns, J. Zhao, and M. P. Harmer, Journal of European Ceramic Society, vo. 10, (1992), pp. 473 - 477

[7] K. Niihara, Private Communication

[8] R. F. Cook, B. R. Lawn, T. P. Dabbs, and P. Chantikul, Journal of the American Ceramic Society, vo. 64, no 9, (1981), pp. c121 - c122.

[9] F. F. Lange, M. R. James, and D. J. Green, Communications of the American Ceramic Society, no.2, (1983), pp. c16 - c17.

[10] L. M. Braun, S. J. Bennison, and B. R. Lawn, Journal of the American Ceramic Society, vo. 75, no. 11, (1992), pp. 3049 - 3057.

[11] P. Chantikul, S. J. Bennison, and B. R. Lawn, Journal of the American Ceramic Society, vo. 73, no. 8, (1990), pp. 2419 - 2427.

2. Publications and Presentations

2. Publications and Presentations

a. Publications

1. J. Zhao, L. Stearns, M. P. Harmer, G. A. Miller, and R. F. Cook, "Mechanical Behavior of Al_2O_3-SiC 'Nanocomposites'", J. Am. Ceram. Soc., 76, 503 (1993).

2. L. Stearns, J. Zhao, and M. P. Harmer, "Processing and Microstructure Development in Al_2O_3-SiC 'Nanocomposites'", J. Eur. Ceram. Soc., 10, 473 (1992).

3. M. P. Harmer, H. M. Chan, and G. A. Miller, "Unique Opportunities for Microstructural Engineering with Duplex and Laminar Ceramic Composites", J. Am. Ceram. Soc., 75[7], 1715-1728 (1992).

4. M. P. Harmer, H. M. Chan, and G. A. Miller, "Unique Opportunities for Microstructural Engineering with Duplex Ceramics", Ceramic Transactions, 22, 617, American Ceramic Society (1991).

b. Presentations

1. L. C. Stearns, J. Zhao, and M. P. Harmer, "Processing and Microstructure Evolution in Al_2O_3-SiC Particulate Composites", 94th Annual Meeting of the American Ceramic Society, Minneapolis, April 1992.

2. J. Zhao, L. Stearns, M. P. Harmer, H. M. Chan, G. A. Miller, and R. F. Cook, "Mechanical properties of Alumina Containing Sub-micron SiC Particles", 94th Annual Meeting of the American Ceramic Society, Minneapolis, April 1992.

3. J. D. French, J. Zhao, M. P. Harmer, H. M. Chan, and G. A. Miller, "Tensile Creep of Duplex Ceramic Microstructures", World Congress on Ceramics, Symposium on Multiphase and Interpenetrating Phase Ceramics", San Francisco, November 1992.

4. H. M. Chan and M. P. Harmer, "Microstructural Design with Duplex Ceramics", Gordon Research Conference on Ceramics, New Hampshire, August 1992.

3. Awards and Accomplishments

3. Awards and Accomplishments

1. Dr. Helen M. Chan has received the ASM International 1992 Bradley Stoughton Award for Young Teachers.

2. Dr. Martin P. Harmer was appointed the Alcoa Foundation Professor of Materials Science and Engineering.

3. Dr. Martin P. Harmer was named to be elected as a Fellow of the American Ceramic Society.

4. Personnel

4. Personnel

Research Associates

1. J. Zhao
2. M. Thompson
3. J. C. Fang

Graduate Students

1. I. A. Chou